MOUNT BAKER BASALT MINERAL TEXTURES AND CHEMISTRY: PROBES INTO MAGMA RESERVOIR PROCESSES

Maria Vasin
Advisor: Sue DeBari
April 2017 – June 2018

ABSTRACT
The purpose of this study is to investigate the magmatic journey of two basaltic lava flows from Mount Baker from mantle melting to eruption. This investigation involves semi-quantitative analysis of phenocryst zoning and disequilbrium textures which are likely to reflect open-system processes. The Park Butter flow was found to involve just one (or two possible but unlikely) mafic magma injection causing zoning and eruption. The Lake Shannon flow was found to involve felsic magma travel through cumulates, mixing of felsic and mafic magmas, and finally a mafic injection into this mixed chamber causing eruption. Both the Park Butte and Lake Shannon flows were found to show strong evidence of diequilibrium textures.

ACKNOWLEDGMENTS
With great gusto I would like to acknowledge Dr. Susan DeBari for her boundless dedication to all aspects of this project. Her guidance and enthusiasm throughout the process have been truly invaluable.

Also, many thanks go to Ben Paulson for assisting with technical aspects such as SEM and thin section work, the SciTech staff at WWU for assisting with the many hours spent in the SEM room, the WWU RSP program for providing funding for thin section manufacturing, and many people (including those listed above) for listening to me talk for much more time than necessary about my fascination with basalt.

INTRODUCTION
Basalt represents the most primitive stage of mantle-derived magma. If a basalt erupts on the surface above a subduction zone, it has made a complete journey from mantle to surface without significantly changing composition (i.e.; differentiating to a more felsic magma). Therefore, basalts have the potential to preserve the entirety of this journey in mineral textures, and to serve as a particularly effective probe into subsurface volcanic processes. Phenocrysts within these basalts can reflect and preserve changes in crystallization condition parameters (e.g.; temperature, pressure, composition) in their concentric crystal structure in a similar way to sedimentary layers preserving evidence of depositional environments.

This study focuses on two basaltic lava flows from Mount Baker, a volcano located in the Cascade Mountains of North America. On the larger scale, it is part of the Cascade magmatic arc, where the Juan de Fuca plate subducts under the North American plate. Previous studies of Cascade basalts have been concentrated on flows located in the south to mid Cascades; there are considerably fewer analyses of basalts erupted north of Mount Rainier, which are less common (Moore and DeBari, 2012). Most of the basalts in the Mt. Baker volcanic field are found on the southwestern side of the stratocone. Lavas erupted in this field almost always have complex phenocrysts, with high amounts of plagioclase and pyroxene (Hildreth et al., 2003). Some of these phenocrysts have textures which reflect open-system processes (Escobar, 2016). The detailed investigation of these mineral textures within primitive flows that travel through

relatively minimal continental basement can help illustrate the journey from parent magma to erupted lava flow.

The current body of research on basaltic lavas from Mt. Baker focuses principally on geochemistry of the whole rocks, without much emphasis on the zoning profiles of the minerals. In 2003, Hildreth et al. published a study providing an extensive investigation into the entire eruptive history of Mount Baker, which included major element data for all flows. Moore and DeBari (2012) expanded on this study by analyzing the whole rock chemistry of Mount Baker's mafic magmas. There has yet to be a detailed mineralogical analysis of these magmas, with the exception of the high-Mg basaltic andesite and andesite flows described by Sas et al. (2017). Furthermore, Moore and DeBari (2012) were principally interested in magma generation from mantle melting. Furthermore, Moore and DeBari (2012) were principally interested in magma generation from mantle melting processes, rather than the path taken by the magma en route to eruption. Escobar (2016) conducted a detailed analysis of crystal clot co-assemblages to infer open system processes affecting Mount Baker andesites. No such study exists for Mount Baker basalts.

This study focuses on two basaltic lava flows from Mount Baker: the Lake Shannon and Park Butte basalts (Figure 1). These flows contain mostly plagioclase, pyroxene, and olivine phenocrysts. Based on Moore and DeBari's 2012 study, the Lake Shannon flow is a typical calc-alkaline basalt (CA), which implies relatively high quantities of dissolved water, while the Park Butte flow is a modified low-potassium olivine tholeiitic basalt (LKOT), which implies a "dry" magma with minimal dissolved water. The Park Butte basalt has similar major element chemistry to other Cascade LKOT lavas (Moore and DeBari, 2012). Thus, this study has the potential to investigate the effect of dissolved water content on open-system volcanic processes.

Even though mineralogical evidence shows that magma mixing and mingling has occurred in the mafic lava flows of Mount Baker, Moore and DeBari (2012) found evidence that their analyzed lava flows (including the Lake Shannon and Park Butte flows) are representative of their mantle-derived parent magmas. Thus, the detailed investigation of mineral textures within these flows can help illustrate the journey from parent magma to erupted lava flow.

By comparing phenocryst compositions to whole rock compositions, they found that the Lake Shannon flow was in near-equilibrium, while the Park Butte flow has both equilibrium and non-equilibrium phenocrysts. This investigation explores in greater detail the phenocryst equilibrium states and textures of the Lake Shannon and Park Butte flows. Some of the phenocryst populations are found to be in equilibrium with the host magma, but there are many examples that are not.

GEOLOGIC BACKGROUND AND TECTONIC SETTING

Lava flowing from a volcano was once magma within the earth. At ocean-continent convergent subduction zones such as that off the coast of the Pacific Northwest of the United States, this magma has its origins in the mantle. As the oceanic plate subducts and experiences an increase in surrounding temperature, hydrous minerals such as chlorite release water from their structures into the mantle of the overriding continental plate. This water lowers the melting temperature of the mantle, and so the solid mantle is converted into a partially molten state (Figure 2).

Magma generated through mantle melting is initially basaltic in composition, but as the magma rises due to density differences between the solid and liquid state, the magma cools and differentiates (changes in chemical composition) and becomes more felsic.(Winter, 2000). This differentiation can occur as a result of crystal fractionation (preferential crystallization of mafic minerals), magma mixing (introduction of a new, more felsic magma, most commonly as a result of crustal melting), or assimilation (introduction and melting of country rock or cumulates). Because basalts are the least differentiated of the magmas, they are the least removed from their mantle source. Therefore, basalts serve as particularly good probes into magma generation and mantle input into magmatic arcs.

Phenocrysts within basaltic lava flows can record magma chamber processes occurring during their crystallization. Crystals begin as a nucleus and grow concentrically outward (like trees). In igneous minerals which exhibit solid solution, and which have not had sufficient time to equilibrate as the containing magma evolves, the composition of the center of a crystal represents the initial crystallization conditions in the containing magma. As the crystal grows, new molecules attach to the outermost edge. The composition of this growing edge is in equilibrium with the containing magma. Thus, the composition of the outermost rim of a crystal represents the crystallization conditions shortly prior to eruption. A change in chemical composition from core to rim is known as zoning. Zoning is a highly advantageous mineral texture, as it records successively changing environments within a magma chamber in much the same way as sedimentary rocks record surface processes. Other textures, such as embayments or sieving, suggest a mineral was not in equilibrium with its containing magma. These mineral textures are a useful indicators of magma chamber processes during a magma's migration to the surface.

Mount Baker is part of the larger Mount Baker volcanic field (MBVF) a Quaternary multivent field which has been active since 1.3 Ma. It is the most conspicuous stratocone in this large cluster, the highest peak in the North Cascades, and the most productive Quaternary eruptive center in the Garibaldi belt, the name given to the volcanic arc of the North Cascades. Other stratocones in this cluster have been more severely eroded by glaciers. The field is subject to a high degree of glacial erosion. It is estimated that over half of erupted material has been removed by glacial activity, and many Pleistocene eruptive centers have been reduced or completely eradicated (Hildreth et al., 2003).

The Cascade volcanic arc is part of a larger system caused by subduction of the Juan de Fuca plate (a remnant of the Farallon plate) beneath the North American plate. The subducting Juan de Fuca plate has some of the hottest subducting plate temperatures worldwide (Hildreth, 2007). Mount Baker is located 320 km east-northeast of the trench; this is reflective of an unusually shallow subduction angle. This low subduction angle combined with the hot temperatures results in early dewatering of the subducting slab. In turn, low degree of melting causes Mount Baker magmas to be less silica-saturated than other basalts. The volcano is approximately 100 km above the top of the subducting slab, 40-45 km of which is sediment or sedimentary rock (Hildreth et al., 2003). Underlying the sedimentary rock are accreted terranes, which are generally mafic (Tabor et al., 2003).

Most lava erupted from the MBVF is andesitic, with basalt and dacite accounting for only 1-3% of the total. This is likely due to the physical barriers to eruption within basaltic and dacitic magmas: basalt is too dense, and dacite is too viscous, but once mixed to form intermediate andesite, eruption is made possible (Kent et al., 2010). The first MBVF basalts began to erupt

from the Black Buttes stratocone 0.5-0.2 Ma. Nearly all erupted basalts from Mount Baker belong to its southwestern focus, near Black Butte. Phenocryst populations within these lava flows tend to be dominated by plagioclase and pyroxene with complex textures (Hildreth et al., 2003). Whole rock data for the Lake Shannon and Park Butte flows is shown in Figure 3.

The Park Butte flow is 716 $\pm$ 45 ka in age, and is a small remnant of a larger flow (Hildreth et al., 2003). The Park Butte flow is a modified low-potassium tholeiitic basalt (LKOT), with similar major element chemistry to other Cascade LKOT lavas. (Moore and DeBari, 2012). The tholeiitic trend of this magma indicates a "dry" magma with minimal dissolved water compared to calc-alkaline magmas. Moore and DeBari (2012) estimated the water content in the Park Butte flow to be about 3%, indicating more water than is typical for an LKOT-type magma. The generally low trace element abundances indicate either a depleted mantle source or high degree of partial melting. It is olivine-rich (50-65% of the phenocrysts) with embayed rims and chemically altered fractures, plagioclase (35-45%) with sieved cores, and normal and oscillatory zoning, and a small amount of clinopyroxene (1%) with embayed rims (Moore and DeBari, 2012).

The Lake Shannon flow is 94 $\pm$ 21 ka in age. The eruption occurred underneath a glacial cover, resulting in hyaloclastic textures (Hildreth et al., 2003). The flow is mostly hyaloclastite tuff and thin lava sheets, with a maximum thickness of 150 meters. Based on Moore and DeBari's 2012 study, the Lake Shannon flow is a typical calc-alkaline basalt (CA) with abundant plagioclase (60-70%) with embayed and sieved cores, and normal and reverse zoning, olivine (30-35%) with resorbed cores and fractured and embayed rims, and some clinopyroxene (<2%).

PROJECT CONTEXT

Streck (2008) shows that open-system processes are reflected in the mineralogical record when they involve magmatic recharge (mixing) or addition of country rock (contamination). Magma mixing can occur as a result of magmatic recharge (introduction of different magma into the magma chamber), or as a result of "self-mixing" – the heterogeneity of magma chamber compositions, temperatures, dissolved gasses, and crystal to liquid ratio can cause movements within the chamber itself. The more dissimilar two mixing magmas are, the greater the difference in viscosity. Contamination typically occurs in the form of incorporation of solid material or crystal mush which subsequently melts and changes the chemical composition. Open-system processes are rarely as simple as a felsic magma being injected once by a mafic magma and subsequently erupting, or a single magma incorporating a single piece of country rock en route to eruption. Magma mixing and mingling tend to occur in multi-stage events, resulting in a complex mineralogical record, which is further complicated by any contamination that occurs during the mingling process. (Streck, 2008).

If disequilibrium mineral textures are observed, then open system processes are apparent. Mineral textures can be observed in phenocrysts (crystals that form in-situ in a magma), antecrysts (crystals part of the same magmatic system, but from a different host magma), or xenocrysts (crystals derived from country rock, completely unrelated to the magma system). Most magmas have some number phenocrysts in disequilibrium, that is, they show evidence for some degree of magma mixing. This evidence includes textures such as embayments or sieved cores, and chemical zoning.

Patterns of zoning, the expression of compositional variability within a crystal, can give clues into magmatic processes during crystal formation. There is a normal pattern of zoning, and if the crystal does not exhibit this normal pattern of zoning, then it reflects some form of magma mixing – reverse zoning indicates incorporation of a more primitive magma. Furthermore, the nature of zoning can reflect much about the nature of mixing which occurred: sharp transitions (known as step zoning) indicate dramatic, fast changes in composition, while smooth transitions (known as progressive zoning) indicate slower compositional changes. Lack of zoning can indicate equilibrium with the surrounding liquid or rapid eruption following incorporation of the crystal.

Other common textures include resorption (dissolution of the mineral back into the melt) and diffusion (exchange of ions in the solid state). Resorption is often reflected through a "sieved" texture (eg; Figure 46) while diffusion is often reflected through progressive zoning (Streck, 2008).

Each mineral (plagioclase, olivine, or pyroxene) forms its own pattern of textures in response to open system processes. Below is a description of the typical textures for these minerals:

Plagioclase has a tendency toward oscillatory zoning even without repeating pulses of more primitive magma. This is because crystallization of anorthite and albite is somewhat kinetically controlled; the ions may be delayed in migrating through the magma and hence the "wait period" is reflected through crystallization from the newly differentiated surrounding magma. This is reflective of temporary magma differentiation through crystal fractionation. Fine banding tends to reflect kinetically controlled oscillatory zoning, while coarse banding could be indicative of external influences of dynamic magma processing. Because plagioclase has a particularly slow diffusion rate, it can serve as a useful record for interpreting magma chamber processes when other crystals have had time to equilibrate (Streck, 2008).

Zoning in plagioclase can reflect either compositional changes, or changes in pressure or temperature. Decompression can cause crystallization due to the exsolution of water. Reverse zoning can either reflect influx of more primitive melt, or increase in temperature or pressure (decrease in pressure in dry magmas). Temperature can increase without introduction of more mafic melt through release of latent heat due to decompression-related crystallization during magma ascent. Distinguishing between compositional or physical causes of zoning can be made possible by examining abundances of minor and trace elements. Increase in iron with increased anorthite content in the crystal structure tends to be indicative of mafic magma recharge, while iron remaining stable with changing anorthite content can reflect physical causes of zoning in the plagioclase crystal. Strontium is a more reliable indicator, as its abundance in plagioclase does not depend on temperature at all (Streck, 2008).

Pyroxenes often display reverse zoning and resorption textures. There are several trace elements which can serve as indicators of compositional versus physical changes, but this study is only focused on major and minor elements (Streck, 2008).

Olivine responds rapidly to disequilibrium through dissolution, re-equilibration through diffusion, or formation of pyroxene rims. Resorption most commonly leads to crystal embayments (eg; Figure 7). Zoned olivines indicate very short times between crystal formation, magma mixing and eruption. A normally zoned olivine can form without magma mixing, but

once again it is indicative of rapid eruption following crystal formation. A reverse zoned olivine is indicative of rapid eruption following compositional change in the surrounding liquid, likely due to injection of a more mafic magma and subsequent exsolution of dissolved gasses (Streck, 2008).

Glomerocrysts, or crystal clots, are clusters of multiple mineral phases which represent co-crystallizing assemblages. They can be used to form associations between different mineral populations to represent a broader magma component or pre-eruption crystallization conditions. These associations can be used as strong evidence for various open system processes, particularly magma mixing or wall rock assimilation (Escobar, 2016).

METHODS

A total of 11 uncovered polished thin sections were made using Moore's previously collected samples. Because the Lake Shannon flow samples displayed a greater compositional variability (see Moore and DeBari, 2012), 7 thin sections were made for the Lake Shannon flow compared to the 4 created for the Park Butte flow. Decision to make a thin section for a given sample was based on composition (attempt to represent mafic or felsic end-members based on weight percent SiO2 and Mg# in Moore's whole rock data), presence and scope of vesicles (vesicular vs. non-vesicular end-member), minimal degree of weathering, and/or presence of potentially interesting anomalies (such as magma mingling) or mineral textures visible in either hand sample or Moore's existing thin sections. Two thin sections were made for sample LS1: LS1-V, representing a highly vesicular component, and LS1-NV, representing a less-vesicular component. The Park Butte flow showed evidence of a vesicular and non-vesicular component as well. The LS2 and PB4 thin section billets were cut so that each component comprised about half of the thin-section area.

The thin sections were analyzed using a combination of petrographic techniques and qualitative to semi-quantitative observations using the WWU Tescan SEM. Thin section petrography was used primarily to identify grain textures, glomerocrysts, or mingled magmas for future analysis in the Tescan SEM, or to verify observations made while using the SEM (for example, ascertaining whether a particular location within the matrix was microcrystalline or glassy).

WWU Tescan SEM data were used to perform semi-quantitative data analysis. Individual mineral grains analyzed in each sample are assigned a number (e.g.; ol5). In cases where multiple analysis points were taken on the same grain, this number is followed by an underscore (_) and another number (e.g. ol5_2). Crystals were classified as phenocrysts if they had a maximum diameter greater than 0.5 mm, microphenocrysts if the diameter was 0.1-0.5 mm, and matrix grains if the diameter was less than 0.1 mm. Values for magnesium number (Mg# = 100*[Mg/Mg+Fe], with values in moles, which is the same as forsterite content for olivines) and anorthite content (An = 100*[Ca/Ca+Na], with values in moles) were generated based on weight percents provided by the Tescan SEM. These values were considered with a margin of error of $\pm$ 2%. Therefore, crystals were considered to have internal compositional variation (i.e.; zoning) if the difference between Mg# or An-content between two analysis points was greater than or equal to 4.

The change in forsterite or anorthite contents from core (initial stages of crystallization) to rim (final stages of crystallization) was plotted as a core-to-rim traverse (eg; Figure 15). In these

charts, the horizontal axis represents the percent of distance traveled from the core to the rim, which is equal to the distance from the core divided by the total core-to-rim distance.

A Rhodes plot is a diagram which can be used to determine mineral equilibrium states based on partition coefficient (Kd) values. Partition coefficient values are a useful tool for establishing equilibrium parameters. The definition of a partition coefficient is:

$$K_d = \frac{C_c}{C_l}$$

where C is the concentration of an element or ratio such as anorthite content, Cc is the concentration of that element or ratio in the crystal, and Cl is the concentration in the liquid. For example, a crystallizing plagioclase in equilibrium with its surrounding liquid will have a specific anorthite content relative to the "anorthite content" (Ca:Ca+Na ratio) of the liquid. This is the equilibrium Kd. If the actual anorthite content is different, then the crystal is not in equilibrium. In this example, an overly high crystal anorthite value can also indicate that the magma had more dissolved water. Water generally reduces melting temperatures, causing low-crystallization-temperature albite to be unstable in "wet" magmas and giving higher preference to anorthite crystallization, increasing the relative concentration of anorthite in the crystal compared to the liquid and thus increasing the Kd value.

Rhodes plots were generated largely based on whole rock X-ray fluorescence (XRF) data from Moore and DeBari (2012) coupled with the SEM semi-quantitative data. The exceptions are PB4, for which two whole rock analyses were made by this study for the two different components, and LS6, for which a single whole rock analysis was made by this study. In some areas of PB4, the two components were too well-mixed to distinguish; in these cases, an average of the two XRF data sets was used. Any new XRF data were used instead of those in Moore and DeBari (2012) for purposes of equilibrium studies. Partition coefficient (K_d) values were considered to be 0.3 $\pm$ 0.03 for olivine, 0.27 $\pm$ 0.03 for clinopyroxene, and 2.55 $\pm$ 0.85 for plagioclase. The Rhodes plots were visually analyzed to identify mineral populations or compositional patterns. Crystals described as "above" or "below" equilibrium are in equilibrium with a more or less primitive rock, respectively. Glass data were plotted in relation to whole rock composition to determine equilibrium states and identify mingled magmas.

PARK BUTTE FLOW

Petrography

The Park Butte basalt is porphyritic with 10% phenocrysts in a holocrystalline matrix. Matrix crystal sizes are very similar to microphenocryst sizes, especially plagioclase – nearly all the matrix crystals can be seen at minimal magnification. The matrix is dominated by subhedral elongate plagioclase, with some anhedral clinopyroxene and olivine visible in varying quantities. High levels of oxidization in some samples (mainly PB2) make mafic matrix crystals difficult to discern, but percentages of clinopyroxene + olivine within the total matrix area range from approximately 20-40%. Average matrix olivine and clinopyroxene diameter varies, with PB7 containing somewhat larger matrix mafic crystals compared to PB4 (Figures 4, 5). Plagioclase crystals are approximately equally sized between the samples. In hand sample, several samples show two distinct matrix colors, deemed "red" and "blue" for the purposes of this study. Sample PB4 shows stark contrast between vesicular red and non-vesicular blue, as shown in Figure 6. No

apparent difference in crystal size and abundance was observed between phenocrysts found within the red and blue matrix areas.

Phenocryst populations are approximately 60% olivine, 35% plagioclase, and 5% clinopyroxene. Olivine phenocrysts occur as 0.2-2 mm sub- to euhedral grains. Disequilibrium textures, especially embayment and diffusion rims, are abundant (Figures 7-9). Plagioclase phenocrysts occur as 0.1-2 mm sub- to euhedral equant to elongate grains. Almost all the plagioclase phenocrysts display oscillatory zoning, and about half show signs of a sharp change in composition in the rim area (Figures 10, 11). When it occurs as crystals, clinopyroxene occurs as 0.5-2 mm subhedral grains, but it is much more common as rims on other crystals.

No glomerocrysts were observed in samples PB3 nor PB7, though all samples contain some small crystal clots of 2-4 olivine or clinopyroxene crystals. Sample PB2 contains one glomerocryst (PB2_Grain1). It is approximately oblong, 4mm long and 1mm across. This glomerocryst contains equant to subspherical, anhedral to subhedral plagioclase (90%, highly fractured) clinopyroxene (10%), and olivine (<1%), all approximately 0.1mm in diameter (Figure 12). These plagioclase crystals are much smaller and more uniform than the phenocrysts in the surrounding thin section.

Sample PB4 contains several subcircular glomerocrysts 2-3mm in diameter which comprise about 8% of the total thin section area. Many of these glomerocrysts appear to have oxidized reaction rims (Figure 13). The glomerocrysts are composed of >95% subhedral equant plagioclase microphenocrysts. The glomerocrysts are absent of phenocrysts (>0.5 mm). Some rounded anhedral clinopyroxene and orthopyroxene are visible in the matrix. The matrix of these glomerocrysts contains somewhat more glass than the surrounding thin section.

Mineral Chemistry
Tables 1-5 show the complete SEM mineral chemistry data for Park Butte.

Olivine:
Figure 14 shows the generalized core and rim data for the Park Butte olivine crystals.The diffusion rims observed in cross-polarized light within olivine phenocrysts are also observed in SEM imagery.

The following olivine populations were identified:

- Population 1: normally zoned olivines, with cores ~Fo75-85 and rims ~Fo65-75, these comprise the majority of the crystals. Within this population, there are two subpopulations:
    - 1a: gradually decreasing forsterite content from core to rim (Figures 15, 16). These crystals have extremely patchy pyroxene rims.
    - 1b: gradually decreasing forsterite content from core to rim, punctuated with sharp decreases and subsequent increases in a somewhat oscillatory zoning pattern (Figures 17, 18). These crystals have slightly patchy pyroxene rims.
- Population 2: reversely zoned olivines, with cores Fo85-86 and rims Fo90-92. Three crystals were observed in this population; all were found in sample PB3 (Figures 19, 20) Two PB2 cores are included in this population; both are located within the PB2 glomerocryst. All population 2 olivines have a clear pyroxene rim.

- Population 3: normally zoned olivines with cores ~Fo80-85 and rims ~Fo55-63. This population is found in PB4 and PB7. Two rims (lacking core data) found in PB7 were included in this population. Within this population, those crystals with completed core-to-rim traverses show constant forsterite contents in the core, then sharp decreases (Figures 21, 22). This pattern is to be contrasted with population 1a, which does not show constant forsterite contents in the cores. All population 3 olivines have little to no clinopyroxene rim present.
- Additional populations that do not fit into these three include cores with Fo70-75 (one with rim data of Fo68), one core with Fo65, and one unzoned olivine crystal with Fo79.

Rims on normally zoned crystals tend to be 75-125µm, while rims on reversely zoned crystals tend to be slightly thinner, 50-75µm (Figure 23).

The Rhodes plot for the Park Butte olivines shows that most PB2 and PB3 grains (population 2) have forsterite contents higher than what is expected equilibrium, while the PB7 rims (population 3) tend to have forsterite contents dramatically below equilibrium (Figure 24). In general, olivine cores and middles for all samples tend to cluster closer to equilibrium than rims.

Pyroxene:

Clinopyroxene appears almost exclusively as rims on the olivine crystals than as isolated phenocrysts. The olivine is also often rimmed by orthopyroxene. Rims are typically patches rather than clear perimeters, and are 20-50µm in thickness. Average forsterite content of olivines with orthopyroxene rims is 79, compared to 74 in olivines with clinopyroxene rims. The Rhodes plot for the clinopyroxene data reveals that all observed clinopyroxene compositions are well below the equilibrium values for the whole rock (Figure 25). Clinopyroxene values represent equilibrium with liquid magnesium numbers of 23-53, while measured whole rock compositions are Mg#58-64 (Moore and DeBari, 2012).

Plagioclase:

Figure 26 shows generalized core and rim data for the Park Butte plagioclase crystals. Few core to rim data traverses exist for the plagioclase crystals; most data is isolated analysis points in cores or middles. Three plagioclase populations are apparent, based mostly on overall anorthite content as opposed to core-to-rim changes:

- Population 1: An_{84}-An_{90} (Figure 27). One crystal has an An_{63} rim. Other than this crystal, there is no evidence of zoning patterns. Found in all samples except PB7.
- Population 2: An_{63}-An_{82} (Figure 28). Contains two normally zoned crystals and one unzoned crystal. Found in all samples.
- Population 3: An_{32}-An_{50} (Figure 29). This population only exists within the PB4 glomerocrysts, which also contain quartz.

Of the three plagioclase crystals with both core and rim data, two are normally zoned and one is unzoned. All three crystals (PB2_plag6, PB3_plag1 and 4) belong to population 2. Both have anorthite contents in the mid- to high 80s within the core and middle regions, then a sharp jump to An_{63} for PB2_plag6 and An_{71} for PB3_plag1. The third crystal (PB2_plag4) is unzoned with $An_{85\text{-}88}$ and belongs to population 2.

Population 3 crystals are found only within PB4 glomerocrysts, which do not contain plagioclase crystals from any other population.

The Rhodes plot for Park Butte plagioclase crystals shows that populations 1 and 2 are generally above equilibrium (with one rim just inside the equilibrium zone), while population 3 is at or below equilibrium (Figure 30).

No significant correlation was found between anorthite content and iron oxide content; the crystals were not analyzed for strontium.

Glomerocrysts and crystal clots:
Sample PB2 contains a single glomerocryst (Figure 12). Based on available data, the glomerocryst contains exclusively population 2 olivines (reversely zoned), two population 1 plagioclase crystals (highest anorthite), and one population 2 plagioclase crystal (mid-anorthite).

Sample PB3 contains a small crystal clot with a population 1 plagioclase and an olivine with an Fo80 core. No rim data was collected on this olivine, but the core composition suggests that it belongs to either population 1 or 3. Sample PB4 contains a crystal clot in the red section with an unzoned Fo79 olivine, Fo73 and 76 cores, and population 2 plagioclase.

Vesicular and non-vesicular components:
Sample PB4, which displays the vesicular red and less-vesicular blue components, does not show extreme difference in olivine mineral chemistry for the two components (Figure 31). The less-vesicular component contains both population 1 and 3 olivines, while the vesicular component contains only population 1 olivines. Besides the glomerocrysts (which contain exclusively population 3 plagioclase and are the only place where population 3 occurs), the plagioclase compositions do not seem to differ significantly between the two components. Both components contain plagioclase populations 1 and 2 (Figure 32). Three quartz grains were observed; all were located within PB4 glomerocrysts.

LAKE SHANNON FLOW

Petrography
The Lake Shannon flow is porphyritic with 30-35% phenocrysts and microphenocrysts. Matrix textures range from almost completely holohyaline (LS6) to hypocrystalline (Figure 33). Areas of fine-grained crystalline matrix tend to be highly oxidized, making mineral identification and observation difficult, but some areas of glass or cryptocrystalline matrix, anhedral olivine, and pilotaxitic plagioclase were observed. Vesicularity varies greatly, but the flow is generally about 25% vesicles. Glomeroporphyritic textures are apparent in most samples (Figure 34). Glomerocrysts are dominated by plagioclase, with some olivine and clinopyroxene, and range from 1-6 mm in diameter, with most between 3 and 4 mm.

Phenocryst populations are dominantly plagioclase (75%) and olivine (20%). Plagioclase occurs generally as subhedral to euhedral equant or elongate crystals, with long axes ranging from 0.1 to 4 mm. Concentric, oscillatory zoning is ubiquitous throughout the plagioclase crystals. Sieved cores are present in about 20% of the plagioclase phenocrysts. Olivine occurs as anhedral to euhedral grains ranging from 0.1 to 2 mm in diameter. Clinopyroxene comprises the remaining 5% of the phenocryst population, save for occasional orthopyroxenes, and occurs as anhedral to subhedral grains ranging from 0.1 to 1.5 mm in diameter. Some rare orthopyroxene

microphenocrysts were observed in sample LS1-NV (≤ 2% of the phenocryst population) and sample LS6 (≤ 5% of the phenocryst population). Occasional embayments and other resorption textures occur in both orthopyroxene and clinopyroxene phenocrysts, particularly within larger-sized crystals, though these textures were observed in some microphenocrysts of both mineral types.

Some samples display certain localities of greater or lesser degree of vesicular texture. For example, two thin sections were made for LS1: LS1-V, which mostly contains the highly vesicular end-member, and LS1-NV, the less vesicular end-member. LS3 was categorized as a highly vesicular sample. LS2 contained distinct bands of both end-members (Figure 35). Based on qualitative approximation, mean vesicle diameter for the highly vesicular end-member is 2 mm, while mean vesicle diameter for the less vesicular end-member is <1 mm. Phenocryst abundances are approximately identical for vesicular and non-vesicular areas.

Sample LS5 has three different matrix colors, categorized for the purposes of this investigation as “red”, “gray”, and “black. These components account for approximately 10%, 80%, and 10% of the total matrix area, respectively. The areas of red matrix tend to be subrounded in shape, the areas of black matrix tend to be elongate and sinuous in shape, the gray matrix is massive, filling in the spaces between the other two matrix bodies (Figure 36). The relative abundance of phenocryst populations is approximately the same for all three components: 80% plagioclase, 15% clinopyroxene, and 5% orthopyroxene. Plagioclase sizes are also similar (the red component may have slightly larger crystals), 0.1-2.2 mm with an average size around 0.7 mm. Aside from color, matrix characteristics are similar between the gray and black components. The matrix is micro- to cryptocrystalline with abundant pilotaxitic plagioclase. Phenocrysts comprise 20-30% of the gray and black components. The red component has significantly more phenocrysts, >80% (Figure 37). The matrix is hypohyaline, with ~35% pilotaxitic plagioclase in red-stained glass. The different matrix colors are good evidence for presence of mingled magmas.

Mineral Chemistry

The Lake Shannon basalt mineral chemistry is highly variable, both within each sample and between samples (Tables 6-10).

Olivine:

Figure 38 shows generalized (core and rim) olivine data for the Lake Shannon flow. No olivine crystals were observed in samples LS5 or LS6. Olivine compositions range from Mg# 73-86. Most olivines are unzoned, but some display normal zoning. Those which are normally zoned and have slightly more detailed traverses show a decrease in forsterite content very close to the rim (eg; Figure 39). Three populations were identified:

- Population 1: unzoned olivines with Fo78-84 (Figure 40). These comprise the majority of the olivine crystals and exist in all samples.
- Population 2: normally zoned olivines with Fo85-86 cores and Fo75-78 rims (Figure 41). These are found in LS1-NV, LS3, and LS4.
- Population 3: normally zoned olivine with Fo80 core and Fo73 rim (Figure 42). Only one crystal was observed in this population, in LS2.

Rhodes plots show that all olivine rims are below equilibrium (Figure 43). The population 3 core is below equilibrium. Population 2 cores and middles are at or above equilibrium. Sample LS4 contains some cores and middles that are above equilibrium as well. Otherwise, cores and middles are at or below equilibrium.

Pyroxene:
Clinopyroxene compositions range from Mg# 69-78. Orthopyroxene compositions range from Mg# 44-74. Chemical zoning was not observed in either of the pyroxene populations, however, little core-to-rim data was collected.

Rhodes plots show that clinopyroxene compositions in LS6 are below equilibrium (Figure 44).

Plagioclase:
Figure 45 shows generalized (core and rim) plagioclase data for the Lake Shannon flow. A majority of the plagioclase population displays concentric, sometimes patchy oscillatory zoning patterns. Sieved crystals were observed in LS1, LS2, and LS4 (eg; Figure 46).

Plagioclase core-to-rim traverses show fairly stable anorthite contents in LS1, LS2, and LS4 (An78-82 throughout the crystal), with two exceptions (Figures 47-49). The first (LS1-NV_plag2) begins at An83, then drops to An74 before returning back to the ~An80 composition of the other crystals. The second (LS2_plag4) begins at An83, then gradually decreases to An76.

In LS5, all crystals with traverse data show some form of zoning (Figures 45, 50, 51). LS5_plag10 (black) and LS5_plag13 (grey) show stable anorthite contents, then a sharp decrease just prior to an increase in anorthite content. LS5_plag10 is particularly dramatic, with a stable anorthite content of 59-62, then a drop to An54, then a sharp increase to An79. LS5_plag6 (grey) shows a sharp increase in anorthite content from An57 to An72, then a gradual decrease. LS5_plag2 shows a decrease from An75 in the core to An52 in the rim.

All LS6 plagioclase crystals with detailed core-to-rim traverses show a jump upward in anorthite content at 80-90% traversed to the rim followed by a sharp decrease (Figure 52). Prior to the jump, LS6_plag1 and LS6_plag7 show stable anorthite contents of An60 and An65 respectively, though LS6_plag1 shows an increased anorthite content in the core. LS6_plag3 and LS6_plag9 show stable anorthite contents, then a sharp decrease in anorthite content just prior to the increase. Though patterns are similar, anorthite contents in these crystals are different.

The following plagioclase populations are identified:

- Population 1: Unzoned, An73-83. All sieved and slightly sieved crystals fall into this population, though not all crystals in this population exhibit that texture. Both LS1 samples, LS2, and LS4 contain only plagioclase crystals belonging to this population (one exception noted below). Two normally zoned crystals are included in this population due to their similar anorthite content:
    - An83 core, An76 rim: LS2_plag4
    - An73 core, An66 rim: LS6_plag1
- Population 2: An57-61 cores and rims found in LS5 and LS6. When traverses are available, they show both normal and reverse zoning (see below).
- Population 3: Normally zoned, with An67-75 core to An46-52 rim: LS5_plag2, LS5_plag12

- Population 4 (one crystal observed): Normally zoned, An94 core and An54-63 rim: LS6_plag2
- Population 5: Plagioclase showing a decrease in anorthite content just prior to an increased anorthite content (Figure 53). This includes two subpopulations:
    - Reversely zoned, with a sharp decrease just prior to the increased anorthite content: LS5_plag10 and 13
    - Decrease in anorthite content following the increased "spike": LS6_plag3 and 9.

Initial Rhodes plots using $K_d = 2.55 \pm 0.85$ show that all Lake Shannon plagioclase crystals are above the equilibrium anorthite content (Figure 54). Based on Sisson & Grove (1992), K_d values of 1.7, 3.4, and 5.5 were tested; only the K_d value of 1.7 allowed for some plagioclase data to fall within the equilibrium error bounds (Figure 55).

No significant correlation was found between anorthite content and iron oxide content; the crystals were not analyzed for strontium.

Glomerocrysts and crystal clots:
The glomerocryst olivines in LS1-V and LS4 all belong to olivine population 1, while the plagioclase crystals all belong to plagioclase population 1. In other words, olivine and plagioclase in LS1-V and LS4 glomerocrysts are unzoned.

The red sections of LS5 are entirely glomerocrysts. Though little data exists, all observed plagioclase crystals belong to population 2 or 5.

Vesicular and non-vesicular components:
Crystal composition in both the vesicular and non-vesicular sections is highly similar, as are zoning patterns. Most crystals in LS1-NV, LS1-V, and LS2 show no change in composition from core to rim.

Magma components of LS5
The three matrix colors observed in LS5 are not observed in SEM imagery. Figure 50 shows compositions of plagioclase crystals color-coded by surrounding matrix. Plagioclase cores in the grey areas tend to have higher anorthite contents (An70-75 with one exception) than those in the red and black areas (An50-60). Rims tend to be An70 or higher. The two normally zoned crystals observed in LS5 have An67-75 cores and An46-52 rims (population 3). With the exception of one inclusion in grey-section plagioclase, the only clinopyroxenes observed in LS5 were located in the red section.

Glass:
Most areas of glass are riddled with cryptocrystalline crystals, making accurate glass data possible to obtain only from LS6. Glass in this sample ranges from Mg# 21-35, with an average Mg# of 30. Average SiO_2 and total alkali content (TAS) is indicative of a rhyolitic glass (Figure 3, Table 10).

DISCUSSION

Even though mineral evidence shows that magma mixing and mingling has occurred in the mafic lava flows of Mount Baker, Moore and DeBari (2012) found evidence that their analyzed lava

flows (including the Lake Shannon and Park Butte flows) remain quite similar to the mantle-derived parent magma. This evidence includes lack of variation in highly incompatible elements, lack of evidence for assimilation of continental crust, and lack of variation between the most mafic and most felsic end-members for each lava flow. Thus, the detailed investigation of mineral textures within these flows can help illustrate the journey from parent magma to erupted lava flow.

Analysis of these mineral textures is based on the end goal of creating a narrative of the various processes affecting a magma along its path from the mantle to the Earth's surface. The intent of this discussion, and subsequent conclusion, is to use mineral zoning profiles to analyze the open-system processes involved in the paths of these two particular flows. A pattern of logic is used to create general hypothesis, with degree of speculation increasing with progression through the pattern. First, presence or lack of disequilibrium features represents the difference between fractional crystallization or open system processes being the dominant mechanisms for differentiation. Open system processes create disequilibrium features. The type of open system processes can be inferred by the chemical and physical properties of the disequilibrium features, as described in Streck (2008).

Plagioclase Rhodes plots are not necessarily direct indicators of plagioclase equilibrium states. Though vertical spread of plagioclase data is reflective of equilibrium state, plagioclase anorthite contents can also reflect water contents in a magma. Therefore, if all plagioclase data clusters above or below equilibrium it is likely that the partition coefficient should be adjusted for a magma with more or less water content, respectively.

It is important to recognize the effect of the differences in age on the expression of compositional variability in the Lake Shannon and Park Butte flows. As magmas move up toward the surface in a volcanic field, not all will reach the surface. Many will stall and form sills, dikes, crystal mushes or, eventually, plutons. Therefore, the older a volcanic field, the more likely it is that magmas will travel through other stalled magmas on their way to the surface. The Park Butte flow is 716 $\pm$ 45 ka in age, while the Lake Shannon flow is 94 $\pm$ 21 ka in age. The Mount Baker Volcanic Field (MBVF) in its entirety is 1.3 Ma in age (Hildreth et al., 2003). Therefore, the Park Butte flow represents magmatic travel through a relatively young volcanic field, while the Lake Shannon flow represents magmatic travel through an older volcanic field. Thus the narrative for the Park Butte could be quite simple, while that for the Lake Shannon flow should represent a more complex journey.

Park Butte

All Park Butte rock samples look very similar in hand sample in terms of color, phenocryst size and abundance, vesicle distribution, etc. Park Butte whole rock data is similar across the samples as well (Figure 3). Though the two PB4 components have slightly different whole rock compositions, there is little indication of this difference when examining crystal compositions (Figures 31, 32). This means that prior to eruption, any mingling magmas were well mixed.

The presence of diffusion rims on the olivines indicate a short period of time between crystallization and eruption. It is possible that in populations 1 and 3, the diffusion rims are simply normal zoning, and these olivines crystallized in-situ and were simply carried out during eruption without interacting with any other magma bodies along the way. However, the presence of pyroxene rims on much of the phenocryst and microphenocryst population is indicative of

disequilibrium with the containing magma. In addition, Population 3 exhibits a sudden jump downward in anorthite content unlikely in a crystal-fractionation scenario. Therefore, it is more likely that the normally zoned olivines were thrust into a more felsic magma and began but did not fully complete the diffusion process en route to eruption.

Initially, the somewhat oscillatory zoning pattern in olivine population 1b (gradual decrease in Fo punctuated with somewhat oscillatory zoning patterns) was hypothesized to be absent from population 1a (gradual decrease in Fo, no punctuations) due to armoring by pyroxene rims. Those olivine crystals which are not armored by a pyroxene rim would be more likely to reflect changes in the crystallization environment and therefore belong to population 1b. However, the data show that this is not the case. Both subpopulations exhibit patchy clinopyroxene rims, and there is little difference between the appearance of the rims between the two populations.

Olivine populations 1 and 3 have similar forsterite contents in the cores, which indicates a likelihood of co-crystallization of these two populations during early stages. For simplicity, this early stage magma will be described as having forsterite content of 80. The difference in these two populations lies in the rim composition, with population 1 exhibiting a forsterite content of ~70, and population 3 exhibiting a forsterite content of ~60. If the Mg# 80 component (population 1 and 3 cores) injected a more differentiated Mg# 60 component (population 3 rims), the resulting mixed magma should have an intermediate Mg# of 70 (population 1 rims). Phenocrysts do not always stay within their original host magma during magmatic injection; they may eject or be plucked off by other magma bodies.

The reverse-zoned olivines of population 2 are reflective of a mafic magma injection. A magma chamber containing these olivine crystals was injected with a more primitive magma. Both cores and rims on these olivines have higher forsterite values than either cores or rims on the rest of the olivine population.

Plagioclase populations 1 and 2 are both representative of a highly primitive magma, while plagioclase population 3 represents a highly developed magma (Figure 30). The zoning profiles of the two zoned crystals in population 2 represent a sharp decrease in the anorthite content of the surrounding liquid, consistent with a thrusting into more developed surroundings.

The presence of both normally and reversely zoned olivine diffusion rims indicates that both normal and reverse zoning must have happened near-simultaneously. Figures 56-62 illustrate two possible scenarios. Both involve magma chambers with forsterite contents (Mg#) of 90, 80, and 60 from deepest to shallowest. The first scenario involves the three olivine populations crystallizing in the Fo80 chamber and forming Fo80 cores. An injection of the Fo90 magma forces populations 1 and 3 upward into the Fo60 magma chamber. There, some olivines are transferred to the felsic magma and form the population 3 Fo60 diffusion rims. Others remain in the injecting Fo80 magma, which is mixed with the felsic host magma to form an intermediate Fo70 component, forming the population 1 rims. Meanwhile, the Fo90 injection into the Fo80 chamber forms an intermediate Fo85 magma. The olivines diffuse and equilibrate with this magma, forming the population 2 Fo85 cores. A second Fo90 injection causes rapid eruption and creates the reversely zoned rims of population 2. This hypothetical scenario addresses the slight difference in rim thickness between the normally zoned and reversely zoned olivine populations. However, it is unclear why population 2 could equilibrate with the Fo85 magma while populations 1 and 3 formed rims. It is possible that because the Fo85 magma is more mafic and

therefore hotter than the Fo60 magma, diffusion rates are increased. It is also unclear if it is possible for these diffusion rims to be preserved after two injections; one injection is far more likely.

A second possible scenario involves a single injection causing eruption. It begins with the cores of all three populations forming simultaneously in the middle magma chamber. In this scenario, this magma chamber is spatially zoned, with Mg# 80 toward the top forming the population 1 and 3 cores, and Mg# 85 toward the base forming the population 2 cores. An injection of the Fo90 component forces the population 1 and 3 cores upward into the Fo60 magma chamber from below. Populations 1 and 3 form rims in the same way as presented in the first scenario. Meanwhile, population 2 forms Fo90 rims. Eruption soon follows and all components are erupted. This hypothesis allows for simultaneous formation of rims. The required speed of eruption supports the idea that this is one injection. In addition, a single pulse of magma will likely self-mix en route to the surface. Therefore, the second scenario is the more probable illustration of the Park Butte magma journey.

Regardless of the scenario, evidence suggests that the eruption event was caused by a mafic injection, which is likely to have caused exsolution of gasses due to depressurization and increased temperature (Figure 62).

No quartz was found in the PB2 glomerocryst. The initial hypothesis was that this, too, was country rock, but the small crystal size is unrealistic for plutonic rocks. The olivine cores within this glomerocryst have the same composition as those in PB3. In addition, the glomerocryst contains high-anorthite plagioclase. Based on this evidence, the glomerocryst is more likely to contain antecrysts of assimilated cumulates, likely sourced from either the mafic base of the middle chamber, or from the lower chamber.

Mount Baker lavas travel through accreted terranes on the way to the surface. The presence of quartz and potassium feldspar in the PB4 glomerocrysts, the differing matrix texture, the presence of reaction rims, and the strikingly low anorthite content relative to other analysis points confirms that these are xenocrysts. They were likely plucked off the magma chamber walls during eruption. However, the narrative is complicated by the apparent increased quantity of glass in these glomerocrysts. While it is possible for the glomerocryst itself to melt upon introduction into the host magma, it is unlikely in this case due to the absence of reaction rims around the glass itself. A potential hypothesis is that the glomerocrysts are a mixture of mingled magma and country rock cumulates. This interpretation makes sense, as the presence of glass implies that any magma mingled into the country rock was erupted rapidly, without significantly altering the composition of this assimilated rock.

Lake Shannon

The high number of discrete mineral populations within the Lake Shannon flow indicates a high degree of magma interaction. The simplest way to conceptualize this degree of interaction is to imagine a dominant magmatic body rising through the crust on its way to the surface and interacting with its surroundings along its way. Some magmas en route to the surface may stall rather than erupting. When this happens, it may take thousands to tens of thousands of years for the stalled magma body to solidify. These crystal mushes and/or liquids will influence other magma bodies passing through them on the way to eruption, like the Lake Shannon flow.

Escobar (2016) associated crystal populations with different cumulate mushes in a similar fashion to this study in the following discussion.

Population 1 is by far the dominant plagioclase population. Because these crystals are for the most part unzoned, they likely represent the bulk portion of the magma body which did not interact with the surrounding crystal mushes. The two normally zoned crystals within this population are LS2_plag4 and LS6_plag1. LS2_plag4, which does not show disequilibrium textures, likely represents fractional crystallization within the dominant rising magma. LS6_plag1, meanwhile, is too dramatically zoned for this assumption. It also contains evidence for formation of a reaction rim just prior to developing a zone of highly increased anorthite content, and formation of disequilibrium fractures just after developing this zone.

The plagioclase crystals which from core-to-rim show a jump upward anorthite content followed by a decrease to initial conditions (ie; those in LS6), or those which show a decreased anorthite content followed by an increase to initial conditions (eg; LS5_plag13) could represent incorporation of small enclaves of magma. In the case of the LS6 crystals, this would mean that a small amount of more primitive magma locally interacted with some crystals, but then it was incorporated into the dominant magma body in small enough volumes that the enclave had negligible effect on the resulting mixed composition.

Populations 2, 3, and 4 all contain points of significantly lower anorthite contents (An46-61) compared to the dominant magma body represented by population 1. The presence of this decreased anorthite content across three populations represents a larger component than could be accounted for through mere interaction with a sill. Therefore, the study proposes that there is a felsic component mingled with the dominant magma. Furthermore, this felsic component injected the dominant magma.

Though magmatic injection is typically described as a more mafic component injecting a dominant, less mafic component, the reverse is possible. During mafic recharge, more time is allowed for mixing of the two components as the mafic injection pools at the base of the magma reservoir. In contrast, a felsic injection will rise rapidly upward through the host magma, and both components more likely will preserve their initial states (Eichelberger, 2000).

The hypothesis for a felsic injection is strongly supported by the presence of rhyolitic glass in LS6. This rhyolitic glass had to come from a felsic liquid. Because the Lake Shannon samples are still basalt or basaltic andesite (with the exception of LS6), the dominant magma body must have been mafic. Furthermore, LS6 has a holohyaline matrix, indicating rapid quenching to glass. It is unclear why the rhyolitic glass has a petrographic resemblance to basaltic glass (Figure 64)

A felsic injection just prior to eruption is supported by the core-to-rim traverses of crystals containing these decreased anorthite contents. Most show a constant, low anorthite content in the core, consistent with crystallization within a felsic magma reservoir. Then, around 80% of the distance from core to rim, there is a sharp increase upward in magma content followed by a decrease back to initial, felsic conditions. This could be achieved as the felsic magma travels through the dominant mafic magma and the crystals interact with this mafic magma temporarily during mingling processes, but they ultimately are reincorporated into the felsic magma which mingles without changing its composition. These crystals remain in the felsic magma as they are

erupted onto the surface. Some crystals may have stayed behind to form reversely zoned rims, while others may have remained deep in the felsic magma, resulting in unzoned felsic crystals (evidence for both is seen in the data).

Following this narrative, plagioclase population 2 represents those crystals which formed within the felsic magma. Population 3 represents crystals which formed in the mafic magma, but then interacted with the felsic magma prior to eruption. Finally, population 4 has anomalously high anorthite contents, higher than even the extreme end of population 1 crystals. The crystal belonging to population 4 shows a sharp change in composition from ~An90 to ~An58, and it is surrounded by rhyolitic glass. This crystal is assumed to have been assimilated by the felsic magma as it traveled through a highly mafic sill. It is most likely that the low-anorthite rims on these crystals shielded the high-anorthite cores from dissolution during later stages.

LS5_plag13 displays an extreme jump upward in anorthite content at 99% crystallization. This jump most likely indicates a mafic injection needed to cause the eruption of the two mingling magma bodies. The composition of this injection is approximately equivalent to the composition of the dominant unzoned plagioclase population, indicating probability of the same mafic source. It is possible that the felsic magma injected the mafic magma and some gasses exsolved due to the decreased pressure from rising and increased temperature from contact with the mafic magma, and this caused eruption. However, the extreme severity, as well as the last-minute timing, of this increase in LS5_plag13 indicates that it is more likely that this final injection caused the degree of gas exsolution necessary for eruption to occur.

LS5 and LS6 are the only two samples to not have any observed plagioclase with sieved cores; they are also the only two samples to contain the low-anorthite plagioclase. This indicates that the low-anorthite plagioclase remained in equilibrium with its surroundings, which is supportive of a felsic magma component.

The three matrix types in LS5 are likely to be mingled magmas. This is supported by the presence of reverse zoning within several LS5 plagioclase crystals, which was not observed in any other sample. In addition, the plagioclase crystals of LS5 display a wide variety of zoning types: normal zoning, reverse zoning, step zoning, and progressive zoning, indicating a complex history of open-system processes easily involving at least three magmas. The red sections of LS5 are exclusively glomerocrysts, which likely indicates that the red sections are crystal cumulates.

Zoned olivines have an intermediate value between core and rim forsterite content approximately equal to the forsterite contents of the unzoned crystals. This likely indicates all olivines are part of the same original population, and while most had time to equilibrate prior to eruption (this is to be expected given the rapid equilibration rate for olivines in particular), some did not. Those olivines that did not equilibrate must have been incorporated just prior to eruption. This evidence supports a mafic pulse just prior to eruption. The initial, dominant mafic magma source provided most of the olivine crystals, which had time to equilibrate. The second pulse could have ejected olivine cumulates from the bottom of its magma chamber into the new magma, with the higher temperature and possible decrease in pressure causing exsolution of gasses and subsequent eruption.

Figures 65-70 show a schematic illustration of the proposed magmatic interactions of the Lake Shannon flow.

CONCLUSION

Both the Lake Shannon and Park Butte flows show evidence of disequilibrium textures. Much more data is necessary to tell the whole story for both the Park Butte and Lake Shannon flows. Whole rock data for LS5 would provide equilibrium states of phenocrysts; core-to-rim traverses for a greater number of analyzed crystals would illustrate more cohesive properties as opposed to simply exposing anamolous anorthite contents. The tale of Mount Baker phenocrysts is very complex and there is much room for investigation in the context of this study.

REFERENCES

Eichelberger, JC, Izbekov, PE, 2000, Eruption of andesite triggered by dyke injection: contrasting cases at Karymsky Volcano, Kamchatka and Mt. Katmai, Alaska, Philosophical Transactions of the Royal Society A, 358, 1465-1485.

Hildreth, W, 2007, Quaternary Magmatism in the Cascades: Geologic perspectives: US Geological Survey, No. 1744.

Hildreth, W, Fierstein, J, Lanphere, M, 2003, Eruptive history and geochronology of the Mount Baker volcanic field, Washington: GSA Bulletin volume 115.6:729-764.

Le Maitre R. W., Bateman P., Dudek A., Keller J., Lameyre Le Bas M.J., Sabine P.A., Schmid R., Sorensen H., Streckeisen A., Woolley A.R., and Zanetti B., 1989, A classification of igneous rocks and glossary of terms. Blackwell, Oxford.

Moore, NE, DeBari, S, 2012, Mafic magmas from Mount Baker in the northern Cascade arc, Washington: probes into mantle and crustal processes: Contributions to Mineralogy and Petrology 163:521-546.

Murphy, JB, 2007, Igneous Rock Assocation 7. Arc Magmatism 1: Relationships between subduction and magma genesis, Geoscience Canada, v.33, no.4.

Kent, A.J.R., Darr, C., Koleszar, A.M., Salisbury, M.J., and Cooper, K.M., 2010, Preferential eruption of andesitic magmas through recharge filtering: Nature Geoscience, v. 3, p. 631-636.

Sisson, T.W. & Grove, T.L. Experimental investigations of the role of H2O in calc-alkaline differentiation and subduction zone magmatism, Contr. Mineral. and Petrol. (1993) 113: 143.

Streck MJ, 2008, Mineral Textures and Zoning as Evidence for Open System Processes: Reviews in Mineralogy & Geochemistry 69:595-622.

Tabor, R.W., Haugerud, R.A., Hildreth, W., and Brown, E.H., 2003, Geologic map of the Mount Baker 30 x 60 minute quadrangle, Washington: U.S. Geological Survey Map I2660, scale 1:100,000.

Winter, JD, 2000, Principles of Igneous and Metamorphic Petrology, Pearson Prentice Hall.

APPENDIX

PARK BUTTE

Table 1. Olivine compositions

Sample	Na2O	MgO	Al2O3	SiO2	K2O	CaO	TiO2	Cr2O3	FeO	Total	Fo	Type	Location
PB2_ol1_1	0.26	44.13	0.27	41.43	0.22	0.45	0.55	0.6	12.09	100	86.68	mph	core
PB2_ol1_2	0.27	43.97	0.29	41.44	0.09	0.22	0.3	0.64	12.79	100	85.97	mph	middle
PB2_ol1_3	0.33	46.81	0	42.18	0.14	0.16	0.14	0	10.25	100	89.06	mph	middle
PB2_ol1_4	0.21	25.51	2.45	42.55	0	0	0.14	0	29.13	100	60.95	mph	rim
PB2_ol2_1	0.25	47.38	0.12	42.45	0.21	0.45	0.47	0.51	8.16	100	91.19	mph	core
PB2_ol2_2	0.5	46.58	0	42.33	0	0	0	0	10.59	100	88.69	mph	middle
PB3_ol1_1	0.24	44.08	0	41.32	0.24	0.45	0.46	0.29	12.92	100	85.88	ph	core
PB3_ol1_2	0.25	44.42	0	41.05	0.06	0.27	0.28	0.21	13.45	100	85.48	ph	middle
PB3_ol1_3	0.34	43.62	0.11	41.36	0.17	0.29	0.2	0.31	13.59	100	85.12	ph	middle
PB3_ol1_4	0.21	43.17	0.18	41.22	0.15	0.28	0.26	0.21	14.31	100	84.32	ph	middle
PB3_ol1_5	0.35	48.55	0	41.78	0.18	0.33	0.48	0.4	7.92	100	91.62	ph	rim
PB3_ol1_6	0.38	47.24	0	41.71	0.15	0.43	0.28	0.47	9.35	100	90.01	ph	rim
PB3_ol2_1	0.34	41.11	0.17	40.55	0.19	0.49	0.41	0.5	16.24	100	81.86	ph	middle
PB3_ol2_2	0.08	41.32	0.17	40.88	0.24	0.36	0.36	0.36	16.22	100	81.95	ph	middle
PB3_ol2_3	0.32	41.31	0	41.28	0	0.31	0.42	0.36	16	100	82.15	ph	middle
PB3_ol2_4	0.32	45.04	0.52	42.39	0.21	0.26	0.18	0	11.08	100	87.87	ph	rim
PB3_ol3_1	0.47	43.4	0	41.86	0.19	0.21	0.29	0.32	13.27	100	85.36	mph	core
PB3_ol3_2	0.22	43.13	0.27	41.59	0.12	0.38	0.15	0	14.13	100	84.47	mph	middle
PB3_ol3_3	0.25	43.38	0.08	41.28	0.18	0.23	0.45	0.64	13.51	100	85.13	mph	middle
PB3_ol3_4	0.48	45.07	0.11	41.11	0.18	0.43	0.35	0.3	11.96	100	87.04	mph	middle
PB3_ol3_5	0.46	47.48	0.41	41.74	0.24	0.34	0.67	0.67	8	100	91.36	mph	rim
PB3_ol4	0.32	47.28	0.37	42.32	0.24	0.08	0.2	0.23	8.95	100	90.40	ph	core
PB3_ol5_1	0.33	41.48	0.2	40.14	0	0.44	0.48	0.47	16.46	100	81.79	ph	core
PB3_ol5_2	0.29	41.93	0.24	40.1	0.22	0.39	0.24	0.55	16.03	100	82.34	ph	middle
PB3_ol6_1	0.38	49.06	0	42.32	0	0.27	0	0.13	7.83	100	91.78	mph	middle
PB3_ol6_2	0.17	49.55	0.2	42.84	0.09	0.27	0.26	0.18	6.43	100	93.21	mph	rim
PB4-NV_ol1_1	0.21	41.1	0.08	41.64	0	0.09	0	0	16.88	100	81.27	ph	core
PB4-NV_ol1_2	0.09	41.34	0	40.52	0.05	0.35	0.37	0.41	16.86	100	81.38	ph	middle
PB4-NV_ol1_3	0.36	41.31	0	41.72	0.07	0.22	0.36	0.28	15.68	100	82.44	ph	middle
PB4-NV_ol1_4	0.44	36.55	0	39.2	0	0.33	0.35	0.57	22.56	100	74.28	ph	middle
PB4-NV_ol1_5	0.43	29.84	0	38.83	0	0.15	0	0	30.75	100	63.37	ph	rim
PB4-NV_ol2_1	0.47	38.2	0	39.39	0.2	0.32	0.33	0.43	20.66	100	76.72	mph	core
PB4-NV_ol2_2	0.24	35.3	0	39.36	0.2	0.35	0.33	0.39	23.83	100	72.53	mph	middle
PB4-NV_ol2_3	0.12	33.06	0	39.45	0	0.2	0.41	0.42	26.33	100	69.12	mph	rim
PB4-NV_ol3_1	0.31	38.57	0	35.28	0.1	0	0.12	0.19	25.43	100	73.00	ph	core
PB4-NV_ol3_2	0.29	36.16	0	33.24	0.08	0.36	0	0	29.86	100	68.34	ph	middle
PB4-V_ol1_1	0.37	39.75	0	40.53	0.17	0.42	0.3	0.5	17.97	100	79.77	mph	core
PB4-Vol1_2	0.17	40.56	0	40.67	0.14	0.09	0	0.11	18.27	100	79.83	mph	middle
PB4-Vol1_3	0.35	39.89	0	40.58	0.05	0.25	0.23	0.12	18.53	100	79.33	mph	rim
PB4-V_ol2	0.26	37.33	0.21	39.76	0.23	0.27	0.46	0.48	21	100	76.01	ma	core
PB4-V_ol3	0.17	35.52	0.09	40.84	0	0.26	0.23	0	22.9	100	73.44	ma	core
PB4-V_ol4_1	0.24	38.84	0.1	40	0.2	0.32	0.52	0.53	19.24	100	78.25	ph	core

PB4-V_ol4_2	0.32	36.79	0.26	39.91	0.13	0.24	0	0.32	22.03	100	74.85	ph	middle
PB4-V_ol4_3	0.12	35.55	0	39.86	0.18	0.5	0.46	0.12	23.2	100	73.20	ph	middle
PB4-V_ol4_4	0.2	34.31	0	39.28	0.12	0.33	0.29	0.49	24.99	100	70.99	ph	rim
PB4-V_ol5	0.35	34.43	0	39.25	0.07	0.31	0.45	0.61	24.54	100	71.44	mph	core
PB4-V_ol6_1	0.37	41.74	0	40.9	0.24	0.31	0.34	0.52	15.58	100	82.69	ph	core
PB4-V_ol6_2	0.33	40.91	0.26	40.69	0	0.14	0	0	17.67	100	80.50	ph	middle
PB4-V_ol6_3	0.24	38.57	0.22	40.54	0.1	0.44	0.17	0.47	19.26	100	78.12	ph	middle
PB4-V_ol6_4	0.32	38.19	0.11	40.99	0.09	0.24	0	0.22	19.84	100	77.43	ph	middle
PB4-V_ol6_5	0.38	37.43	0	39.16	0	0.27	0.12	0.59	22.05	100	75.16	ph	rim
PB4-V_ol7_1	0.3	36.22	0.17	40.18	0	0.16	0	0	22.97	100	73.76	ph	core
PB4-V_ol7_2	0.23	34.62	0.27	39.58	0.25	0.34	0.66	0.55	23.5	100	72.42	ph	middle
PB4-V_ol7_3	0.26	34.21	0	38.85	0.2	0.4	0.48	0.44	25.16	100	70.79	ph	middle
PB4-V_ol7_4	0.26	32.43	0.1	38.98	0.28	0.23	0.44	0	27.28	100	67.94	ph	rim
PB4-V_ol8_1	0.16	40.83	0	41.1	0.18	0.33	0.34	0.41	16.66	100	81.37	ph	core
PB4-V_ol8_2	0.24	41.76	0	41.08	0.21	0.33	0.26	0.3	15.82	100	82.47	ph	middle
PB4-V_ol8_3	0.28	38.17	0.11	39.92	0.08	0.44	0.33	0.75	19.93	100	77.34	ph	middle
PB4-V_ol8_4	0.33	35.63	0	38.66	0.17	0.25	0.35	0.26	24.35	100	72.29	ph	middle
PB4-V_ol8_5	0.37	34.4	0	39.4	0.2	0.39	0.31	0.39	24.54	100	71.42	ph	rim
PB4_ol9	0.29	40.44	0	40.36	0.18	0.32	0.29	0.32	17.8	100	80.20	ph	middle
PB4_ol10	0.15	39.72	0.12	40.48	0.23	0.37	0.38	0.72	17.83	100	79.88	ph	middle
PB4_ol11	0.15	40.93	0	41.09	0.13	0.27	0.35	0.61	16.48	100	81.57	ph	middle
PB4-V_ol12_1	0.35	39.06	0.2	40.42	0.1	0.26	0.27	0.29	19.04	100	78.53	ph	core
PB4-V_ol12_2	0.32	39.18	0.21	39.68	0.2	0.34	0.29	0.45	19.32	100	78.33	ph	middle
PB4-V_ol12_3	0.34	36.95	0	39.15	0.2	0.5	0.46	0.48	21.94	100	75.01	ph	middle
PB4-V_ol12_4	0.37	32.73	0.22	39.33	0	0.31	0.31	0.2	26.53	100	68.74	ph	rim
PB4-mix_ol1_1	0.3	41.63	0.08	40.62	0.11	0.38	0.36	0.09	16.42	100	81.88	ph	core
PB4-mix_ol1_2	0.34	41.88	0	40.85	0.1	0.46	0.28	0.18	15.89	100	82.45	ph	middle
PB4-mix_ol1_3	0.14	34.73	0.37	40.24	0.15	0.27	0	0	24.1	100	71.98	ph	rim
PB4-mix_ol2_1	0.43	40.75	0	41.03	0	0.26	0.4	0.44	16.69	100	81.32	ph	core
PB4-mix_ol2_2	0.28	40.45	0.11	40.65	0.11	0.41	0.41	0.6	16.99	100	80.93	ph	middle
PB4-mix_ol2_3	0.25	37.4	0.21	40.72	0.2	0.28	0.33	0.41	20.2	100	76.75	ph	middle
PB4-mix_ol2_4	0.38	34.71	0.12	40.19	0.29	0.35	0.39	0.2	23.38	100	72.58	ph	rim
PB4-mix_ol2_5	0.47	41.35	0.16	40.81	0	0.15	0.25	0.28	16.53	100	81.68	ph	middle
PB7_ol1_1	N/A	41.39	0.13	42.14	N/A	0.36	0.41	0.45	15.12	100	82.99	ph	middle
PB7_ol1_2	N/A	41.16	0.13	42.19	N/A	0.32	0.6	0.63	14.96	100	83.06	ph	middle
PB7_ol1_3	N/A	42.47	0.1	41.54	N/A	0.47	0.38	0.46	14.58	100	83.85	ph	core
PB7_ol1_4	N/A	42.29	0.14	42.3	N/A	0.37	0.37	0.47	14.07	100	84.27	ph	middle
PB7_ol1_5	N/A	42.22	0.1	42.49	N/A	0.38	0.26	0.39	14.16	100	84.16	ph	middle
PB7_ol1_6	N/A	39.57	0.13	40.73	N/A	0.44	0.32	0.56	18.25	100	79.44	ph	middle
PB7_ol1_7	N/A	32.79	0.16	40.16	N/A	0.13	0.12	0.13	26.51	100	68.80	ph	rim
PB7_ol1_8	N/A	32.61	0.25	39.04	N/A	0.46	0.34	0.27	27.03	100	68.26	ph	rim
PB7_ol1_9	N/A	33.28	0	40.43	N/A	0.22	0.11	0.39	25.57	100	69.88	ph	rim
PB7_ol2_1	N/A	40.99	0	41.81	N/A	0.34	0.42	0.63	15.81	100	82.21	ph	core

PB7_ol2_2	N/A	39.19	0.24	41.12	N/A	0.46	0.45	0.66	17.88	100	79.62	ph	middle
PB7_ol2_3	N/A	35.53	0	40.68	N/A	0.62	0.56	0.89	21.73	100	74.45	ph	middle
PB7_ol2_4	N/A	31.83	0	39.67	N/A	0.46	0.38	0.23	27.43	100	67.41	ph	rim
PB7_ol2_5	N/A	31.21	0	39.33	N/A	0.48	0.44	0.16	28.37	100	66.23	ph	rim
PB7_ol3_1	0.22	35.49	0.09	39.21	0.2	0.36	0.58	0	23.84	100	72.63	ph	rim
PB7_ol3_2	0.25	39.45	0	40.18	0	0.32	0.46	0.3	19.04	100	78.69	ph	middle
PB7_ol3_3	0.2	42.07	0.07	40.26	0.22	0.31	0.27	0.24	16.36	100	82.09	ph	core
PB7_ol3_4	0.21	40.92	0	41.09	0.12	0.27	0.13	0.24	17.03	100	81.07	ph	middle
PB7_ol3_5	0	40.25	0.08	41.19	0.08	0.27	0.22	0.37	17.54	100	80.36	ph	rim
PB7_ol3_6	0.24	32.56	0	38.46	0.14	0.39	0.26	0.18	27.78	100	67.63	ph	rim
PB7_ol4_1	0.23	43.43	0	40.63	0	0.29	0.22	0.26	14.95	100	83.81	ph	core
PB7_ol4_2	0.37	43	0.09	40.14	0.19	0.62	0.36	0.52	14.71	100	83.90	ph	middle
PB7_ol4_3	0.5	42.2	0.12	40.08	0.16	0.24	0.16	0.35	16.17	100	82.31	ph	middle
PB7_ol4_4	0.27	38.58	0.2	39.93	0.07	0.39	0.43	0.42	19.72	100	77.72	ph	middle
PB7_ol4_5	0.42	37.24	0.12	39.82	0.13	0.29	0.44	0.32	21.21	100	75.79	ph	rim
PB7_ol4_6	0.19	32.34	0.13	38.29	0	0.41	0.32	0.3	28.03	100	67.28	ph	rim
PB7_ol5	0.18	30.97	0	38.3	0.26	0.33	0.5	0.2	29.27	100	65.35	mph	core
PB7_ol6_1	0.41	43.06	0.09	40.85	0.06	0.32	0.21	0.43	14.57	100	84.05	ph	core
PB7_ol6_2	0.32	42.99	0	41.04	0.09	0.29	0.52	0.43	14.31	100	84.26	ph	middle
PB7_ol6_3	0.29	37.92	0.23	39.41	0.14	0.26	0.27	0.37	21.11	100	76.20	ph	middle
PB7_ol6_4	0.35	33.22	0.25	38.85	0.22	0.35	0.33	0.17	26.26	100	69.28	ph	rim
PB7_ol6_5	0.24	40.33	0.11	40.22	0	0.25	0.24	0.32	18.29	100	79.72	ph	rim
PB7_ol6_6	0.12	37.36	0.41	39.43	0.12	0.21	0.4	0.62	21.33	100	75.74	ph	rim
PB7_ol7	N/A	24.79	0	38.17	N/A	0.45	0.1	0.26	36.23	100	54.95	ph	rim
PB7_ol8_1	N/A	23.31	0.18	37.2	N/A	0.31	0.44	0.47	38.09	100	52.17	ph	rim
PB7_ol8_2	N/A	23.53	0.14	37.14	N/A	0.21	0.72	0.21	38.05	100	52.43	ph	middle
PB7_ol9_1	N/A	39.69	0	41.45	N/A	0.25	0.12	0.26	18.23	100	79.51	ph	core
PB7_ol9_2	N/A	38.85	0	40.88	N/A	0.37	0.42	0.44	19.04	100	78.44	ph	middle
PB7_ol9_3	N/A	40.51	0	41.94	N/A	0.16	0	0	17.39	100	80.59	ph	middle
PB7_ol9_4	N/A	34.51	0.17	39.78	N/A	0.28	0.29	0.23	24.74	100	71.32	ph	middle
PB7_ol9_5	N/A	30.3	0.45	38.99	N/A	0.26	0.42	0.42	29.17	100	64.93	ph	rim
PB7_ol10_1	N/A	41.65	0.17	42.06	N/A	0.47	0.2	0.28	15.17	100	83.03	ph	core
PB7_ol10_2	N/A	40.97	0	42.46	N/A	0.33	0.28	0.47	15.49	100	82.50	ph	middle
PB7_ol10_3	N/A	39.38	0	41.11	N/A	0.5	0.44	0.65	17.93	100	79.65	ph	middle
PB7_ol10_4	N/A	35.71	0.25	40.03	N/A	0.5	0.47	0.45	22.58	100	73.82	ph	middle
PB7_ol10_5	N/A	31.08	0	40.45	N/A	0.26	0	0.27	27.95	100	66.47	ph	rim
PB7_ol11_1	N/A	39.5	0	41.33	N/A	0.32	0.42	0.57	17.85	100	79.78	ph	core
PB7_ol11_2	N/A	38.26	0.18	40.57	N/A	0.12	0	0.27	20.6	100	76.80	ph	middle
PB7_ol11_3	N/A	35.14	0.11	40.1	N/A	0.36	0.33	0.35	23.6	100	72.63	ph	middle
PB7_ol11_4	N/A	32.95	0	39.12	N/A	0.5	0.4	0.4	26.62	100	68.81	ph	rim
PB7_ol11_5	N/A	32.81	0.11	39.68	N/A	0.17	0	0.32	26.9	100	68.50	ph	rim

Fo – forsterite content. Grain types are: ph – phenocryst, mph – microphenocryst, ma – matrix, incl – inclusion. If incl is preceeded by a mineral abbreviation (e.g.; plag incl), then the grain is an inclusion in that mineral (e.g.; inclusion in plagioclase). For details on classification, see Methods section. Light blue fill = less-vesicular blue component (PB4-NV). Light red fill = vesicular red component (PB4-V). "PB4-mix" = matrix is too well mingled to distinguish between components. *Italics* = glomerocrysts with reaction rims (e.g.; Figure 13).

Table 2. Clinopyroxene compositions

Sample	Na2O	MgO	Al2O3	SiO2	K2O	CaO	TiO2	Cr2O3	FeO	Total	Mg#	Type	Location
PB3_cpx1	0.35	16.46	1.4	54.78	0.06	15.1	0.66	0.43	10.76	100	73.16743	ol rim	middle
PB3_cpx2	0.66	12.78	2.73	50.98	0.26	18.49	2.63	0.53	10.94	100	67.55711	ol incl	middle
PB3_cpx3	0.7	12.21	2.18	51.39	0.22	15.77	2.45	0.82	14.26	100	60.4161	ol rim	middle
PB3_cpx4	0.74	13.79	2.32	51.93	0.13	17.35	2.21	0.74	10.78	100	69.51457	ol rim	middle
PB4-NV_cpx1	*0.46*	*18*	*0.89*	*54.38*	*0.17*	*7.75*	*0.8*	*0.11*	*17.44*	*100*	*64.78591*	*ma*	*core*
PB4-NV_cpx2	*0.47*	*14.93*	*1.15*	*54.49*	*0.1*	*14.48*	*1.21*	*0.36*	*12.82*	*100*	*67.48936*	*ma*	*core*
PB4-NV_cpx3	*0.18*	*20.06*	*0.56*	*54.53*	*0.13*	*4.2*	*0.89*	*0*	*19.43*	*100*	*64.79285*	*mph*	*middle*
PB4-NV_cpx4	*0.46*	*17.64*	*0.56*	*54.65*	*0.13*	*6.05*	*0.85*	*0.62*	*19.04*	*100*	*62.28502*	*mph*	*middle*
PB4-NV_cpx5	0.62	13.79	3.67	51.55	0.23	17.19	1.71	0.43	10.81	100	69.45565	ol rim	middle
PB4-NV_cpx6	*0.79*	*14.49*	*1.4*	*45.3*	*0.22*	*16.76*	*1*	*0*	*20.04*	*100*	*56.3103*	*mph*	*core*
PB4-V_cpx1	0.3	22.89	0.41	55.22	0.23	3.38	0.86	0.35	16.37	100	71.36721	ol rim	middle
PB7_cpx1	N/A	15.04	1.32	54.75	N/A	17.93	0.88	0.82	9.24	100	74.36845	ol rim	middle
PB7_cpx2_1	N/A	14.63	2.16	54.57	N/A	18.84	0.85	0.51	8.45	100	75.52745	ol rim	core
PB7_cpx2_2	N/A	12.82	1.95	52.8	N/A	18	1.79	0.2	12.44	100	64.75132	ol rim	middle
PB7_cpx2_3	N/A	14.16	1.12	54.3	N/A	17.84	1.2	0.49	10.89	100	69.85942	ol rim	rim
PB7_cpx3	0.49	16.03	2.51	53.4	0.15	16.82	0.89	0.39	9.31	100	75.425	ol rim	middle
PB7_cpx4_1	0.41	15.33	2.3	53.52	0.29	18.58	0.77	0.16	8.64	100	75.97749	ol rim	middle
PB7_cpx4_2	0.62	13.99	0.64	54.55	0.21	17.08	0.4	0.44	12.08	100	67.36693	ol rim	middle
PB7_cpx4_3	0.41	14.44	0.92	54.16	0.14	18.14	0.6	0.27	10.94	100	70.17432	ol rim	middle
PB7_cpx4_4	0.56	16	2.75	53.85	0.14	18.18	0.62	0.95	6.95	100	80.40629	ol rim	middle
PB7_cpx5	0.34	15.8	1.83	53.56	0.22	17.71	1.31	0.55	8.68	100	76.44124	ol rim	middle
PB7_cpx6_1	N/A	12.86	1.83	52.78	N/A	17.99	1.55	0.15	12.84	100	64.09737	ol rim	rim
PB7_cpx6_2	N/A	13.95	2.11	53.65	N/A	17.93	1.35	0.58	10.43	100	70.45021	ol rim	middle
PB7_cpx7	N/A	13.74	2.2	54.09	N/A	19.08	1.15	0.58	9.15	100	72.80188	ol rim	middle
PB7_cpx8	N/A	13.95	2.17	52.19	N/A	17.69	1.72	0.76	11.51	100	68.35857	ol rim	middle
PB7_cpx9	N/A	14.52	1.32	53.66	N/A	18.12	1.07	0.8	10.51	100	71.12035	ol rim	middle

Abbreviations and colors as in Table 1.

Table 3. Feldspar compositions

Sample	Na2O	MgO	Al2O3	SiO2	K2O	CaO	TiO2	Cr2O3	FeO	Total	An	Type	Location
PB2_plag1	1.95	0.34	30.98	50.54	0.29	14.06	0.43	0.46	0.95	100	88.85055	mph	core
PB2_plag2	3.65	0.48	28.73	53.59	0.32	11.27	0.27	0.61	1.09	100	77.33769	mph	core
PB2_plag3	1.81	0.29	32.67	49.25	0.2	15.33	0	0	0.45	100	90.34837	mph	middle
PB2_plag4_1	2.12	0.31	30.75	51.31	0.3	13.85	0.15	0.27	0.95	100	87.83535	ph	core
PB2_plag4_2	2.48	0.34	30.38	52.19	0.17	12.9	0.26	0.31	0.97	100	85.18304	ph	middle
PB2_plag4_3	2.06	0.3	31.1	51.03	0.18	14.36	0.18	0.12	0.68	100	88.51166	ph	middle
PB2_plag4_4	2.26	0.23	30.94	50.32	0.23	14.86	0	0.53	0.64	100	87.90399	ph	rim
PB2_plag5_1	3.79	0.23	28.12	55.02	0.28	11.23	0.19	0.19	0.95	100	76.60758	mph	core
PB2_plag5_2	3.79	0.38	27.93	53.98	0.29	11.47	0.47	0.59	1.1	100	76.98439	mph	middle
PB2_plag5_3	3.76	0	28.19	55.71	0.09	10.95	0	0.43	0.88	100	76.29609	mph	rim
PB2_plag6_1	2.13	0.34	31.49	49.84	0.08	14.43	0.11	0.49	1.08	100	88.21811	mph	core
PB2_plag6_2	1.97	0.35	31.73	50.07	0.19	14.34	0.33	0	1.01	100	88.94446	mph	middle
PB2_plag6_3	1.96	0.24	31.31	49.31	0.2	15.16	0.38	0.35	1.09	100	89.52735	mph	middle
PB2_plag6_4	4.91	0.26	24.1	59.98	0.44	7.7	0.42	0.48	1.72	100	63.41373	mph	rim
PB3_plag1_1	1.99	0	31.16	49.53	0.36	14.93	0.54	0.29	1.21	100	89.23813	ph	core
PB3_plag1_2	1.83	0.24	32.45	49.4	0.08	14.59	0.13	0.28	0.99	100	89.8081	ph	middle
PB3_plag1_3	2.76	0.49	30.79	52.31	0.16	13.24	0	0	0.24	100	84.13187	ph	middle
PB3_plag1_4	4.43	0.48	26.84	56.03	0.5	9.73	0.35	0.5	1.14	100	70.8245	ph	rim
PB3_plag2_1	2.34	0.37	30.62	50.52	0.2	13.99	0.28	0.5	1.18	100	86.85562	ph	middle
PB3_plag2_2	2.59	0.07	30.99	50.78	0.17	13.54	0.47	0.44	0.96	100	85.24631	ph	middle
PB3_plag2_3	2.1	0.08	31.42	50.26	0.23	13.99	0.38	0.46	1.08	100	88.04256	ph	middle
PB4-NV_plag1	*7.18*	*0.06*	*22.2*	*63.04*	*1.19*	*4.73*	*0.33*	*0.3*	*0.98*	*100*	*42.13307*	*mph*	*core*
PB4-NV_plag2	*7.23*	*0.36*	*21.27*	*64.24*	*1.39*	*4.06*	*0.5*	*0.24*	*0.71*	*100*	*38.2962*	*mph*	*core*
PB4-NV_plag3	*6.74*	*0*	*23.13*	*62.29*	*0.84*	*5.28*	*0.45*	*0.27*	*1*	*100*	*46.4044*	*mph*	*middle*
PB4-NV_plag4	*6.77*	*0.07*	*23.23*	*62.33*	*0.8*	*5.36*	*0.22*	*0.36*	*0.84*	*100*	*46.66805*	*mph*	*middle*
PB4-NV_plag5	*7.04*	*0.15*	*22.66*	*62.08*	*0.9*	*5.39*	*0.6*	*0.39*	*0.79*	*100*	*45.83463*	*mph*	*core*
PB4-NV_plag6	4.42	0.17	28.32	54	0.35	10.8	0.32	0.29	1.32	100	72.97723	ma	middle
PB4-NV_kspar1	*4.2*	*0.21*	*14.87*	*71.09*	*5.99*	*0.65*	*0.51*	*0.65*	*1.82*	*100*	*14.60646*	*ma*	*middle*
PB4-NV_kspar2	*3.74*	*0.13*	*14.75*	*73.26*	*6.45*	*0.15*	*0.58*	*0.16*	*0.78*	*100*	*4.24462*	*ma*	*middle*
PB4-NV_plag7	3.75	0.1	29.26	53.33	0.37	11.5	0.19	0.25	1.24	100	77.21783	ol incl	middle
PB4-NV_kspar3	*7.43*	*0.08*	*20.92*	*64.9*	*1.9*	*3.09*	*0.53*	*0.36*	*0.8*	*100*	*31.49035*	*mph*	*middle*
PB4-NV_kspar4	*7.56*	*0*	*20.41*	*64.63*	*2.55*	*3.07*	*0.49*	*0.31*	*0.97*	*100*	*30.97833*	*mph*	*middle*
PB4-NV_kspar5	*7.48*	*0*	*20.13*	*64.6*	*2.6*	*2.47*	*0.9*	*0.65*	*1.17*	*100*	*26.73805*	*mph*	*middle*
PB4-NV_kspar6	*7.88*	*0*	*20.5*	*64.05*	*1.71*	*4.54*	*0.41*	*0.23*	*0.68*	*100*	*38.90423*	*mph*	*middle*
PB4-NV_plag8	2.45	0.37	30.57	50.93	0.27	13.62	0.37	0.36	1.07	100	86.00268	ph	middle
PB4-NV_plag9	4.07	0.18	28.38	55.2	0.19	10.55	0.19	0.14	1.1	100	74.12631	ph	middle
PB4-NV_kspar7	*3.47*	*0.12*	*13.39*	*74.38*	*5.9*	*0.44*	*0.74*	*0.34*	*1.22*	*100*	*12.2919*	*ma*	*middle*
PB4-NV_plag10	*7.63*	*0.25*	*21.63*	*60.02*	*2.02*	*6.82*	*0.61*	*0.43*	*0.58*	*100*	*49.69582*	*mph*	*core*
PB4-NV_plag11_1	*6.65*	*0.25*	*17.86*	*60.87*	*8.26*	*2.81*	*0.85*	*0.59*	*1.86*	*100*	*31.83486*	*mph*	*core*
PB4-NV_plag11_2	*7.8*	*0.11*	*19.43*	*60.83*	*4.27*	*4.55*	*0.81*	*0.71*	*1.5*	*100*	*39.19947*	*mph*	*middle*
PB4-NV_plag11_3	*7.06*	*0.08*	*19.23*	*61.73*	*5.74*	*3.21*	*0.66*	*0.77*	*1.52*	*100*	*33.4453*	*mph*	*rim*

PB4-NV_plag12	*6.67*	*0.22*	*22.72*	*62.18*	*1.08*	*5.36*	*0.37*	*0.36*	*1.04*	*100*	*47.0386*	*mph*	*core*
PB4-NV_plag13	1.94	0.4	31.75	48.83	0.17	15.26	0.3	0.25	1.08	100	89.68411	mph	middle
PB4-V_plag1	3.28	0.35	29.14	52.31	0.31	12.48	0.41	0.37	1.36	100	80.7888	ol incl	middle
PB4-V_plag2	3.07	0.18	29.3	51.86	0.29	13.02	0.24	0.53	1.51	100	82.41716	mph	core
PB4-V_plag3_1	2.47	0.19	31.27	49.76	0.36	13.85	0.47	0.67	0.97	100	86.10607	ph	middle
PB4-V_plag3_2	2.46	0.21	30.64	50.01	0.33	14.18	0.49	0.42	1.26	100	86.43304	ph	middle
PB4-V_plag3_3	2.33	0.45	32.17	49.81	0.19	14.75	0.18	0.12	0	100	87.49481	ph	middle
PB4-mix_plag1	4.5	0.21	27.35	55.34	0.42	10.37	0.35	0.24	1.22	100	71.80685	ol incl	middle
PB4-mix_plag2	3.49	0.25	28.88	53.09	0.15	12.13	0.3	0.29	1.41	100	79.34489	ol incl	core
PB7_plag1	4.13	0.18	28.36	55.02	0.15	10.58	0	0.23	1.35	100	73.89945	ol incl	middle
PB7_plag2	4.39	1.54	24.5	57.59	0.62	8.59	0.82	0	1.94	100	68.38087	ol incl	core

Kspar = potassium feldspar. All other abbreviations, colors as in Table 1.

Table 5. Orthopyroxene compositions

Sample	Na2O	MgO	Al2O3	SiO2	K2O	CaO	TiO2	Cr2O3	FeO	Total	Mg#	Type	Location
PB2_opx1	0.16	25.14	2.91	41.01	0.17	0.41	0.3	0	29.89	100	59.98818	ol rim	middle
PB3_opx1	0.26	22.1	1.83	39.51	0.36	0.57	0.9	1.56	32.91	100	54.48386	ol incl	core
PB3_opx2	0.45	24.5	0.12	41.26	0.3	0.6	0.45	0.65	31.69	100	57.94969	ol incl	core
PB3_opx3	0.28	31.17	0.61	57.52	0.22	0.75	0.61	0.63	8.21	100	87.12593	ol rim	middle
PB3_opx4	0.24	26.6	0.15	40.75	0.14	0.37	0.39	0.18	31.19	100	60.32081	ol incl	core
PB4-NV_opx1	*0.33*	*17.75*	*0.17*	*44.61*	*0.16*	*1.95*	*0.22*	*0.53*	*34.28*	*100*	*47.99757*	*mph*	*middle*
PB4-NV_opx2	*0.13*	*17.88*	*0.38*	*53.32*	*0.22*	*1.16*	*0.74*	*0.47*	*25.7*	*100*	*55.36003*	*ma*	*middle*
PB4_opx1	0.09	20.97	0	39.96	0	0.23	0.16	0	38.59	100	49.20347	ol rim	middle
PB4_opx2	0.56	18.91	0.15	38.31	0.13	0.96	0.89	0.56	39.53	100	46.02509	ol rim	middle
PB4_opx3	0.34	19.32	0.2	38.73	0	0.31	0.47	0.3	40.33	100	46.06023	ol incl	middle
PB4_opx4	0.52	28.38	0.96	56.46	0.18	0.68	0.42	0.31	12.1	100	80.69817	ma	middle
PB4_opx5	0.22	29.26	1.21	55.56	0.16	0.62	0.31	0.47	12.2	100	81.04323	ma	core
PB4_opx6	0.3	20.19	0.71	54.96	0.26	3.93	0.93	0.15	18.58	100	65.9516	ol rim	middle
PB7_opx1_1	0.26	26.96	0.36	56.36	0.1	1.2	0.59	0.19	13.97	100	77.4776	ol rim	middle
PB7_opx1_2	0.47	27.19	0.42	55.68	0.14	1.39	0.67	0.25	13.8	100	77.83742	ol rim	middle
PB7_opx2	0.24	18.37	0.66	54.49	0	1.85	0.39	0.29	23.7	100	58.01235	ol rim	middle

All abbreviations and colors as in Table 1.

LAKE SHANNON

Table 6. Olivine compositions

Sample	Na2O	MgO	Al2O3	SiO2	K2O	CaO	TiO2	Cr2O3	FeO	Total	Fo	Type	Location
LS1-NV_ol1_1	0.37	41.01	0.19	41.52	0.00	0.31	0.32	0.34	15.94	100.00	82.10	ph	core
LS1-NV_ol1_2	0.46	40.52	0.00	41.99	0.15	0.21	0.00	0.37	16.31	100.00	81.58	ph	middle
LS1-NV_ol1_3	0.20	40.69	0.00	42.38	0.00	0.21	0.00	0.00	16.52	100.00	81.45	ph	middle
LS1-NV_ol1_4	0.31	40.19	0.00	41.56	0.10	0.37	0.24	0.32	16.93	100.00	80.89	ph	middle
LS1-NV_ol1_5	0.51	41.26	0.00	41.05	0.10	0.41	0.19	0.66	15.81	100.00	82.31	ph	rim
LS1-NV_ol2_1	0.23	42.90	0.12	42.30	0.00	0.25	0.00	0.31	13.89	100.00	84.63	mph	core
LS1-NV_ol2_2	0.34	43.23	0.23	42.83	0.11	0.14	0.00	0.00	13.11	100.00	85.46	mph	middle
LS1-NV_ol2_3	0.38	41.21	0.14	40.77	0.00	0.38	0.71	0.75	15.65	100.00	82.44	mph	middle
LS1-NV_ol2_4	0.22	38.47	0.00	40.85	0.22	0.32	0.34	0.62	18.96	100.00	78.34	mph	rim
LS1-NV_ol2_5	0.29	36.82	0.37	40.78	0.00	0.24	0.00	0.00	21.50	100.00	75.33	mph	rim
LS1-NV_ol2_6	0.30	38.15	0.17	40.59	0.00	0.35	0.36	0.31	19.77	100.00	77.48	mph	rim
LS1-NV_ol3_1	0.25	40.31	0.22	40.84	0.00	0.34	0.00	0.19	17.86	100.00	80.09	ma	core
LS1-NV_ol3_2	0.30	38.30	0.00	41.00	0.00	0.37	0.21	0.34	19.48	100.00	77.80	ma	rim
LS1-NV_ol4_1	0.46	39.62	0.00	41.59	0.08	0.27	0.32	0.22	17.45	100.00	80.19	mph	core
LS1-NV_ol4_2	0.32	40.08	0.26	41.48	0.28	0.43	0.28	0.34	16.53	100.00	81.21	mph	middle
LS1-NV_ol4_3	0.30	40.03	0.09	41.13	0.20	0.30	0.54	0.38	17.03	100.00	80.73	mph	rim
LS1-NV_ol5	0.32	36.60	0.42	41.07	0.00	0.32	0.00	0.00	21.27	100.00	75.41	plag incl	middle
LS1-NV_ol6_1	0.26	40.60	0.21	40.81	0.25	0.30	0.37	0.44	16.76	100.00	81.20	mph	core
LS1-NV_ol6_2	0.33	40.10	0.00	40.75	0.10	0.45	0.40	0.47	17.38	100.00	80.44	mph	middle
LS1-NV_ol6_3	0.29	39.68	0.00	40.86	0.26	0.53	0.42	0.69	17.26	100.00	80.38	mph	rim
LS1-NV_ol7_1	0.30	40.30	0.00	40.90	0.18	0.42	0.46	0.52	16.92	100.00	80.94	mph	core
LS1-NV_ol7_2	0.43	40.84	0.19	41.25	0.00	0.36	0.00	0.00	16.93	100.00	81.13	mph	rim
LS1-NV_ol8_1	0.21	40.58	0.24	40.65	0.13	0.64	0.56	0.52	16.47	100.00	81.45	mph	core
LS1-NV_ol8_2	0.58	40.91	0.30	41.60	0.08	0.25	0.00	0.00	16.28	100.00	81.75	mph	middle
LS1-NV_ol8_3	0.22	39.63	0.00	41.22	0.29	0.38	0.36	0.33	17.57	100.00	80.08	mph	rim
LS1-V_ol1_1	0.33	40.95	0.25	41.54	0.23	0.42	0.60	0.00	15.68	100.00	82.32	mph	core
LS1-V_ol1_2	0.31	40.52	0.00	41.91	0.12	0.23	0.25	0.22	16.44	100.00	81.46	mph	rim
LS1-V_ol2	0.24	40.95	0.19	40.72	0.24	0.52	0.49	0.21	16.44	100.00	81.62	mph	core
LS1-V_ol3	0.23	41.36	0.14	41.30	0.00	0.25	0.25	0.31	16.17	100.00	82.01	mph	core
LS1-V_ol4	0.38	41.17	0.25	40.90	0.19	0.50	0.23	0.16	16.21	100.00	81.91	mph	core
LS1-V_ol1	0.26	43.16	0.00	42.30	0.00	0.00	0.00	0.00	14.27	100.00	84.35	mph	core
LS1-V_ol2	0.34	41.91	0.13	41.67	0.00	0.13	0.00	0.25	15.56	100.00	82.76	mph	core
LS1-V_ol3	0.44	41.33	0.08	41.60	0.07	0.54	0.11	0.38	15.44	100.00	82.67	mph	core
LS1-V_ol4_1	0.24	41.38	0.24	40.64	0.09	0.24	0.00	0.31	16.86	100.00	81.40	mph	core
LS1-V_ol4_2	0.34	41.16	0.48	41.25	0.28	0.39	0.00	0.42	15.68	100.00	82.39	mph	middle
LS1-V_ol4_3	0.11	38.87	0.13	41.26	0.00	0.32	0.00	0.00	19.31	100.00	78.20	mph	rim
LS1-V_ol5_1	0.23	42.99	0.11	42.27	0.13	0.21	0.00	0.11	13.93	100.00	84.62	mph	core
LS1-V_ol5_2	0.10	42.87	0.00	41.90	0.23	0.46	0.11	0.17	14.17	100.00	84.36	mph	rim

LS2_ol1	0.21	40.57	0.00	41.09	0.00	0.26	0.18	0.09	17.60	100.00	80.43	mph	core
LS2_ol2_1	0.31	38.95	0.08	40.78	0.13	0.50	0.28	0.47	18.50	100.00	78.96	ma	core
LS2_ol2_2	0.25	39.00	0.00	40.79	0.11	0.43	0.44	0.52	18.46	100.00	79.02	ma	middle
LS2_ol2_3	0.35	38.31	0.10	41.21	0.00	0.30	0.28	0.49	18.96	100.00	78.27	ma	rim
LS2_ol3_1	0.26	39.82	0.16	41.67	0.00	0.19	0.00	0.20	17.70	100.00	80.04	mph	core
LS2_ol3_2	0.73	32.63	2.06	40.91	0.15	1.15	0.39	0.31	21.68	100.00	72.85	mph	rim
LS2_ol4_1	0.40	40.54	0.20	41.67	0.00	0.28	0.00	0.16	16.74	100.00	81.19	mph	core
LS2_ol4_2	0.24	41.09	0.00	41.71	0.00	0.25	0.29	0.41	16.02	100.00	82.05	mph	middle
LS2_ol4_3	0.28	40.61	0.13	41.52	0.07	0.41	0.25	0.35	16.39	100.00	81.54	mph	middle
LS2_ol4_4	0.21	38.50	0.10	41.14	0.00	0.32	0.49	0.47	18.78	100.00	78.51	mph	rim
LS2_ol5_1	0.23	40.46	0.00	42.42	0.00	0.13	0.00	0.00	16.75	100.00	81.15	mph	core
LS2_ol5_2	0.23	40.80	0.07	41.67	0.12	0.28	0.00	0.00	16.84	100.00	81.20	mph	middle
LS2_ol5_3	0.24	42.02	0.00	41.74	0.16	0.27	0.14	0.20	15.24	100.00	83.09	mph	middle
LS2_ol5_4	0.26	38.25	0.00	40.54	0.22	0.45	0.29	0.39	19.60	100.00	77.67	mph	rim
LS3_ol1_1	0.15	43.45	0.19	40.42	0.12	0.30	0.62	0.91	13.83	100.00	84.85	mph	core
LS3_ol1_2	0.36	43.74	0.10	41.44	0.15	0.31	0.32	0.17	13.39	100.00	85.34	mph	middle
LS3_ol1_3	0.29	44.20	0.00	40.85	0.13	0.24	0.26	0.21	13.83	100.00	85.07	mph	middle
LS3_ol1_4	0.25	43.75	0.28	41.12	0.00	0.22	0.38	0.38	13.62	100.00	85.13	mph	middle
LS3_ol1_5	0.28	42.85	0.46	41.03	0.20	0.43	0.29	0.62	13.85	100.00	84.65	mph	middle
LS3_ol1_6	0.20	38.39	0.08	39.93	0.08	0.25	0.19	0.43	20.44	100.00	77.00	mph	rim
LS3_ol2	0.21	38.02	0.16	39.67	0.14	0.26	0.50	0.41	20.64	100.00	76.65	ma	middle
LS3_ol3	0.34	39.21	0.14	40.30	0.14	0.37	0.45	0.30	18.75	100.00	78.85	ma	core
LS3_ol4	0.32	37.12	0.10	40.14	0.11	0.24	0.00	0.17	21.81	100.00	75.21	ma	core
LS3_ol5_1	0.29	39.32	0.00	40.24	0.16	0.39	0.15	0.40	19.06	100.00	78.62	mph	core
LS3_ol5_2	0.17	39.13	0.10	40.47	0.00	0.24	0.30	0.29	19.29	100.00	78.34	mph	middle
LS3_ol5_3	0.37	38.49	0.09	40.31	0.25	0.34	0.24	0.39	19.51	100.00	77.86	mph	rim
LS3_ol6_1	0.23	39.22	0.00	40.73	0.05	0.31	0.13	0.28	19.05	100.00	78.59	mph	core
LS3_ol6_2	0.37	38.74	0.00	40.52	0.05	0.38	0.22	0.28	19.43	100.00	78.04	mph	middle
LS3_ol6_3	0.32	39.15	0.00	40.24	0.12	0.45	0.32	0.46	18.95	100.00	78.64	mph	rim
LS3_ol7_1	0.27	39.80	0.00	40.34	0.17	0.35	0.30	0.30	18.46	100.00	79.35	mph	core
LS3_ol7_2	0.26	39.38	0.15	40.21	0.16	0.29	0.43	0.39	18.74	100.00	78.93	mph	middle
LS3_ol7_3	0.38	39.75	0.00	40.33	0.13	0.36	0.20	0.36	18.49	100.00	79.31	mph	rim
LS4_ol1_1	0.39	40.37	0.00	39.92	0.07	0.41	0.26	0.44	18.14	100.00	79.87	mph	core
LS4_ol1_2	0.20	40.77	0.19	41.47	0.00	0.14	0.00	0.13	17.11	100.00	80.94	mph	middle
LS4_ol1_3	0.32	40.38	0.00	41.06	0.00	0.23	0.34	0.30	17.37	100.00	80.56	mph	middle
LS4_ol1_4	0.19	40.56	0.13	41.10	0.18	0.30	0.38	0.18	16.98	100.00	80.98	mph	middle
LS4_ol1_5	0.40	40.55	0.09	40.53	0.00	0.26	0.34	0.52	17.31	100.00	80.68	mph	rim
LS4_ol2_1	0.20	40.53	0.00	40.04	0.00	0.27	0.27	0.24	18.45	100.00	79.66	mph	core
LS4_ol2_2	0.15	40.61	0.07	40.85	0.19	0.27	0.20	0.33	17.34	100.00	80.68	mph	middle
LS4_ol2_3	0.42	40.51	0.00	40.60	0.08	0.25	0.12	0.31	17.71	100.00	80.30	mph	middle
LS4_ol2_4	0.20	40.06	0.00	40.27	0.19	0.43	0.55	0.33	17.98	100.00	79.89	mph	rim
LS4_ol3_1	0.30	40.08	0.38	40.55	0.00	0.26	0.29	0.36	17.78	100.00	80.07	mph	core
LS4_ol3_2	0.32	40.90	0.18	40.79	0.00	0.16	0.00	0.13	17.52	100.00	80.62	mph	middle

LS4_ol3_3	0.38	39.69	0.10	40.88	0.00	0.28	0.15	0.11	18.40	100.00	79.36	mph	rim
LS4_ol4_1	0.19	42.48	0.00	40.84	0.00	0.49	0.20	0.36	15.43	100.00	83.07	mph	core
LS4_ol4_2	0.37	42.61	0.11	41.18	0.21	0.46	0.35	0.28	14.44	100.00	84.03	mph	middle
LS4_ol4_3	0.17	42.41	0.00	41.35	0.10	0.39	0.31	0.30	14.97	100.00	83.47	mph	middle
LS4_ol4_4	0.34	43.15	0.00	41.49	0.00	0.14	0.00	0.30	14.59	100.00	84.06	mph	rim
LS4_ol5_1	0.33	44.54	0.18	40.86	0.00	0.28	0.42	0.63	12.76	100.00	86.15	mph	core
LS4_ol5_2	0.28	44.33	0.00	41.67	0.13	0.43	0.29	0.32	12.55	100.00	86.29	mph	middle
LS4_ol5_3	0.31	44.43	0.00	40.96	0.00	0.21	0.17	0.24	13.68	100.00	85.27	mph	middle
LS4_ol5_4	0.22	44.12	0.12	41.35	0.32	0.55	0.30	0.55	12.47	100.00	86.31	mph	middle
LS4_ol5_5	0.25	44.63	0.09	41.73	0.16	0.28	0.29	0.17	12.40	100.00	86.52	mph	middle
LS4_ol5_6	0.34	44.11	0.00	40.33	0.18	0.50	0.55	0.47	13.52	100.00	85.33	mph	middle
LS4_ol5_7	0.38	39.23	0.00	39.64	0.06	0.35	0.30	0.33	19.71	100.00	78.01	mph	rim

For guide to abbreviations, see Table 1.

Table 7. Clinopyroxene compositions

Sample	Na2O	MgO	Al2O3	SiO2	K2O	CaO	TiO2	Cr2O3	FeO	Total	Mg#	Type	Location
LS5_cpx1	0.41	13.32	1.44	54.01	0.21	18.78	0.73	0.57	10.52	100.00	69.29665	mph	middle
LS5_cpx2	0.41	15.99	3.28	52.95	0.05	13.26	1.34	0.28	12.45	100.00	69.5991	plag incl	core
LS5_cpx3	0.61	14.67	1.45	54.25	0.26	18.49	0.68	0.00	9.58	100.00	73.18764	mph	middle
LS5_cpx4	0.48	14.63	1.58	54.50	0.26	18.59	0.60	0.60	8.75	100.00	74.87689	mph	rim
LS5_cpx5	0.44	14.15	1.58	54.38	0.00	18.62	0.60	0.27	9.96	100.00	71.69077	mph	middle
LS5_cpx6	0.43	14.30	1.32	55.03	0.16	19.25	0.45	0.24	8.83	100.00	74.27175	mph	middle
LS6_cpx1	0.39	14.81	1.46	55.91	0.00	18.34	0.24	0.00	8.85	100.00	74.89315	plag incl	core
LS6_cpx2	0.53	14.40	1.80	54.10	0.28	18.16	0.97	0.57	9.19	100.00	73.63627	plag incl	core
LS6_cpx3_1	0.53	14.87	1.60	55.00	0.11	18.29	0.28	0.00	9.31	100.00	74.00624	mph	core
LS6_cpx3_2	0.55	14.84	1.65	54.40	0.18	18.48	0.56	0.32	9.01	100.00	74.59311	mph	middle
LS6_cpx3_3	0.53	15.37	1.70	54.51	0.18	18.64	0.56	0.26	8.26	100.00	76.83521	mph	middle
LS6_cpx3_4	0.63	14.95	1.05	54.40	0.06	18.74	0.46	0.09	9.62	100.00	73.4759	mph	rim
LS6_cpx4_1	0.58	14.62	1.29	54.69	0.17	18.54	0.75	0.28	9.07	100.00	74.1821	mph	core
LS6_cpx4_2	0.73	14.25	2.91	53.74	0.10	18.08	0.94	0.18	9.08	100.00	73.66675	mph	middle
LS6_cpx4_3	0.57	15.30	2.11	54.28	0.21	18.46	0.93	0.38	7.77	100.00	77.8271	mph	middle
LS6_cpx4_4	0.40	14.72	1.52	54.53	0.14	17.90	0.51	0.34	9.94	100.00	72.52543	mph	rim

Mg# = 100*[Mg/(Mg+Fe)]. Light red fill = red component. Light gray fill = gray component. For other abbreviations, see Table 1.

Table 8. Plagioclase compositions

Sample	Na2O	MgO	Al2O3	SiO2	K2O	CaO	TiO2	Cr2O3	FeO	Total	An	Type	Location
LS1-NV_plag1_1	3.24	0.29	28.96	53.74	0.17	11.92	0.42	0.47	0.79	100.00	80.26	ph_s	middle
LS1-NV_plag1_2	2.89	0.39	29.33	52.74	0.26	12.72	0.34	0.40	0.93	100.00	82.95	ph_s	middle
LS1-NV_plag1_3	3.36	0.25	29.00	53.56	0.19	12.22	0.30	0.23	0.89	100.00	80.08	ph_s	rim
LS1-NV_plag2_1	3.00	0.25	29.35	53.10	0.16	12.85	0.36	0.42	0.52	100.00	82.56	mph	core
LS1-NV_plag2_2	3.42	0.28	29.30	52.95	0.32	12.37	0.26	0.28	0.82	100.00	79.99	mph	middle

LS1-NV_plag2_3	4.08	0.14	26.73	55.63	0.53	10.50	0.51	0.73	1.14	100.00	73.99	mph	middle
LS1-NV_plag2_4	3.32	0.30	28.66	54.06	0.27	12.05	0.17	0.22	0.94	100.00	80.05	mph	rim
LS1-V_plag1	3.10	0.14	29.65	54.49	0.00	12.34	0.00	0.00	0.28	100.00	81.48	mph	core
LS1-V_plag2	2.97	0.49	29.68	52.08	0.19	12.94	0.25	0.32	1.08	100.00	82.80	mph	core
LS1-V_plag3_1	3.10	0.41	28.62	53.38	0.22	12.46	0.28	0.48	1.06	100.00	81.63	ph_s	core
LS1-V_plag3_2	3.27	0.36	29.27	53.53	0.21	11.77	0.28	0.52	0.78	100.00	79.91	ph_s	middle
LS1-V_plag3_3	3.28	0.30	29.17	53.99	0.23	12.26	0.13	0.00	0.65	100.00	80.51	ph_s	rim
LS1-V_plag4_1	3.08	0.30	29.33	52.69	0.29	12.68	0.42	0.20	1.02	100.00	81.98	ph	middle
LS1-V_plag4_2	3.22	0.18	29.42	52.56	0.23	12.85	0.20	0.34	1.00	100.00	81.52	ph	middle
LS1-V_plag4_3	3.11	0.41	29.01	52.81	0.34	12.97	0.39	0.32	0.64	100.00	82.17	ph	rim
LS2_plag1_1	3.15	0.44	30.48	52.67	0.14	12.50	0.00	0.00	0.62	100.00	81.43	ph	core
LS2_plag1_2	3.36	0.23	30.22	53.17	0.12	12.38	0.00	0.00	0.52	100.00	80.28	ph	middle
LS2_plag1_3	3.63	0.33	29.34	53.18	0.26	12.31	0.12	0.16	0.66	100.00	78.94	ph	middle
LS2_plag1_4	3.94	0.30	28.29	54.78	0.33	11.10	0.38	0.23	0.66	100.00	75.69	ph	rim
LS2_plag2_1	3.57	0.07	28.82	53.91	0.16	11.77	0.43	0.40	0.87	100.00	78.47	ph_s	core
LS2_plag2_2	3.55	0.18	29.46	53.87	0.20	11.85	0.12	0.11	0.66	100.00	78.67	ph_s	middle
LS2_plag2_3	3.50	0.30	29.33	54.13	0.20	11.77	0.09	0.19	0.48	100.00	78.80	ph_s	middle
LS2_plag2_4	3.43	0.21	29.25	54.28	0.26	11.48	0.23	0.10	0.76	100.00	78.72	ph_s	rim
LS2_plag3_1	3.56	0.31	29.42	53.47	0.18	11.65	0.20	0.32	0.88	100.00	78.34	mph	core
LS2_plag3_2	3.30	0.41	30.18	53.30	0.16	12.28	0.00	0.00	0.38	100.00	80.44	mph	middle
LS2_plag3_3	3.43	0.24	29.85	53.20	0.30	12.06	0.14	0.00	0.78	100.00	79.53	mph	middle
LS2_plag3_4	3.87	0.08	28.38	53.85	0.27	11.61	0.57	0.47	0.91	100.00	76.83	mph	middle
LS2_plag3_5	4.28	0.35	27.67	54.91	0.30	10.48	0.40	0.42	1.19	100.00	73.02	mph	rim
LS2_plag4_1	2.91	0.37	29.86	52.99	0.17	12.98	0.00	0.19	0.52	100.00	83.14	mph	core
LS2_plag4_2	3.04	0.39	29.54	52.68	0.09	12.77	0.16	0.36	0.98	100.00	82.28	mph	middle
LS2_plag4_3	3.26	0.22	29.30	53.40	0.15	12.86	0.15	0.00	0.66	100.00	81.34	mph	middle
LS2_plag4_4	3.79	0.26	27.94	55.53	0.26	11.10	0.27	0.29	0.57	100.00	76.40	mph	rim
LS2_plag5_1	3.43	0.40	28.42	53.43	0.27	12.19	0.36	0.51	1.00	100.00	79.71	mph_ss	core
LS2_plag5_2	3.09	0.20	28.77	53.99	0.19	12.75	0.13	0.21	0.67	100.00	82.02	mph_ss	middle
LS2_plag5_3	3.48	0.32	28.37	54.70	0.33	11.98	0.21	0.10	0.52	100.00	79.19	mph_ss	rim
LS2_plag6_1	3.65	0.34	28.30	54.61	0.18	11.66	0.30	0.28	0.68	100.00	77.93	mph	core
LS2_plag6_2	3.54	0.29	28.42	53.85	0.33	12.22	0.36	0.33	0.66	100.00	79.23	mph	middle
LS2_plag6_3	3.54	0.16	27.92	55.28	0.25	11.34	0.22	0.26	1.02	100.00	77.98	mph	rim
LS3_plag1	3.47	0.44	29.92	52.93	0.28	11.85	0.17	0.29	0.65	100.00	79.05	mph	middle
LS3_plag2	4.59	0.47	27.06	56.10	0.14	10.06	0.24	0.37	0.97	100.00	70.78	mph	middle
LS3_plag3_1	3.71	0.31	28.76	54.28	0.35	11.27	0.28	0.18	0.87	100.00	77.05	mph	core
LS3_plag3_2	4.07	0.27	28.59	55.38	0.00	11.05	0.00	0.00	0.64	100.00	75.00	mph	middle
LS3_plag3_3	4.33	0.21	28.05	55.77	0.16	10.63	0.14	0.09	0.63	100.00	73.07	mph	rim
LS4_plag1_1	4.34	0.29	28.67	55.63	0.22	10.57	0.00	0.00	0.28	100.00	72.91	mph	core
LS4_plag1_2	3.82	0.25	28.71	54.60	0.31	11.14	0.40	0.23	0.55	100.00	76.32	mph	middle
LS4_plag1_3	4.00	0.38	28.87	54.88	0.09	11.02	0.00	0.00	0.76	100.00	75.28	mph	middle
LS4_plag1_4	4.21	0.35	28.18	54.83	0.27	10.67	0.41	0.09	0.98	100.00	73.69	mph	rim
LS4_plag2	4.36	0.22	27.59	55.29	0.13	10.38	0.38	0.37	1.29	100.00	72.46	ol rim	core

LS4_plag3_1	3.87	0.46	28.95	54.41	0.24	11.08	0.12	0.15	0.72	100.00	75.99	ph_ss	core
LS4_plag3_2	3.81	0.24	29.41	52.87	0.40	11.60	0.29	0.53	0.85	100.00	77.09	ph_ss	middle
LS4_plag3_3	3.88	0.30	28.90	54.57	0.22	10.89	0.40	0.17	0.68	100.00	75.62	ph_ss	middle
LS4_plag3_4	3.61	0.37	30.01	52.47	0.27	11.88	0.34	0.26	0.80	100.00	78.44	ph_ss	middle
LS4_plag3_5	3.74	0.00	29.25	53.53	0.18	11.86	0.28	0.40	0.76	100.00	77.80	ph_ss	middle
LS4_plag3_6	4.25	0.19	27.90	54.62	0.30	10.42	0.60	0.61	1.11	100.00	73.04	ph_ss	rim
LS4_plag4_1	3.44	0.27	29.44	53.57	0.26	11.84	0.18	0.21	0.78	100.00	79.18	ph_s	core
LS4_plag4_2	3.73	0.36	29.31	53.37	0.18	11.49	0.44	0.19	0.93	100.00	77.30	ph_s	middle
LS4_plag4_3	3.43	0.31	29.37	53.51	0.39	11.46	0.35	0.42	0.76	100.00	78.69	ph_s	middle
LS4_plag4_4	3.55	0.25	29.31	53.38	0.10	12.00	0.38	0.10	0.93	100.00	78.89	ph_s	middle
LS4_plag4_5	3.70	0.28	29.47	53.14	0.29	11.49	0.26	0.24	1.13	100.00	77.44	ph_s	rim
LS5_plag1_1	5.22	0.17	26.12	57.73	0.51	8.54	0.48	0.32	0.90	100.00	64.39	mph	core
LS5_plag1_2	4.90	0.20	27.08	56.81	0.51	9.20	0.57	0.13	0.61	100.00	67.48	mph	middle
LS5_plag1_3	5.23	0.00	25.88	58.30	0.54	8.61	0.36	0.32	0.76	100.00	64.53	mph	middle
LS5_plag1_4	5.99	0.16	23.04	62.03	0.93	5.87	0.26	0.38	1.36	100.00	51.99	mph	rim
LS5_plag2	6.40	0.22	23.23	61.54	0.91	5.82	0.44	0.60	0.83	100.00	50.13	mph	core
LS5_plag3	5.48	0.19	24.42	60.95	0.63	7.27	0.18	0.10	0.77	100.00	59.45	ph	core
LS5_plag4	5.29	0.19	25.67	58.89	0.35	8.12	0.41	0.41	0.66	100.00	62.92	ph	middle
LS5_plag5_1	5.79	0.00	24.88	60.73	0.87	6.91	0.00	0.20	0.62	100.00	56.88	mph	core
LS5_plag5_2	4.28	0.05	27.42	56.81	0.33	10.22	0.00	0.00	0.88	100.00	72.52	mph	middle
LS5_plag5_3	4.76	0.29	26.68	56.76	0.43	9.48	0.43	0.42	0.75	100.00	68.76	mph	middle
LS5_plag5_4	5.04	0.31	26.18	57.87	0.58	8.83	0.15	0.20	0.84	100.00	65.94	mph	middle
LS5_plag5_5	4.67	0.15	27.09	56.20	0.46	9.59	0.24	0.35	1.25	100.00	69.42	mph	rim
LS5_plag6	4.85	0.25	26.41	56.87	0.56	9.20	0.30	0.52	1.03	100.00	67.71	ph	middle
LS5_plag7_1	4.95	0.20	26.90	57.32	0.44	9.46	0.13	0.14	0.48	100.00	67.87	mph	core
LS5_plag7_2	4.16	0.22	28.05	54.92	0.41	10.55	0.37	0.52	0.80	100.00	73.70	mph	core
LS5_plag7_3	6.16	0.22	24.39	60.82	0.69	6.23	0.41	0.19	0.89	100.00	52.78	mph	middle
LS5_plag7_4	6.21	0.13	24.70	61.12	0.77	6.52	0.08	0.00	0.47	100.00	53.71	mph	middle
LS5_plag7_5	4.21	0.26	28.00	54.71	0.47	10.32	0.42	0.54	1.06	100.00	73.04	mph	rim
LS5_plag8_1	5.49	0.00	24.45	60.81	0.76	7.13	0.22	0.45	0.69	100.00	58.94	mph	core
LS5_plag8_2	5.14	0.07	24.72	59.92	0.64	7.83	0.58	0.34	0.76	100.00	62.74	mph	middle
LS5_plag8_3	5.28	0.26	25.51	59.07	0.49	7.95	0.29	0.27	0.87	100.00	62.46	mph	middle
LS5_plag8_4	5.83	0.21	23.81	61.82	0.95	6.20	0.36	0.29	0.52	100.00	54.03	mph	middle
LS5_plag8_5	3.87	0.05	27.95	54.75	0.44	11.26	0.28	0.36	1.04	100.00	76.28	mph	rim
LS5_plag8_6	3.40	0.10	29.03	54.61	0.35	11.84	0.00	0.00	0.67	100.00	79.38	mph	rim
LS5_plag8_7	3.70	0.00	27.88	55.98	0.36	10.55	0.33	0.11	1.09	100.00	75.91	mph	rim
LS5_plag9_1	4.72	0.11	27.16	56.68	0.39	9.52	0.35	0.23	0.83	100.00	69.03	ph	core
LS5_plag9_2	5.62	0.12	25.74	59.44	0.53	7.82	0.00	0.00	0.73	100.00	60.60	ph	middle
LS5_plag10_1	4.08	0.27	28.61	54.43	0.24	11.35	0.19	0.25	0.58	100.00	75.46	ph	core
LS5_plag10_2	6.55	0.00	22.89	63.35	1.18	5.06	0.20	0.22	0.55	100.00	46.06	ph	rim
LS5_plag11_1	3.97	0.00	28.53	55.12	0.28	10.80	0.27	0.30	0.74	100.00	75.04	ph	core
LS5_plag11_2	4.21	0.27	28.45	53.97	0.40	10.89	0.26	0.35	1.22	100.00	74.09	ph	middle
LS5_plag11_3	5.25	0.28	26.12	57.91	0.56	8.15	0.39	0.26	1.07	100.00	63.18	ph	middle

LS5_plag11_4	3.94	0.27	28.35	54.98	0.24	10.82	0.24	0.11	1.06	100.00	75.22	ph	rim
LS5_plag12_1	5.55	0.10	24.78	60.24	0.66	7.31	0.25	0.36	0.75	100.00	59.28	mph	core
LS5_plag13	5.41	0.18	24.54	60.65	0.72	7.07	0.26	0.28	0.89	100.00	59.09	mph	core
LS5_plag14	3.45	0.21	29.08	54.53	0.38	11.33	0.20	0.09	0.74	100.00	78.40	mph	core
LS5_plag15	5.46	0.24	25.35	59.60	0.51	7.77	0.23	0.24	0.60	100.00	61.13	mph	core
LS5_plag12_2	4.03	0.11	27.92	56.00	0.38	10.28	0.33	0.17	0.76	100.00	73.82	mph	rim
LS5_plag16	4.06	0.09	28.06	55.89	0.29	10.79	0.10	0.00	0.72	100.00	74.60	mph	rim
LS6_plag1_1	4.14	0.14	27.57	57.03	0.37	9.91	0.00	0.16	0.69	100.00	72.57	ph	core
LS6_plag1_2	5.20	0.19	26.54	57.45	0.48	8.78	0.46	0.10	0.80	100.00	65.11	ph	middle
LS6_plag1_3	4.97	0.07	26.25	58.57	0.45	8.75	0.16	0.14	0.64	100.00	66.05	ph	middle
LS6_plag1_4	5.16	0.32	26.43	57.32	0.51	8.87	0.30	0.34	0.74	100.00	65.52	ph	middle
LS6_plag1_5	5.43	0.24	26.33	57.11	0.49	8.72	0.34	0.53	0.82	100.00	63.96	ph	middle
LS6_plag1_6	4.84	0.09	25.54	58.77	0.54	8.60	0.38	0.34	0.91	100.00	66.26	ph	middle
LS6_plag1_7	3.89	0.07	29.55	53.54	0.26	11.60	0.24	0.23	0.63	100.00	76.72	ph	middle
LS6_plag1_8	3.13	0.21	29.60	53.05	0.38	12.54	0.32	0.00	0.76	100.00	81.58	ph	middle
LS6_plag1_9	4.89	0.20	26.08	58.94	0.42	8.56	0.10	0.15	0.66	100.00	65.93	ph	rim
LS6_plag2_1	5.81	0.26	25.27	59.81	0.59	7.36	0.11	0.20	0.58	100.00	58.33	mph	rim
LS6_plag2_2	1.09	0.10	33.70	46.96	0.15	16.14	0.46	0.44	0.97	100.00	94.24	mph	core
LS6_plag2_3	1.49	0.16	33.40	47.65	0.17	15.83	0.32	0.29	0.69	100.00	92.15	mph	middle
LS6_plag2_4	6.21	0.24	24.34	60.76	0.67	6.71	0.31	0.24	0.52	100.00	54.43	mph	rim
LS6_plag2_5	6.01	0.16	24.92	59.74	0.76	6.82	0.38	0.20	0.99	100.00	55.64	mph	rim
LS6_plag2_6	1.19	0.23	34.10	46.89	0.24	16.17	0.33	0.18	0.68	100.00	93.76	mph	core
LS6_plag2_7	5.12	0.21	25.20	60.16	0.44	7.93	0.20	0.00	0.74	100.00	63.12	mph	rim
LS6_plag2_8	5.58	0.16	23.43	62.40	0.69	6.38	0.31	0.24	0.80	100.00	55.82	mph	rim
LS6_plag3_1	5.38	0.10	26.34	59.08	0.40	8.18	0.00	0.09	0.42	100.00	62.69	mph	core
LS6_plag3_2	5.41	0.27	26.46	58.02	0.50	8.27	0.28	0.16	0.64	100.00	62.82	mph	middle
LS6_plag3_3	5.90	0.31	25.53	59.05	0.41	7.81	0.31	0.00	0.69	100.00	59.40	mph	middle
LS6_plag3_4	5.35	0.23	26.56	57.78	0.50	8.28	0.26	0.22	0.83	100.00	63.11	mph	middle
LS6_plag3_5	5.53	0.00	26.35	59.33	0.33	7.87	0.00	0.00	0.60	100.00	61.13	mph	middle
LS6_plag3_6	5.54	0.27	26.52	58.41	0.33	8.25	0.00	0.09	0.60	100.00	62.21	mph	middle
LS6_plag3_7	6.36	0.12	24.46	61.08	0.65	6.43	0.00	0.10	0.79	100.00	52.77	mph	middle
LS6_plag3_8	4.25	0.29	28.18	54.94	0.42	10.43	0.37	0.38	0.73	100.00	73.06	mph	middle
LS6_plag3_9	5.86	0.11	25.10	60.04	0.62	7.25	0.28	0.13	0.60	100.00	57.76	mph	rim
LS6_plag4	4.87	0.10	27.84	55.84	0.45	9.43	0.33	0.41	0.74	100.00	68.15	cpx rim	core
LS6_plag5	5.66	0.24	26.02	58.89	0.34	7.83	0.00	0.00	1.01	100.00	60.46	cpx incl	core
LS6_plag6	2.32	0.05	32.02	50.32	0.22	14.12	0.00	0.23	0.73	100.00	87.06	cpx infill	middle
LS6_plag7_1	5.64	0.14	25.18	59.31	0.68	7.43	0.29	0.47	0.86	100.00	59.28	mph	core
LS6_plag7_2	5.67	0.21	25.67	59.50	0.57	7.34	0.22	0.19	0.64	100.00	58.86	mph	middle
LS6_plag7_3	5.56	0.23	26.51	58.74	0.46	8.00	0.00	0.00	0.49	100.00	61.39	mph	middle
LS6_plag7_4	5.73	0.24	25.53	59.09	0.48	7.64	0.30	0.29	0.71	100.00	59.57	mph	middle
LS6_plag7_5	4.93	0.25	27.06	57.15	0.43	9.11	0.14	0.26	0.66	100.00	67.13	mph	middle
LS6_plag7_6	5.87	0.26	25.38	59.44	0.67	7.25	0.35	0.26	0.51	100.00	57.72	mph	middle
LS6_plag7_7	6.05	0.06	24.75	59.61	0.59	7.39	0.38	0.36	0.81	100.00	57.45	mph	middle

LS6_plag7_8	6.23	0.29	24.71	59.89	0.74	6.63	0.27	0.33	0.91	100.00	54.05	mph	rim
LS6_plag8_1	4.85	0.22	25.74	58.80	0.37	8.93	0.00	0.23	0.87	100.00	67.05	ma	middle
LS6_plag8_2	4.47	0.26	25.86	57.50	0.42	9.17	0.47	0.68	1.17	100.00	69.39	ma	middle
LS6_plag9_1	3.60	0.22	28.14	55.80	0.29	11.13	0.00	0.00	0.82	100.00	77.36	mph	middle
LS6_plag9_2	3.48	0.20	28.07	54.53	0.32	11.88	0.31	0.27	0.93	100.00	79.05	mph	middle
LS6_plag9_3	4.26	0.16	26.57	57.00	0.48	9.98	0.41	0.20	0.95	100.00	72.14	mph	middle
LS6_plag9_4	3.53	0.20	27.74	55.49	0.33	11.29	0.18	0.45	0.78	100.00	77.95	mph	middle
LS6_plag9_5	4.38	0.10	26.36	58.50	0.37	9.66	0.00	0.09	0.55	100.00	70.91	mph	middle
LS6_plag9_6	4.73	0.18	25.91	59.28	0.46	8.71	0.21	0.00	0.51	100.00	67.05	mph	rim
LS6_plag10_1	3.93	0.23	26.94	57.12	0.43	10.37	0.18	0.17	0.62	100.00	74.47	ma	middle
LS6_plag10_2	4.16	0.24	26.34	56.89	0.45	9.66	0.66	0.39	1.21	100.00	71.96	ma	middle

An = 100*[Ca/(Ca+Na)]. Underscores following mineral type represent observed sieving: ph_s is a sieved phenocryst, ph_ss is a slightly sieved phenocryst. Mineral names preceeding the word "rim" represent plagioclase rimming the given mineral (e.g.; cpx rim means the data point is a plagioclase rim on a clinopyroxene crystal). The grain denoted "cpx infill" represents an embayment within a clinopyroxene crystal which is infilled with plagioclase. Light red fill = red component. Light gray fill = gray component. Dark gray fill = black component. For other abbreviations, see Table 1.

Table 9. Orthopyroxene compositions

Sample	Na2O	MgO	Al2O3	SiO2	K2O	CaO	TiO2	Cr2O3	FeO	Total	Mg#	Type	Location
LS2_opx1	0.69	17.59	1.20	38.84	0.25	1.06	0.24	0.34	39.81	100.00	44.06	ol rim	middle
LS3_opx1	0.47	22.14	0.59	38.37	0.24	0.51	0.56	0.30	36.82	100.00	51.73	ol rim	middle
LS5_opx1	0.29	20.21	0.77	54.19	0	2.35	0.67	0.31	21.2	100	62.95	mph	core
LS5_opx2	0.36	20.41	0.72	54.68	0	1.46	0.44	0.26	21.68	100	62.66	mph	middle
LS5_opx3	0.18	20.77	0.69	54.98	0.18	1.61	0.75	0.13	20.7	100	64.14	mph	middle
LS5_opx4	0.2	24.43	1.19	56.15	0	1.46	0.5	0.29	15.77	100	73.41	mph	middle
LS5_opx5	0.24	25.06	1.08	55.76	0	1.45	0.58	0.26	15.56	100	74.17	mph	core
LS6_opx1	0.21	22.88	0.59	54.98	0.09	1.63	0.62	0.46	18.53	100.00	68.76	ma	core
LS6_opx2_1	0.19	23.42	1.04	56.02	0	1.59	0.62	0.42	16.71	100	71.41	mph	core
LS6_opx2_2	0.17	22.73	1.08	56.49	0.05	1.36	0.53	0.15	17.44	100	69.91	mph	middle
LS6_opx2_3	0.32	23.25	0.56	56.1	0.06	1.38	0.29	0.3	17.74	100	70.03	mph	rim
LS6_opx2_4	0.29	23.08	0.52	56.01	0.08	1.58	0.64	0.39	17.41	100	70.27	mph	rim

For equations and guide to abbreviations and colors, see Tables 6, 7, and 8.

Table 10. Glass compositions

Sample	Na2O	MgO	Al2O3	SiO2	K2O	CaO	TiO2	Cr2O3	FeO	Total	Mg#
LS6_glass_1	3.69	0.68	13.79	72.66	3.69	1.72	1.09	0.00	2.67	100.00	31.22
LS6_glass_2	3.78	0.73	13.85	72.80	3.89	1.63	0.68	0.00	2.64	100.00	33.02
LS6_glass_3	3.67	0.67	13.47	73.46	3.84	1.50	0.55	0.09	2.74	100.00	30.36
LS6_glass_4	3.94	0.55	13.57	72.90	3.71	1.42	0.95	0.29	2.65	100.00	27.01
LS6_glass_5	3.67	0.45	13.62	73.16	3.86	1.61	0.61	0.00	3.03	100.00	20.93
LS6_glass_6	3.68	0.75	13.65	72.69	3.56	1.73	0.73	0.17	3.04	100.00	30.54
LS6_glass_7	4.55	0.82	14.12	71.74	3.55	1.87	0.70	0.00	2.66	100.00	35.46
LS6_glass_8	4.44	0.84	14.56	70.86	3.39	1.89	0.91	0.36	2.76	100.00	35.17
LS6_glass_9	3.64	0.55	13.55	73.65	3.89	1.57	0.59	0.00	2.55	100.00	27.77
LS6_glass_10	3.82	0.63	13.8	72.58	3.63	2.08	0.61	0.13	2.72	100.00	29.22
LS6_glass_11	3.83	0.73	13.94	71.73	3.75	1.75	0.74	0.44	3.08	100.00	29.70
LS6_glass_12	3.77	0.75	14.07	72.17	3.84	1.61	0.71	0.25	2.84	100.00	32.01
LS6_glass_13	3.49	0.67	14.11	72	3.89	1.82	0.88	0.12	3.04	100.00	28.21
LS6_glass_14	3.65	0.64	14.14	72.21	3.47	1.8	0.86	0.34	2.89	100.00	28.30

All glass observations are from matrix data.

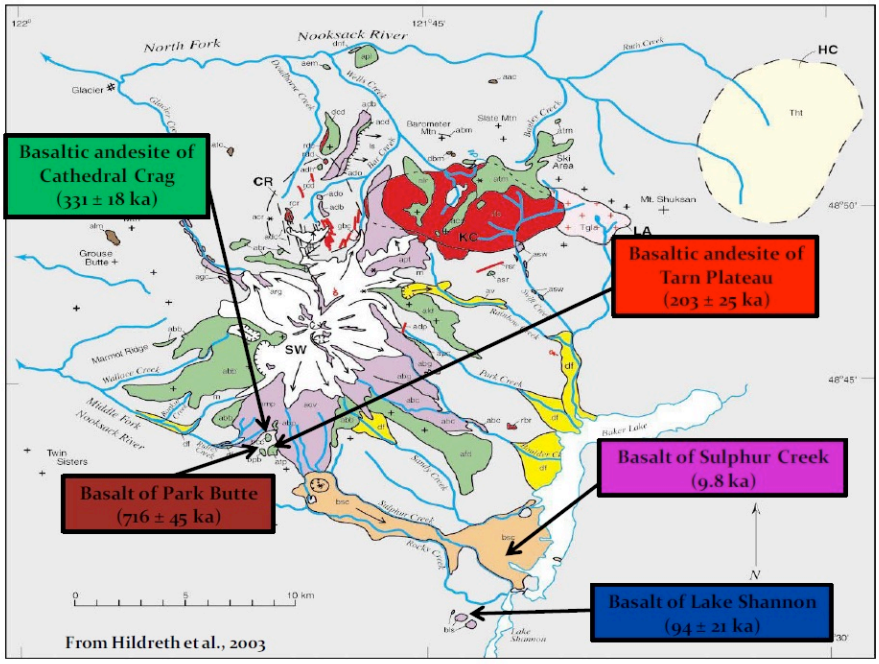

Figure 1. From Moore and DeBari (2012) – map of mafic Mount Baker flow units. Note the two flows analyzed in this study, located at the southern end of the map.

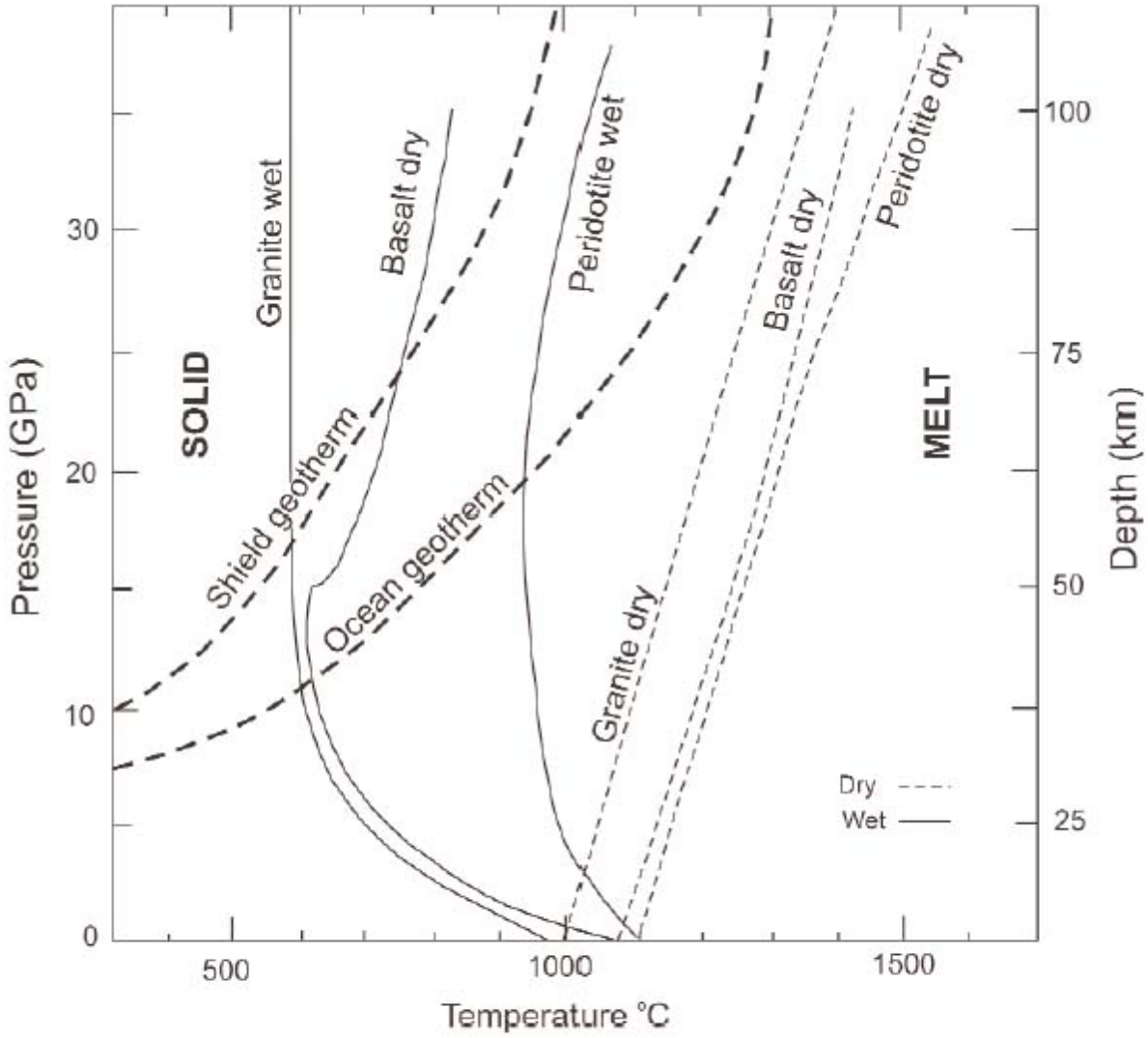

Figure 8. The effect of water on magma genesis. Phase diagram emphasizing the role of water in magma source rock (modified from Winter 2001) showing a comparison between the dry and water-saturated *solidi* for granite, basalt and peridotite, and typical shield and oceanic geotherms. The breakdown curves for hydrous phases in the mantle such as amphibole and phlogopite are shown.

Figure 2. Diagram showing wet vs. dry melting curves emphasizing the fact that magma can be generated at lower temperatures if there is sufficient water (Murphy, J.B., 2007).

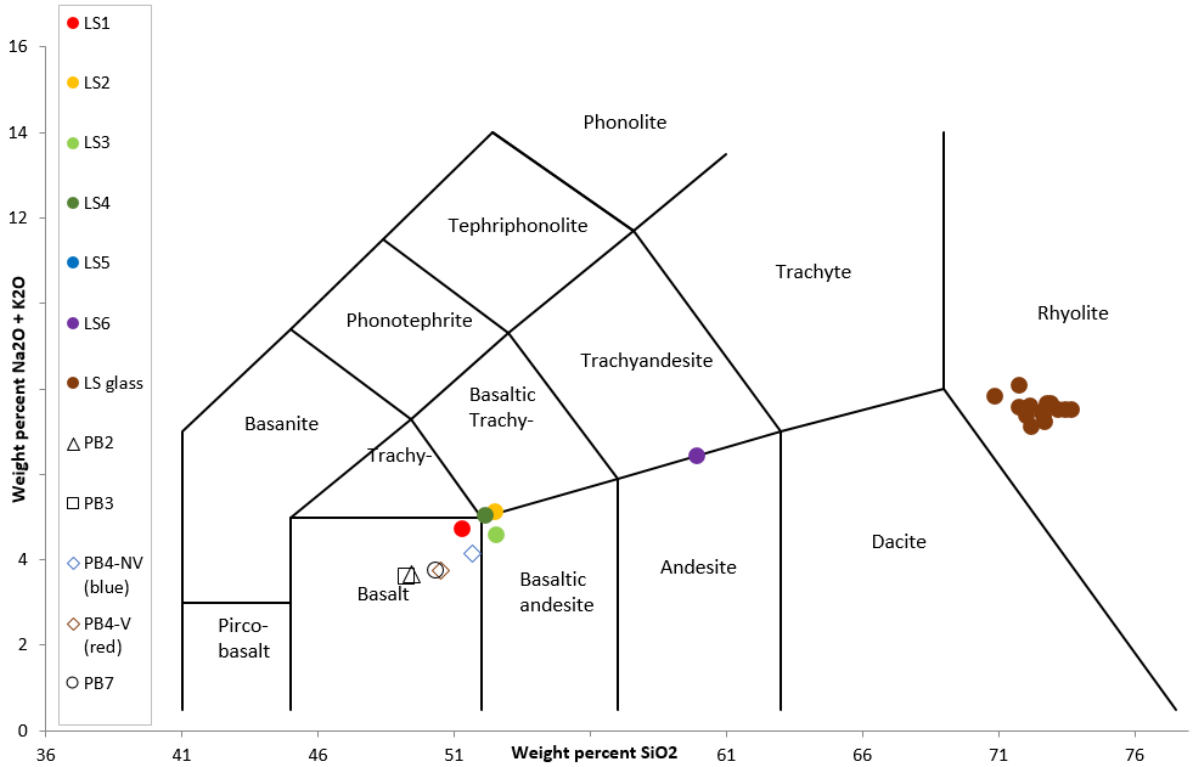

Figure 3. Total alkali content versus silica (TAS) diagram showing whole rock data for the analyzed Lake Shannon and Park Butte samples (Le Maitre et al., 1989).

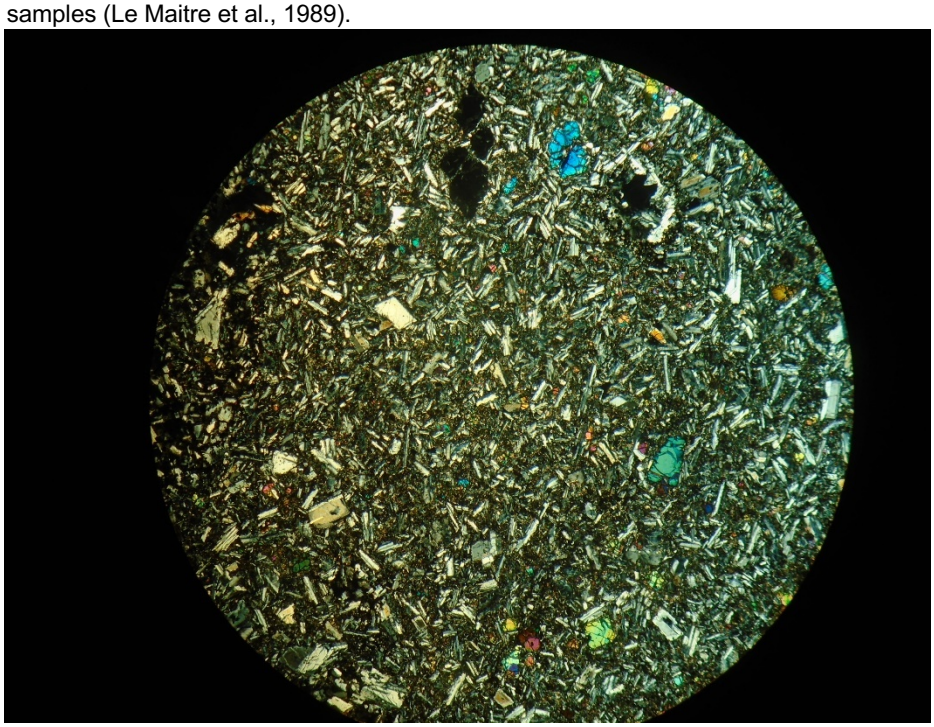

Figure 4. Cross-polarized light (XPL) view of PB4 matrix. Field of view diameter = 1 cm. Note the difference in mafic crystal size compared to PB7 (Figure 5). In PB7, the mafic matrix crystals are larger.

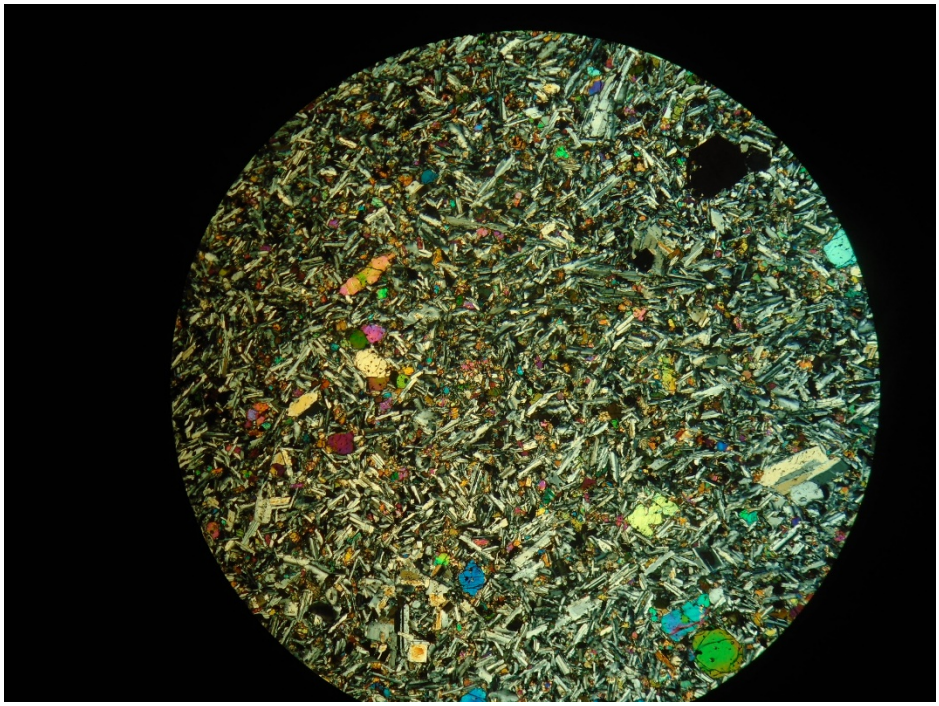

Figure 5. Cross-polarized light (XPL) view of PB7 matrix. Field of view diameter = 1 cm. Note the difference in mafic crystal size compared to PB4 (Figure 4). In PB4, the mafic matrix crystals are larger.

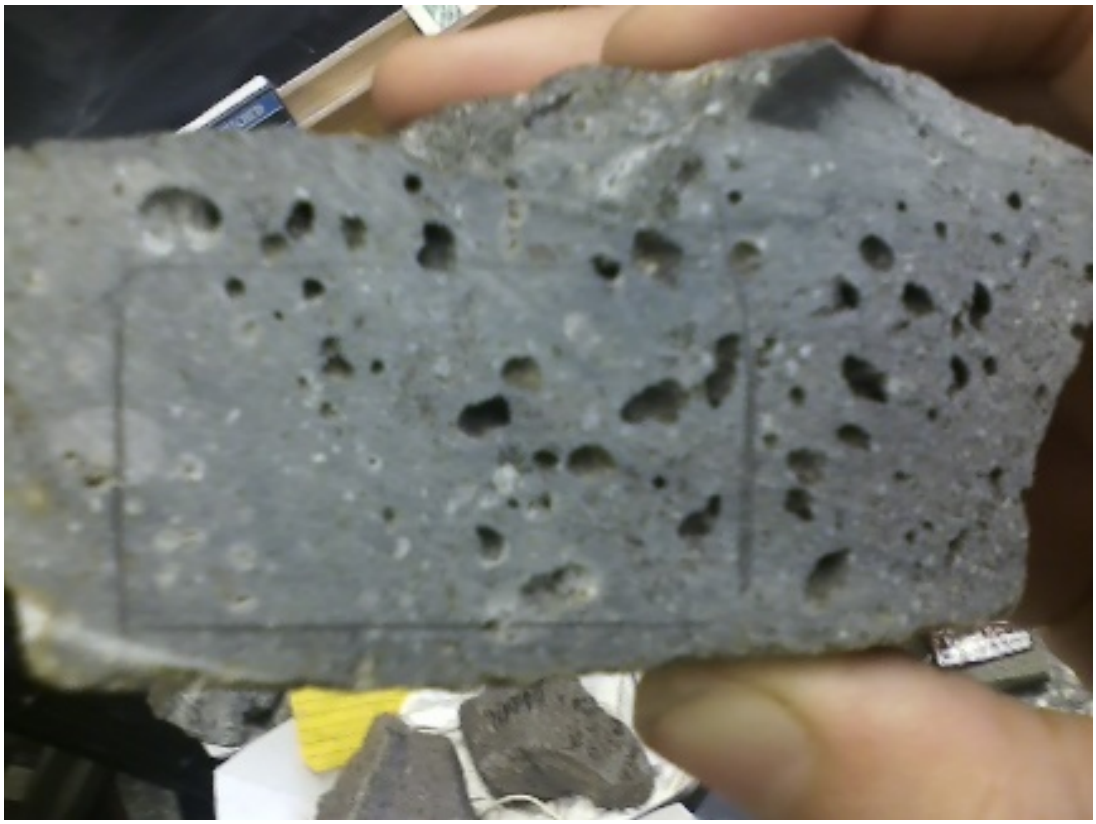

Figure 6. Hand sample of PB4 showing vesicular “red” section on right and less-vesicular “blue” section on left. Long edge of rectangle = 3.5 cm.

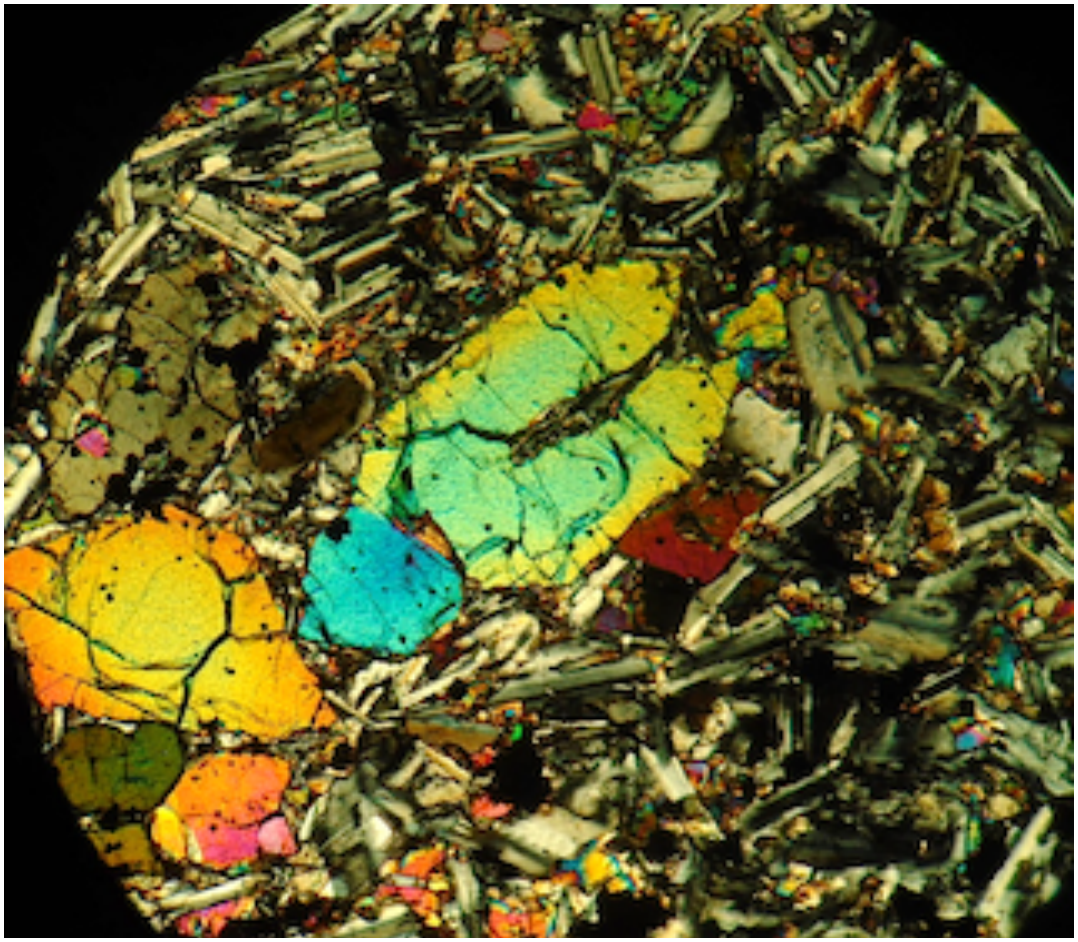

Figure 7. Cross-polarized light (XPL) view of zoned and embayed olivine crystal in sample PB7. Zoning is indicated by color change from blue core to green rim, embayment is located in the upper right corner of the crystal. Field of view diameter 2.5mm.

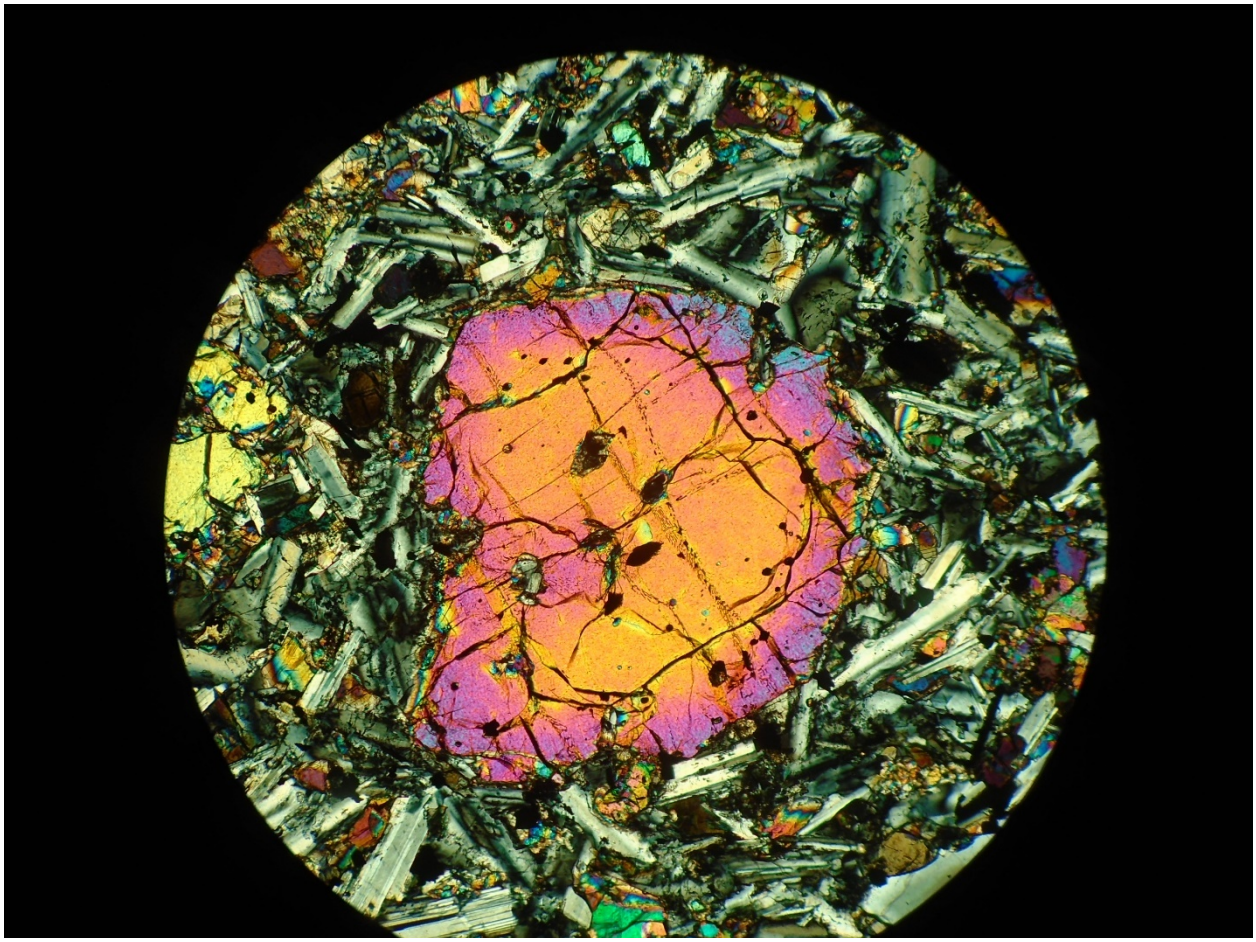

Figure 8. Cross-polarized light (XPL) view of zoned and embayed olivine crystal in sample PB7. Zoning is indicated by color change from yellow-orange core to pink-blue rim. This crystal also shows evidence of embayment along the edges. Field of view diameter 2.5mm.

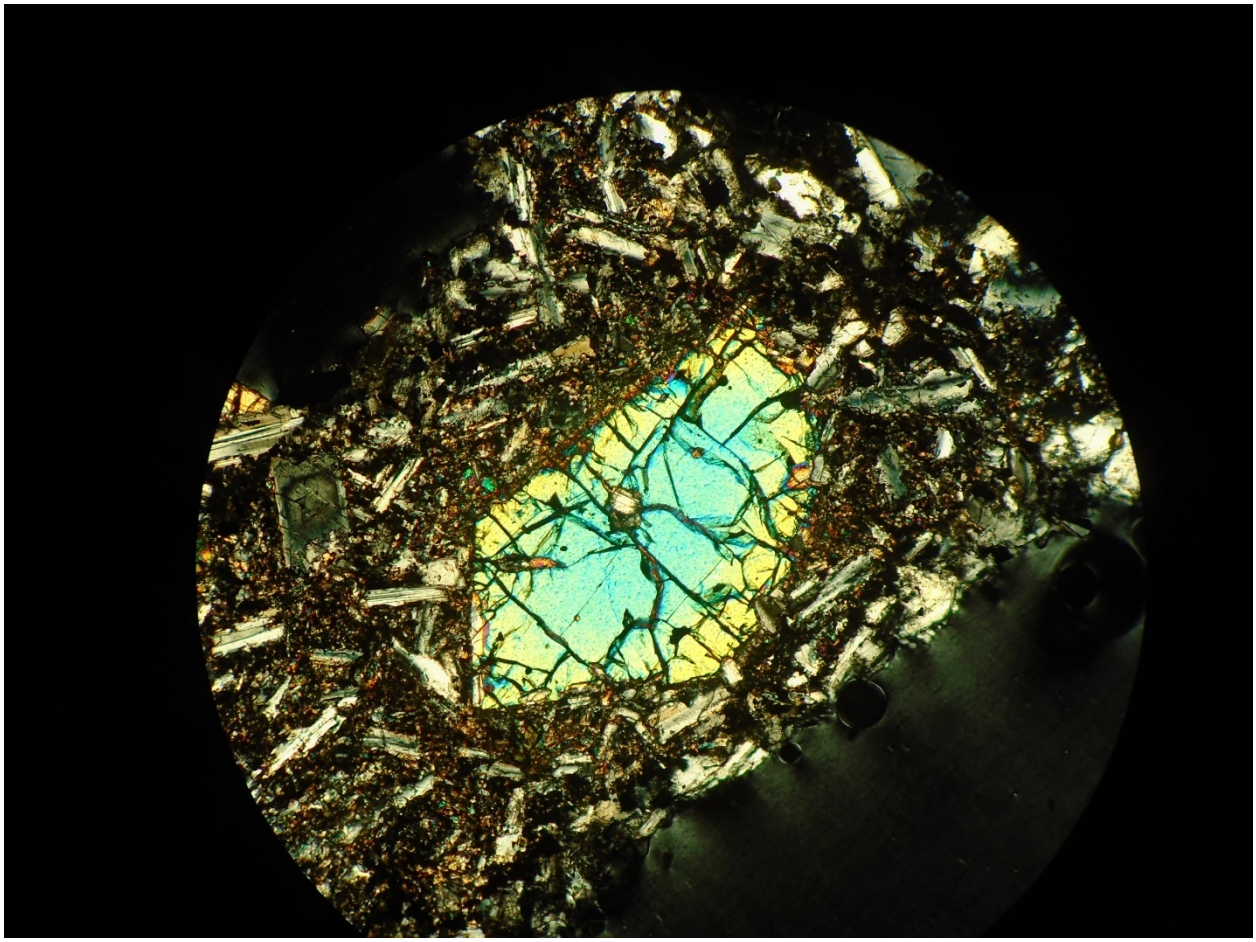

Figure 9. Cross-polarized light (XPL) view of zoned and embayed olivine crystal in sample PB7. Zoning is indicated by color change from blue core to green rim, embayment is located in the upper right corner of the crystal. Field of view diameter 2.5mm.

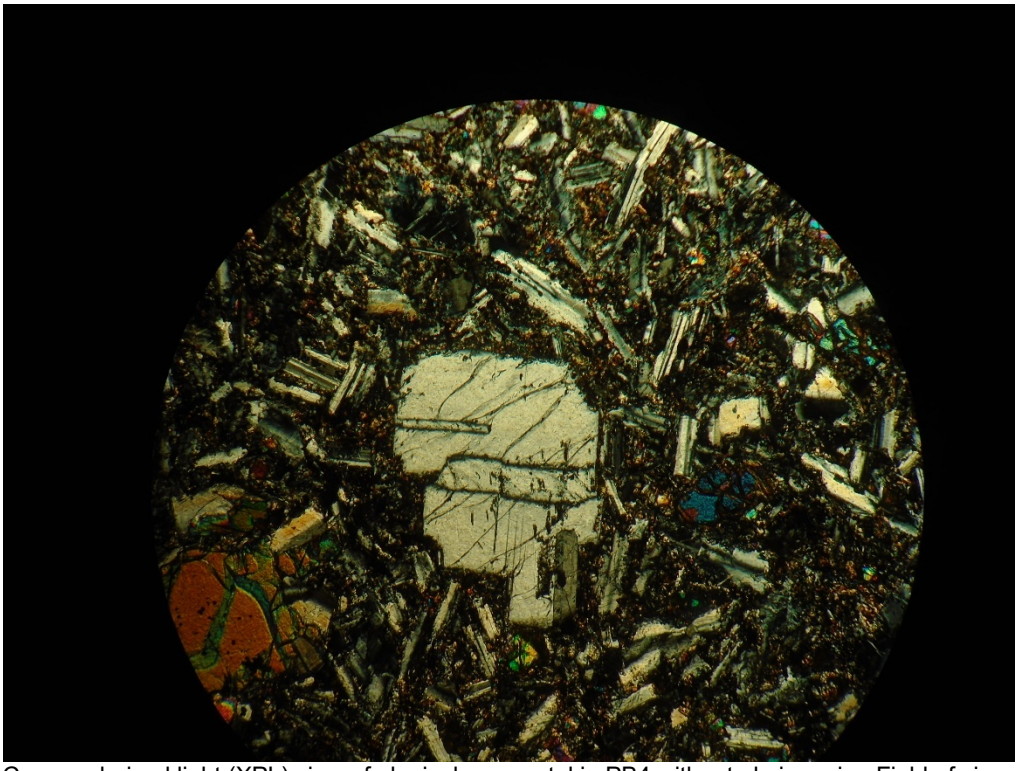

Figure 10. Cross-polarized light (XPL) view of plagioclase crystal in PB4 without obvious rim. Field of view diameter = 2.5 mm.

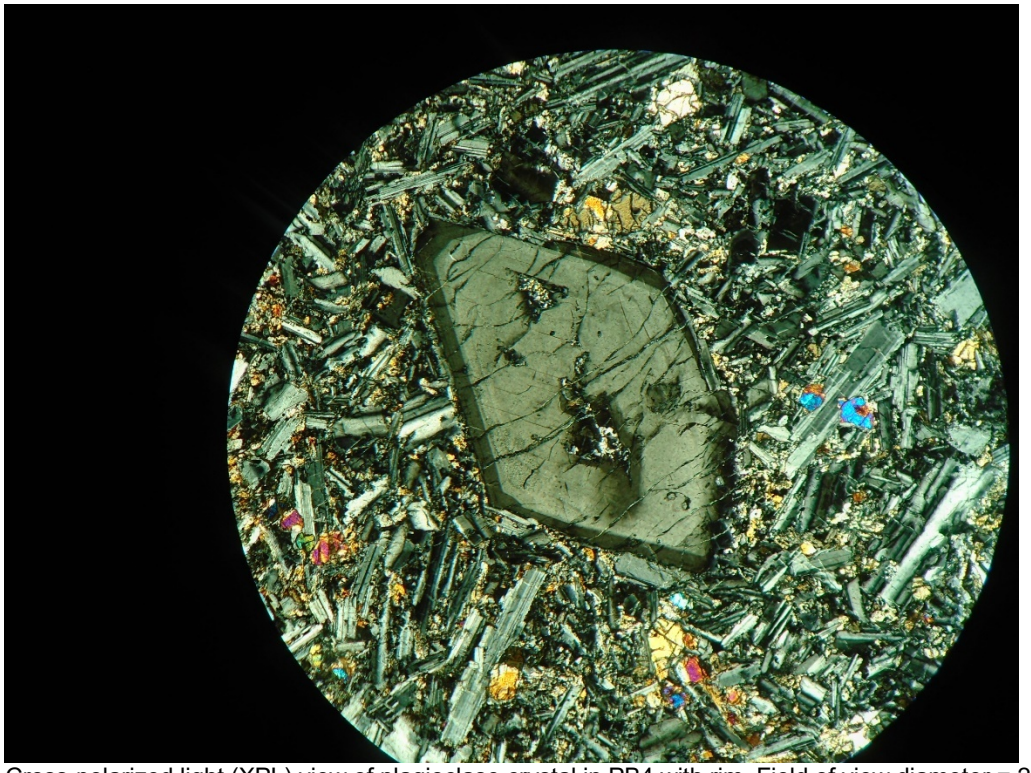

Figure 11. Cross-polarized light (XPL) view of plagioclase crystal in PB4 with rim. Field of view diameter = 2.5 mm.

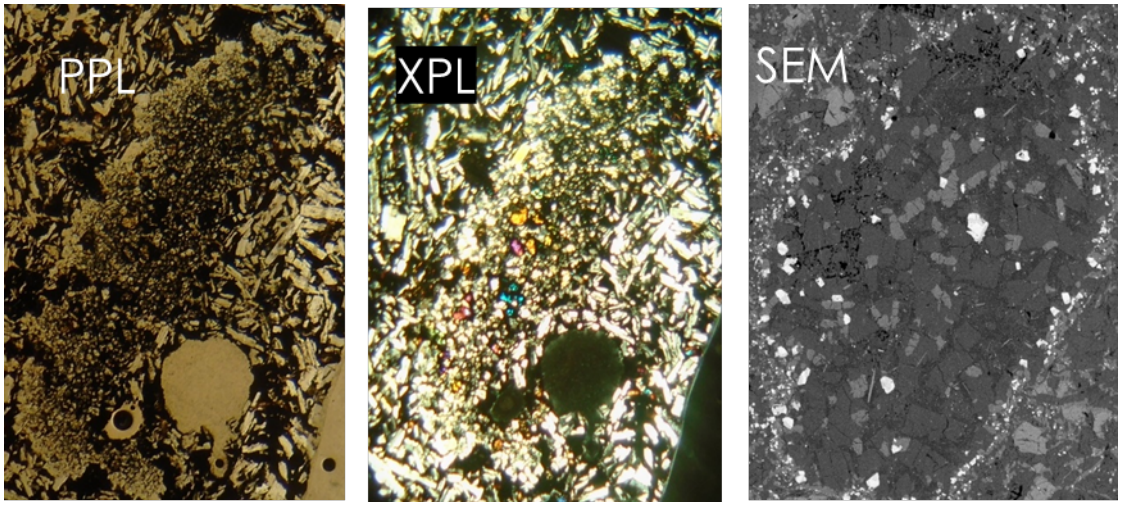

Figure 12. Three views of the PB2 glomerocryst. From left to right: plane polarized light (PPL), cross-polarized light (XPL), and scanning electron microscope (SEM). Glomerocryst is approximately 1 mm across and 4 mm long.

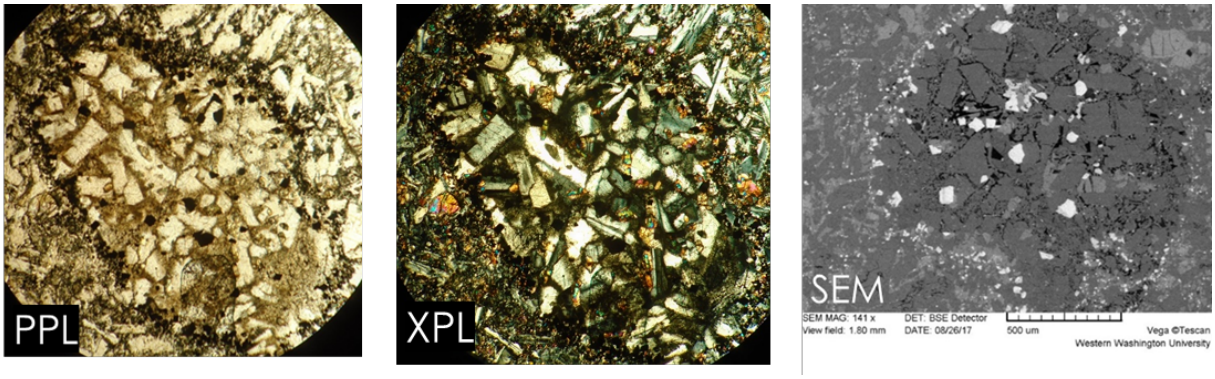

Figure 13. Three views of a PB4 glomerocryst. From left to right: plane polarized light (PPL), cross-polarized light (XPL), and scanning electron microscope (SEM). Note the reaction rim around the cluster.

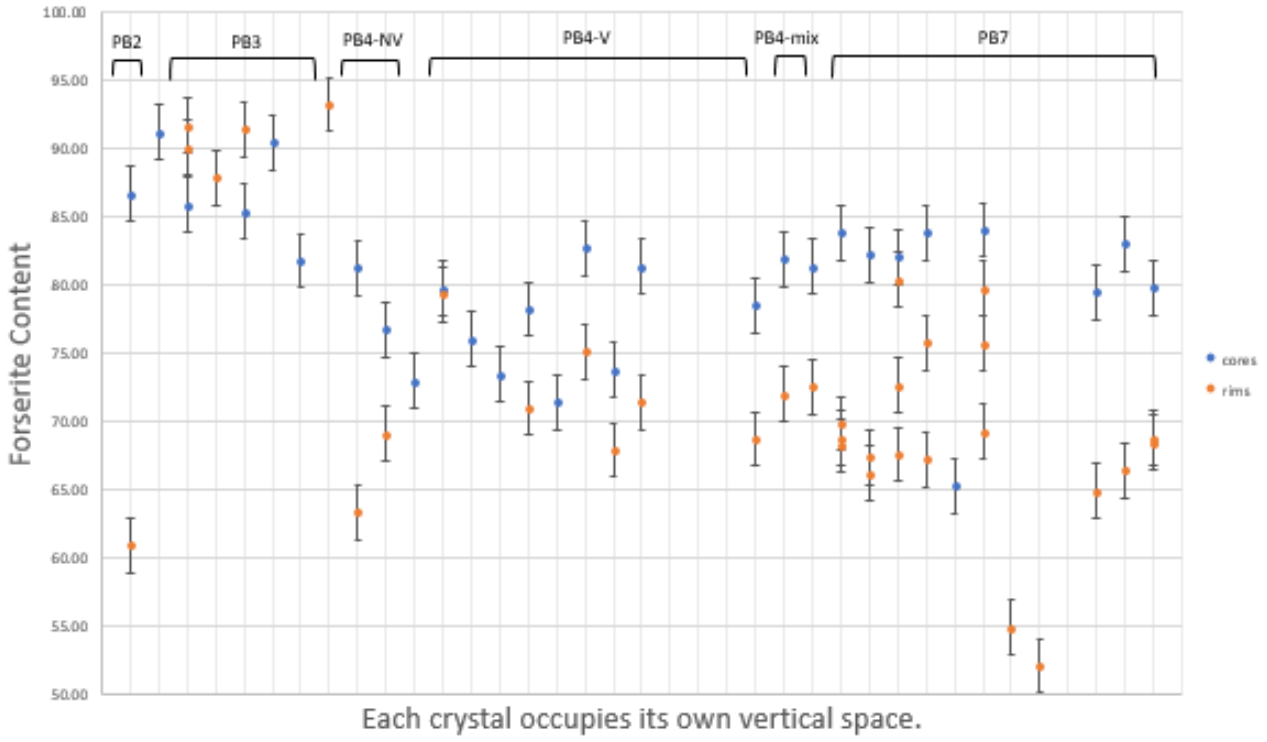

Figure 14. Core and rim analyses for Park Butte olivine crystals. Each vertical line represents one crystal. Note the generally higher forsterite contents in PB2 and PB3, representing population 2, and the low-Fo rims representing the rims of population 3.

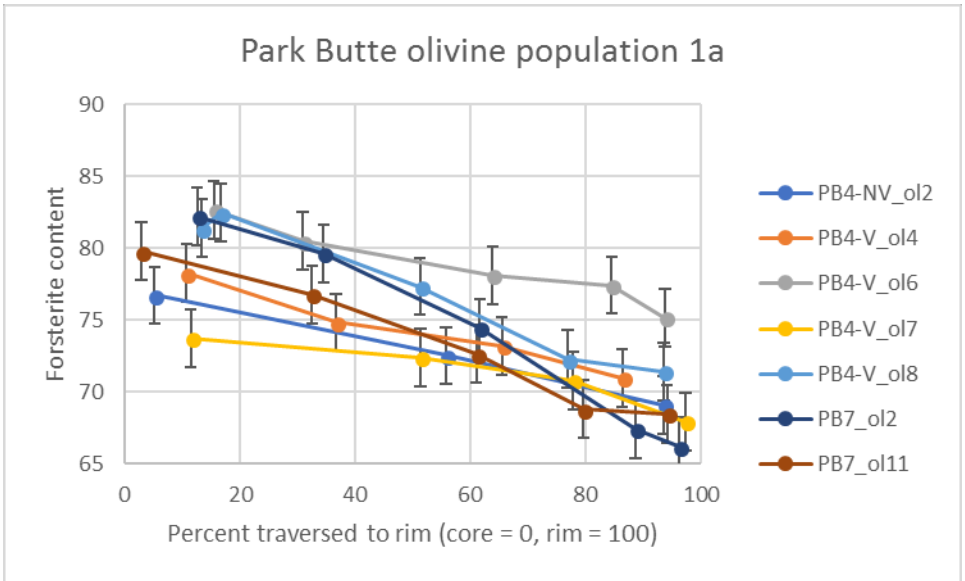

Figure 15. Core-to-rim traverses for Park Butte olivines placed in population 1a, which shows gradual normal zoning from core to rim.

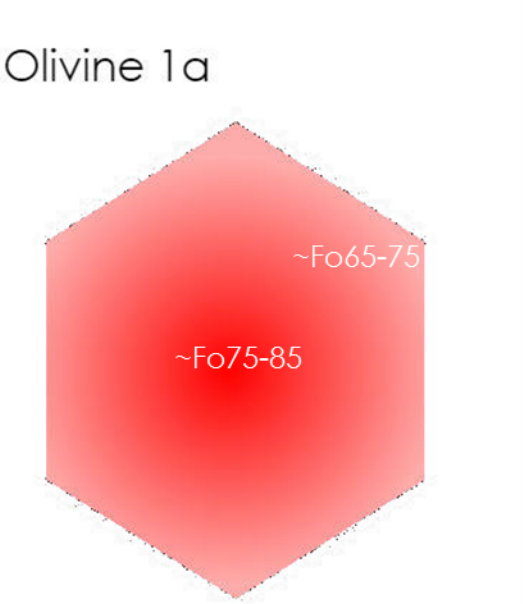

Figure 16. Schematic illustration of Park Butte olivine population 1a crystals. Darker red = more mafic.

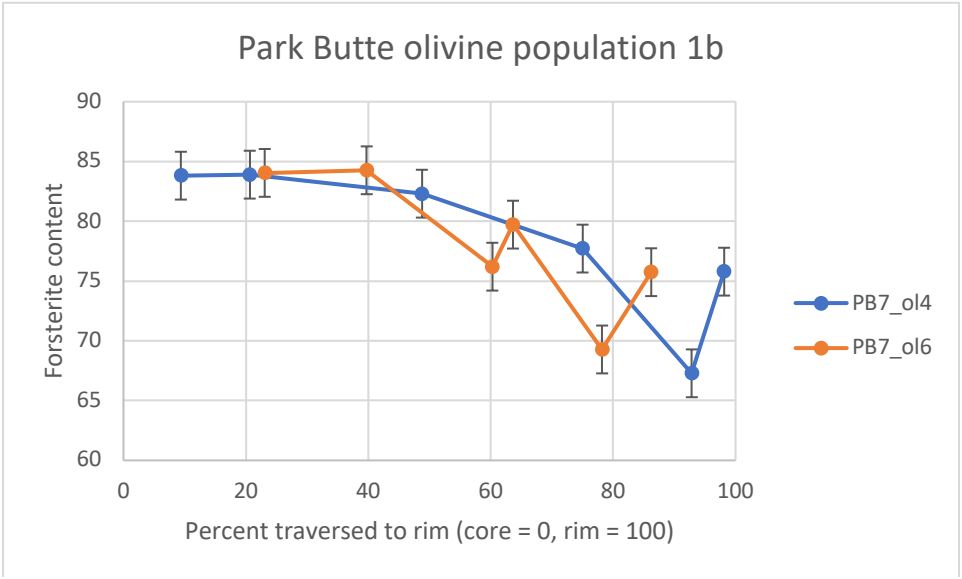

Figure 17. Core-to-rim traverses for Park Butte olivines placed in population 1b, which shows gradual normal zoning from core to rim punctuated by somewhat-oscillatory zoning patterns.

Figure 18. Schematic illustration of Park Butte olivine population 1b crystals. Darker red = more mafic.

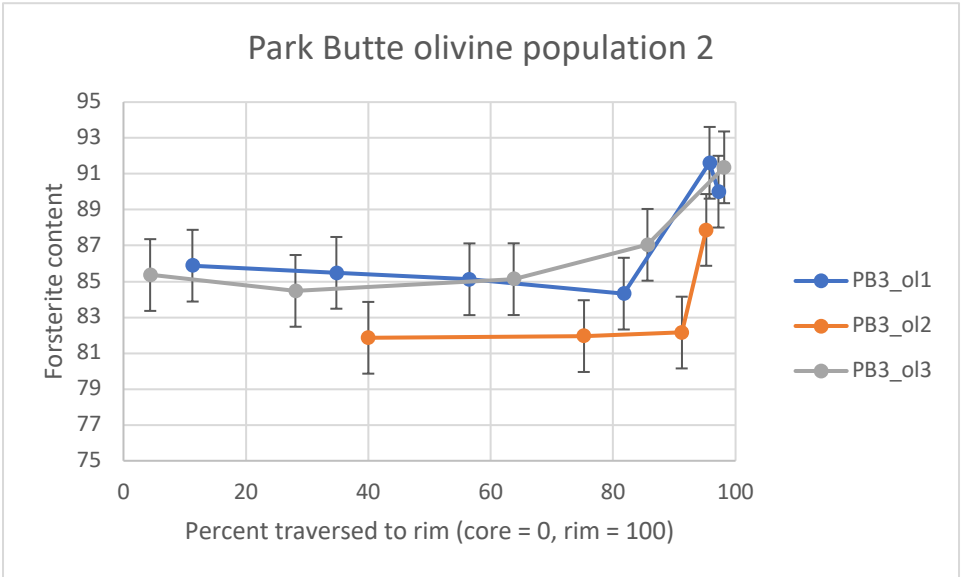

Figure 19. Core-to-rim traverses for Park Butte olivines placed in population 2, which shows sharp reverse zoning and slightly higher-Fo cores than populations 1 and 3.

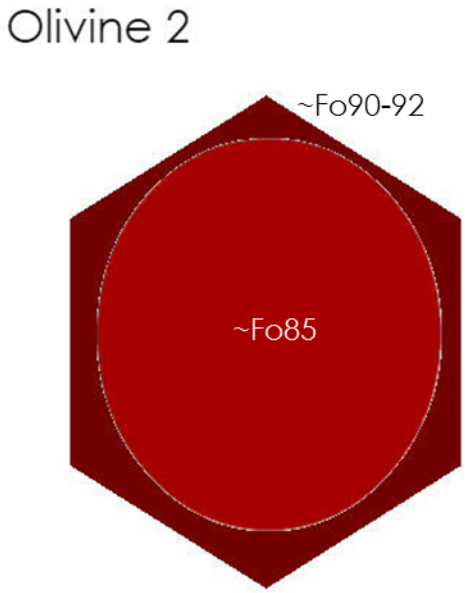

Figure 20. Schematic illustration of Park Butte olivine population 2 crystals. Darker red = more mafic.

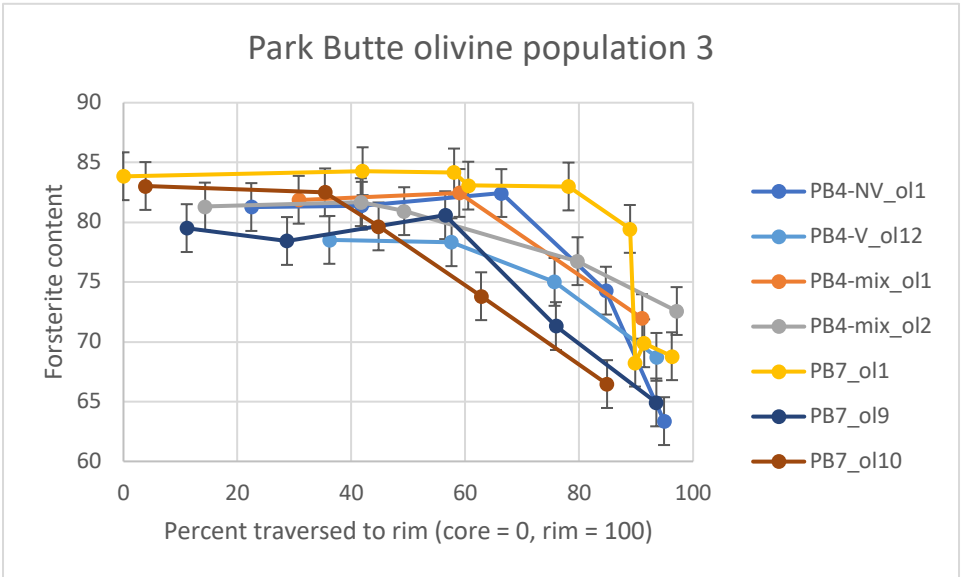

Figure 21. Core-to-rim traverses for Park Butte olivines placed in population 3, which shows very sharp normal zoning.

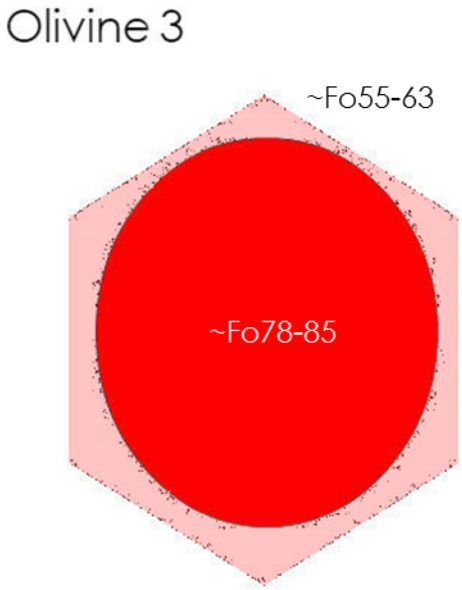

Figure 22. Schematic illustration of Park Butte olivine population 3 crystals. Darker red = more mafic.

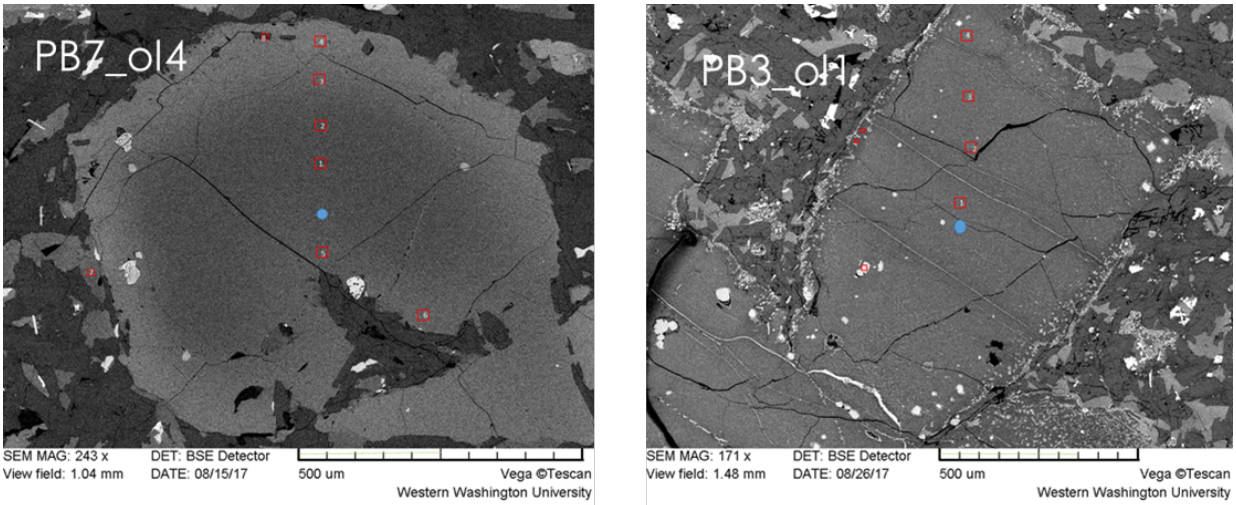

Figure 23. Park Butte flow: normally zoned crystal on left, reversely zoned crystal on right. Note the difference in rim thickness (images are same scale).

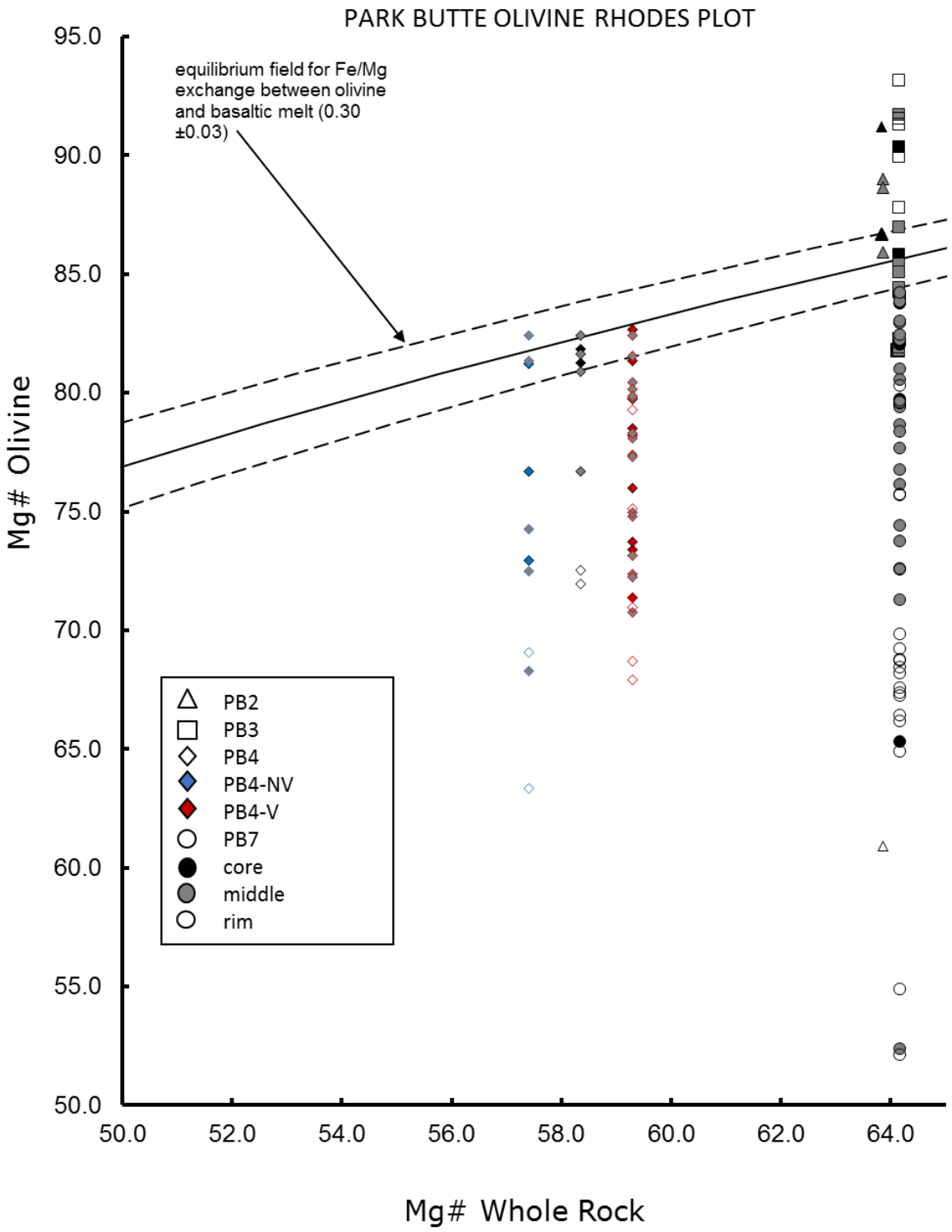

Figure 24. Park Butte olivine Rhodes plot showing equilibrium states for olivine crystals.

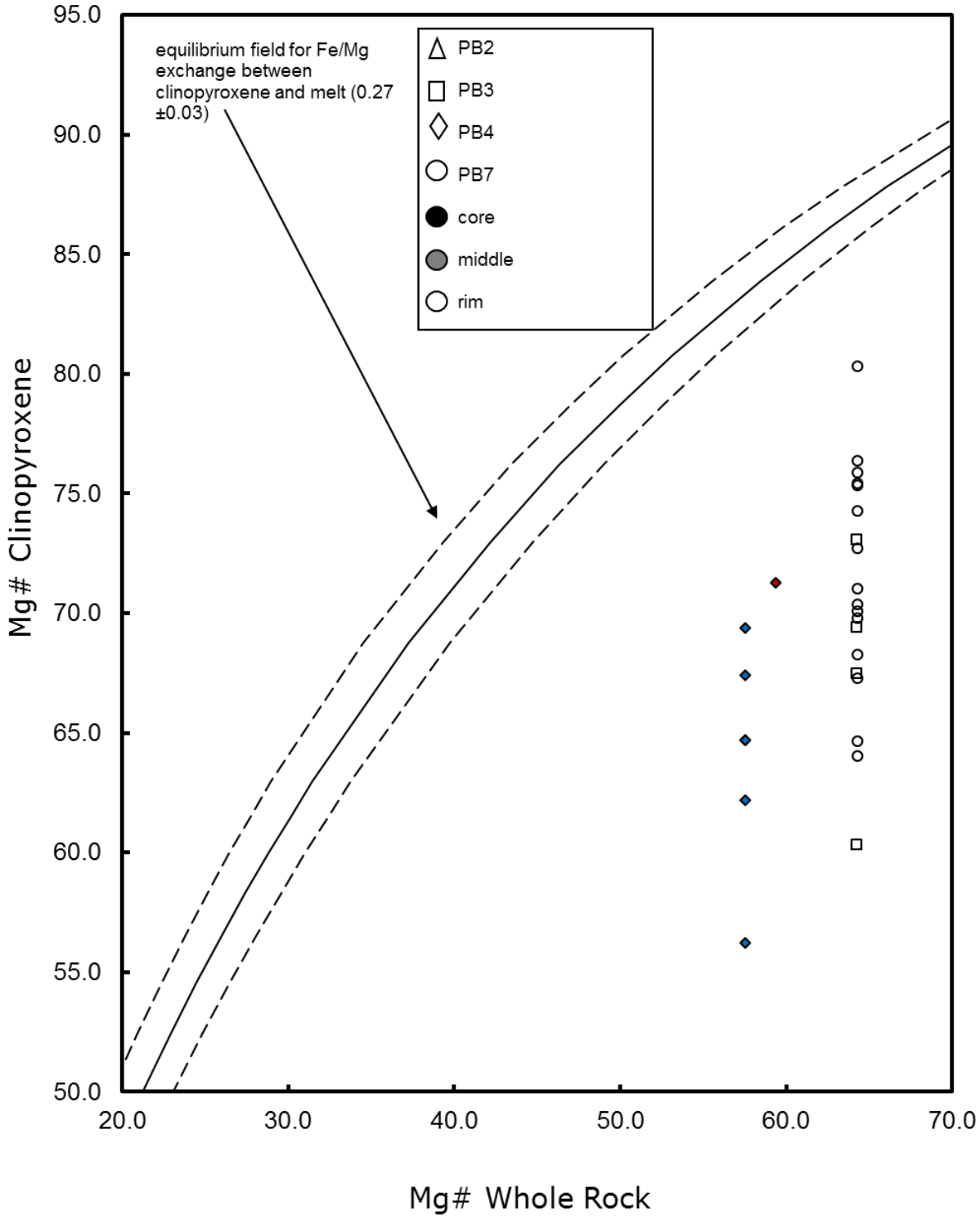

Figure 25. Park Butte clinopyroxene rhodes plot showing equilibrium states for clinopyroxene crystals.Not shown in legend: blue diamond = PB4-NV, red diamond = PB4-V.

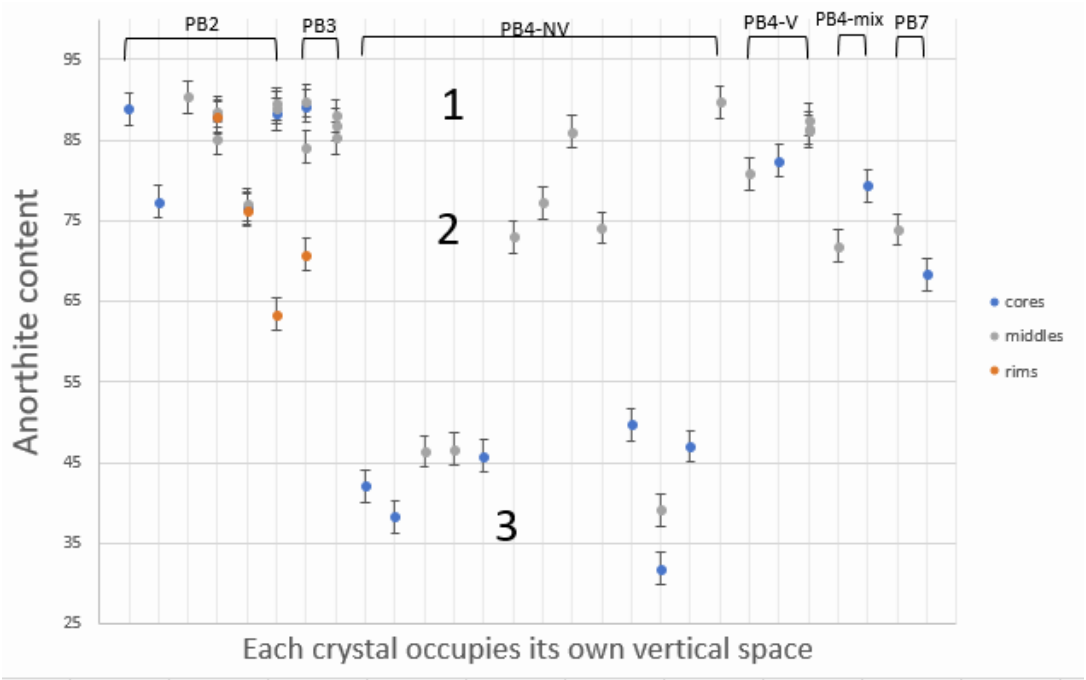

Figure 26. Core, middle, and rim analyses for Park Butte plagioclase crystals. Each vertical line represents one crystal. Populations are labelled.

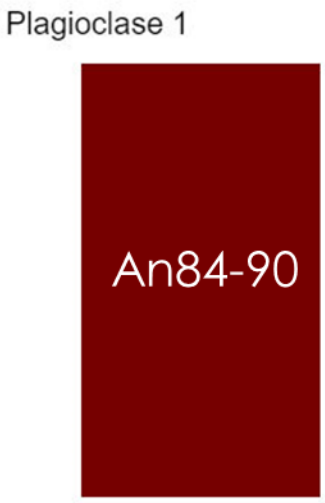

Figure 27. Schematic illustration of Park Butte plagioclase population 1 crystals. Darker red = more mafic; this population has the highest anorthite content.

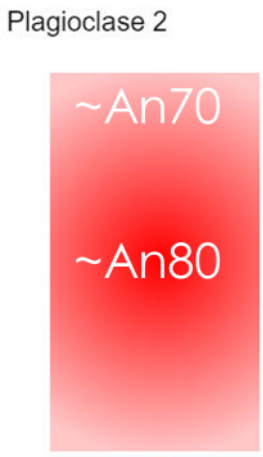

Figure 28. Schematic illustration of Park Butte plagioclase population 2 crystals. Darker red = more mafic. Because those crystals in population 2 with core and rim data available displayed normal zoning, this is shown on the illustration.

Figure 29. Schematic illustration of Park Butte population 3 crystals. These are colored blue to represent their much more felsic composition relative to the other plagioclase populations.

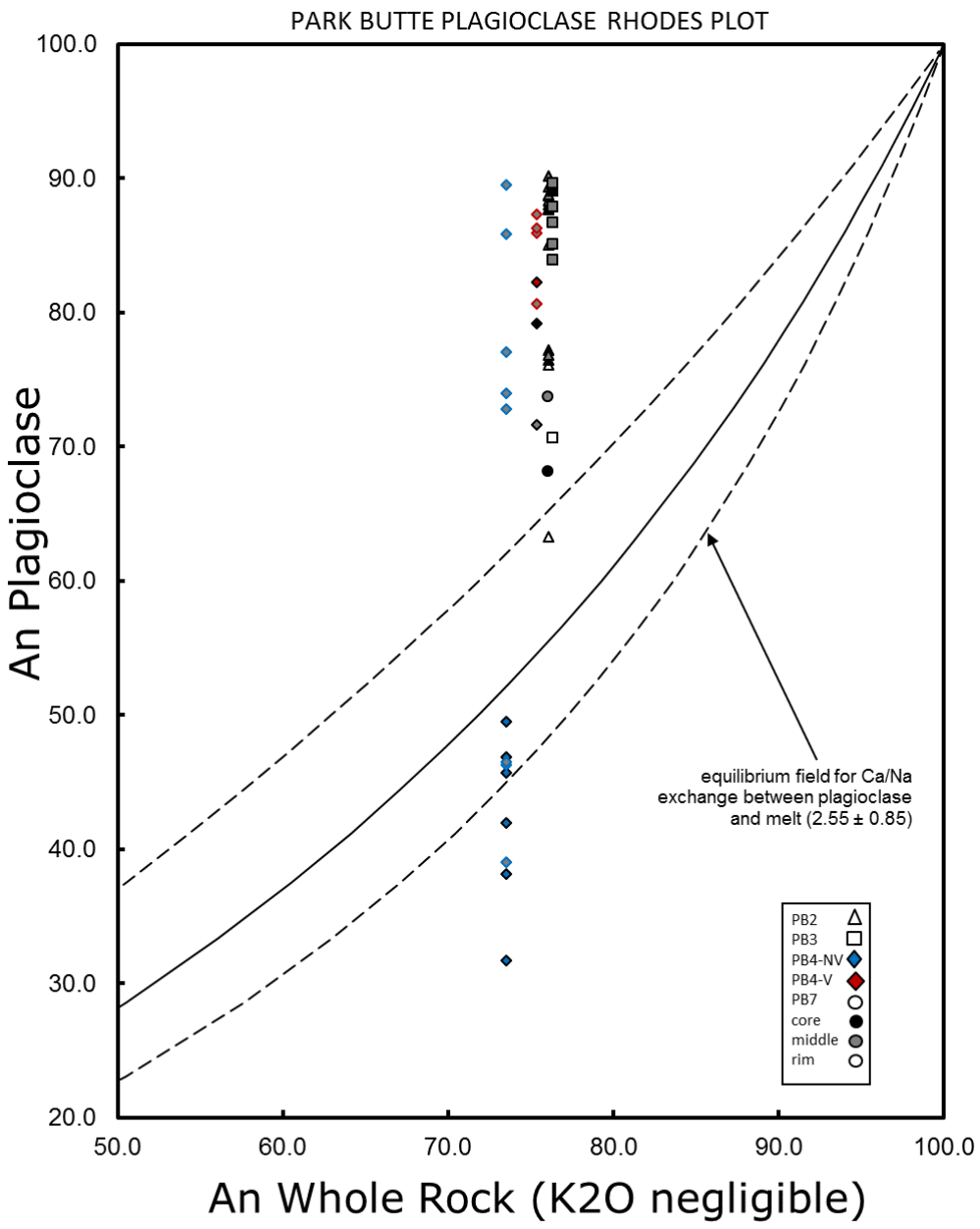

Figure 30. Park Butte plagioclase Rhodes plot showing equilibrium states for plagioclase crystals.

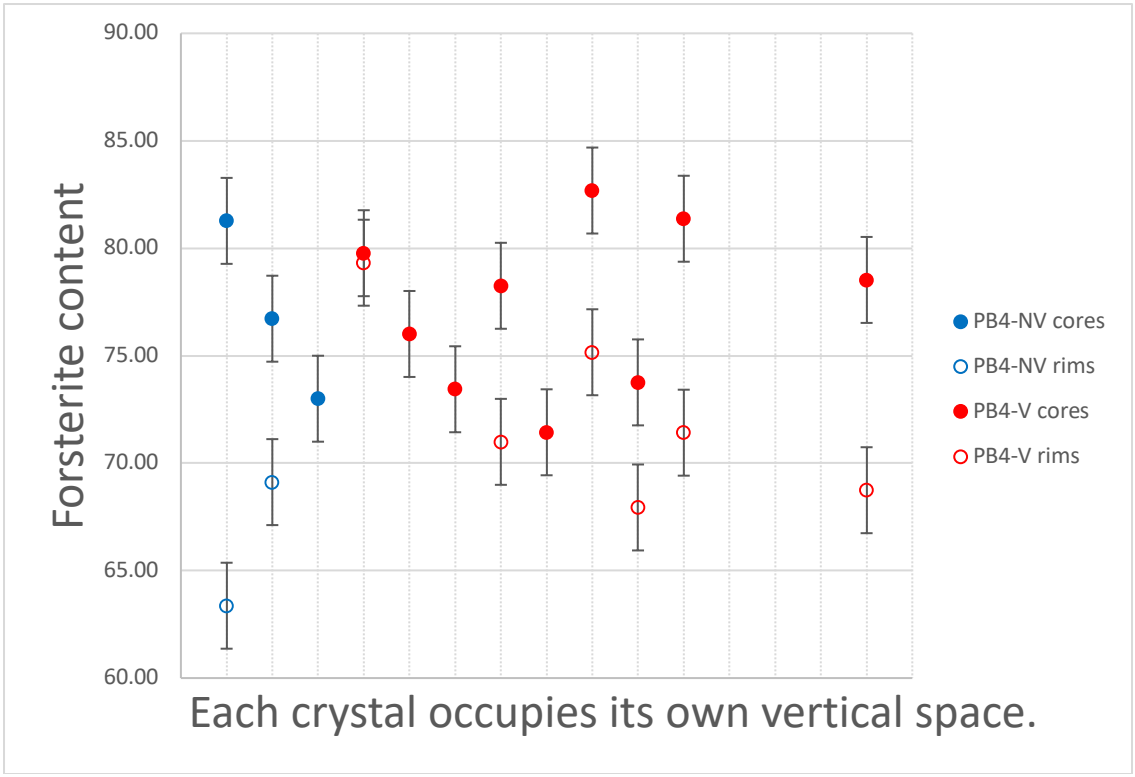

Figure 31. Core and rim analyses for sample PB4 olivine crystals. Each vertical line represents one crystal.

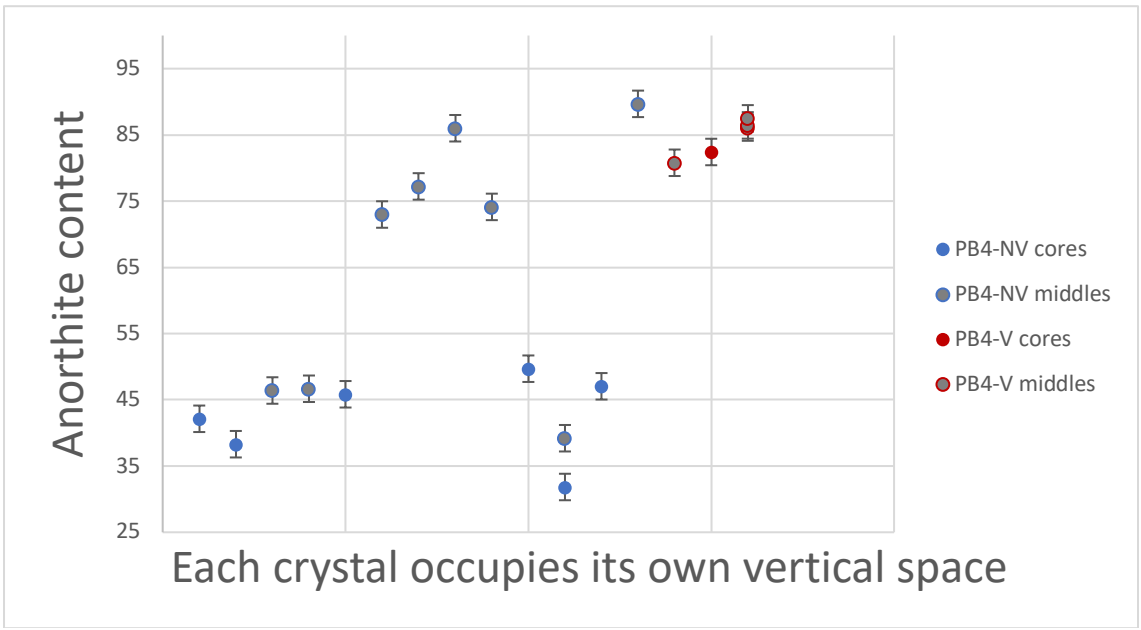

Figure 32. Core, middle, and rim analyses for sample PB4 plagioclase crystals. Each vertical line represents one crystal.

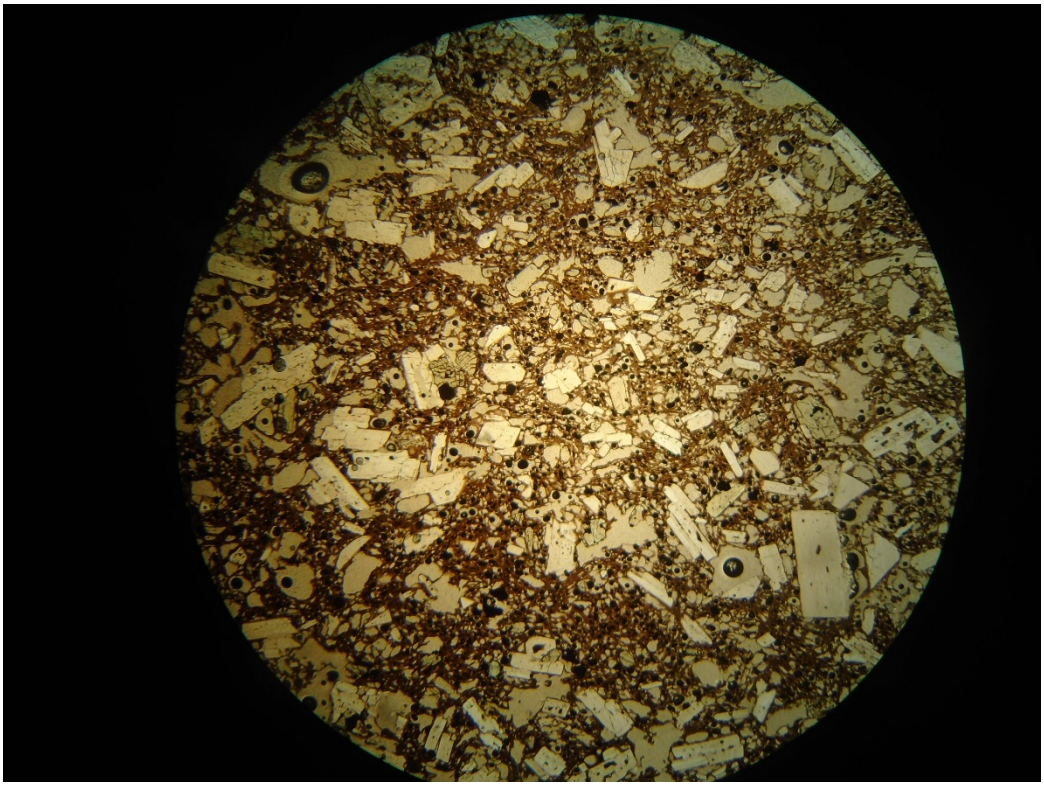

Figure 33. Plane-polarized light (PPL) image showing highly vesicular holohyaline matrix of sample LS6. Note the brown color of the glass, which typically indicates basaltic glass composition. Field of view diameter = 1 cm.

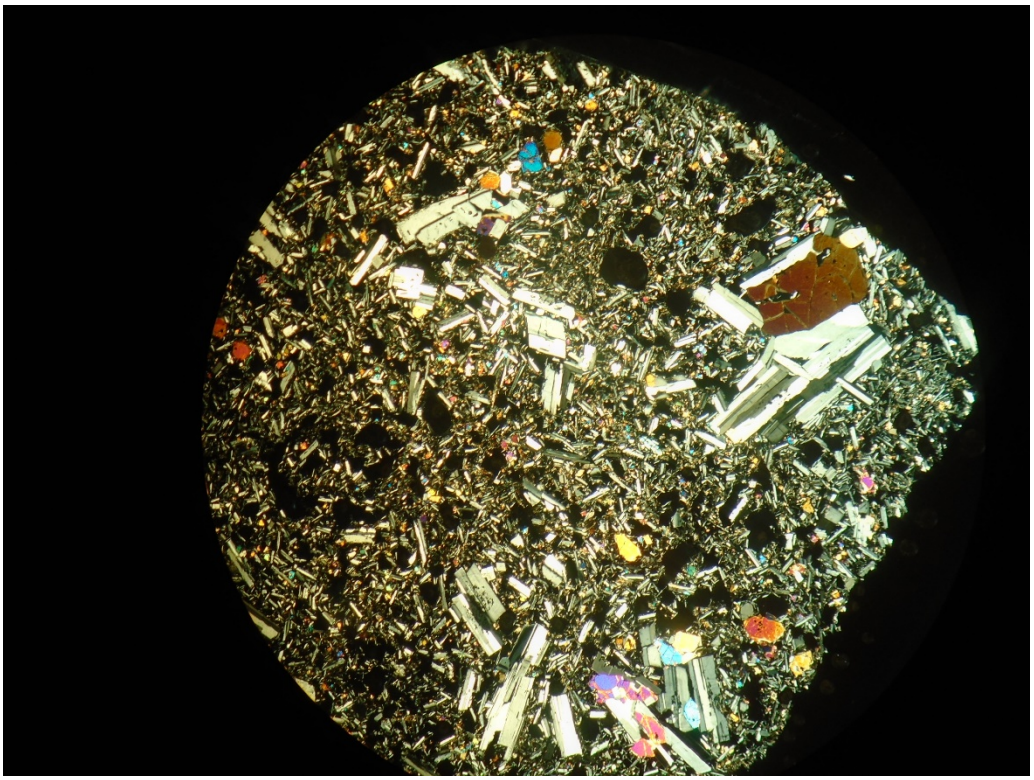

Figure 34. Glomeroporphyritic texture observed in sample LS2. Maximum field of view diameter = 1 cm.

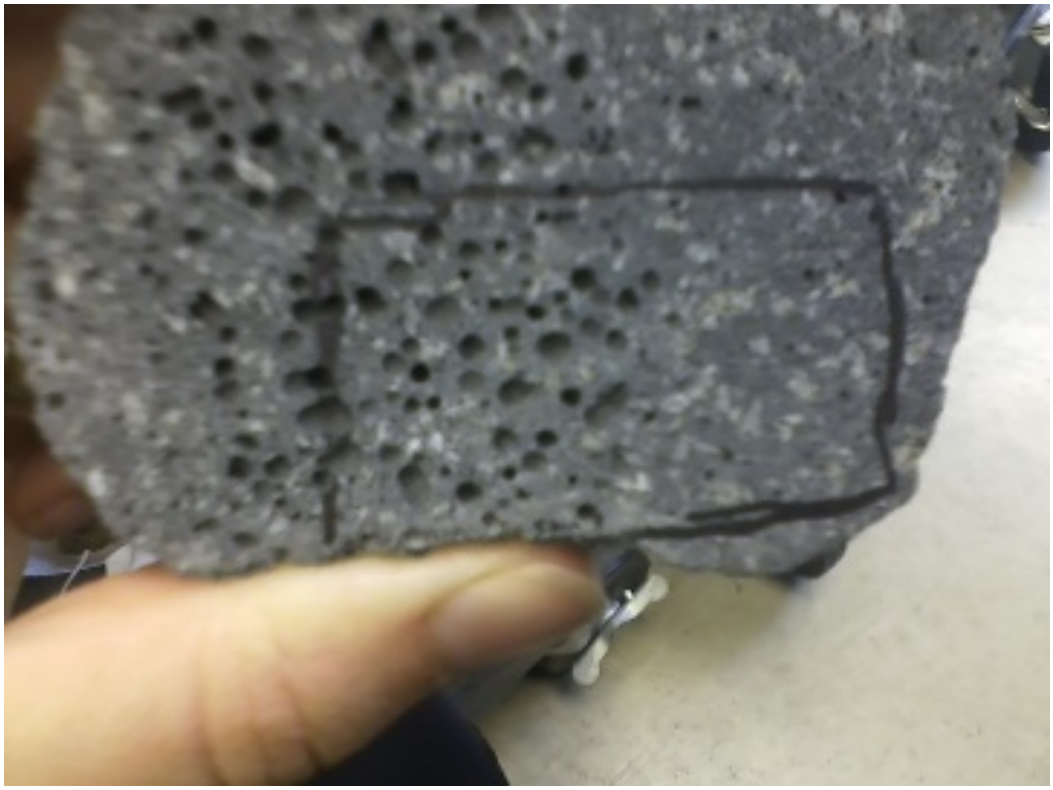

Figure 35. Hand sample of LS2 showing distinct contrast between vesicular (left end of rectangle) and much-less-vesicular (right end of rectangle) components. Long edge of rectangle is approximately 3.5 cm.

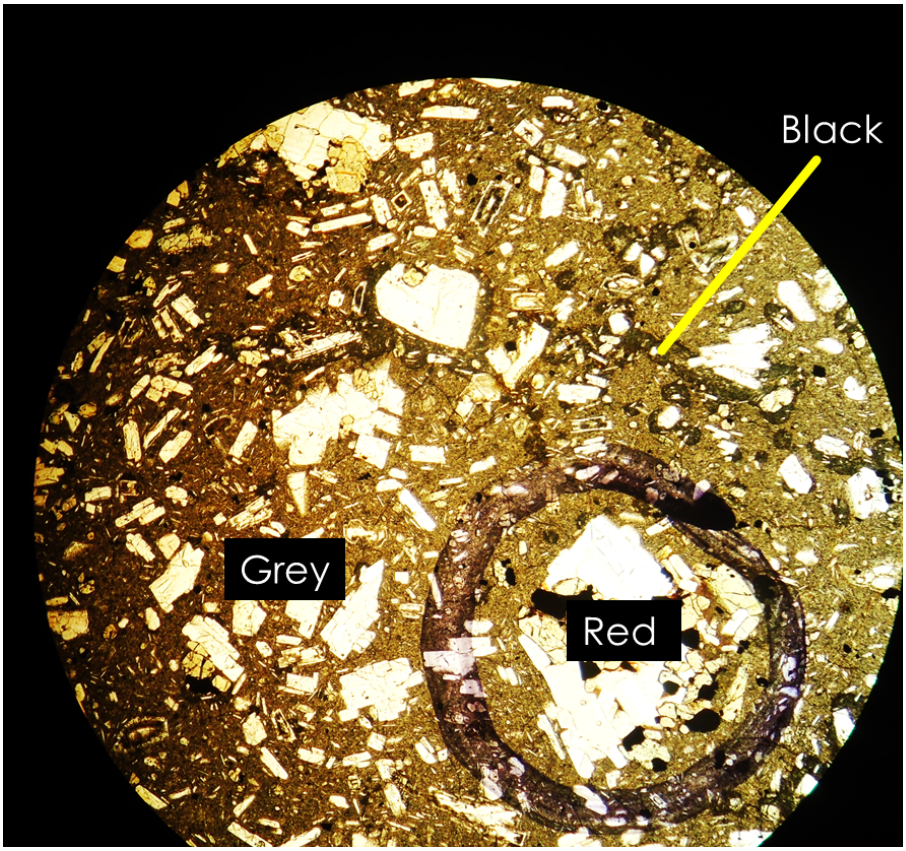

Figure 36. Plane-polarized light (PPL) view of three matrix colors in sample LS5. Red is circled in permanent marker. Black appears as sinuous elongate shapes. Grey is massive and dominates the matrix. Field of view diameter = 1cm.

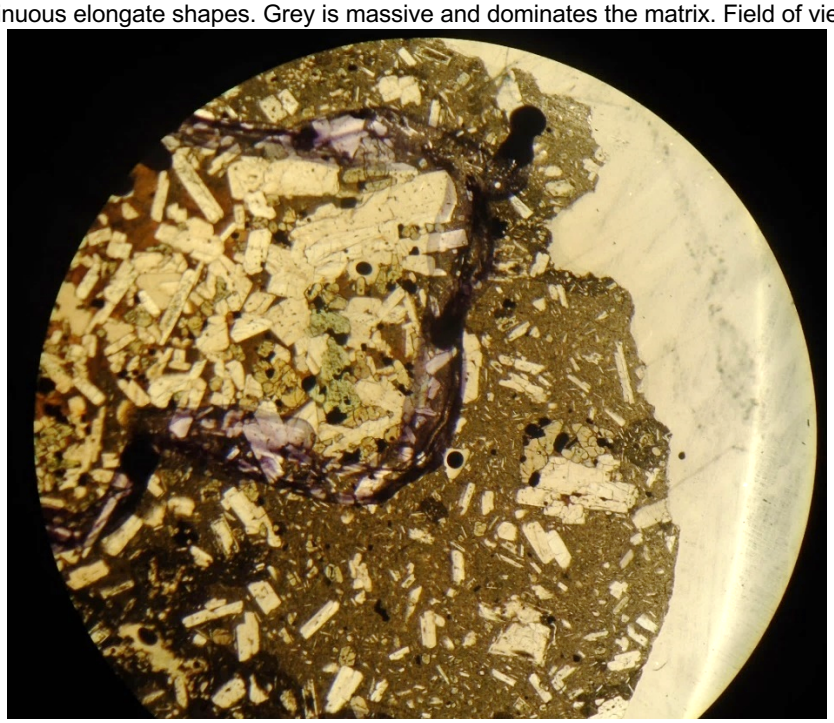

Figure 37. Plane-polarized light (PPL) view of red component circled in marker juxtaposed against grey component. Note the distinct difference in matrix color, as well as the difference in phenocryst abundance. Field of view diameter = 1cm.

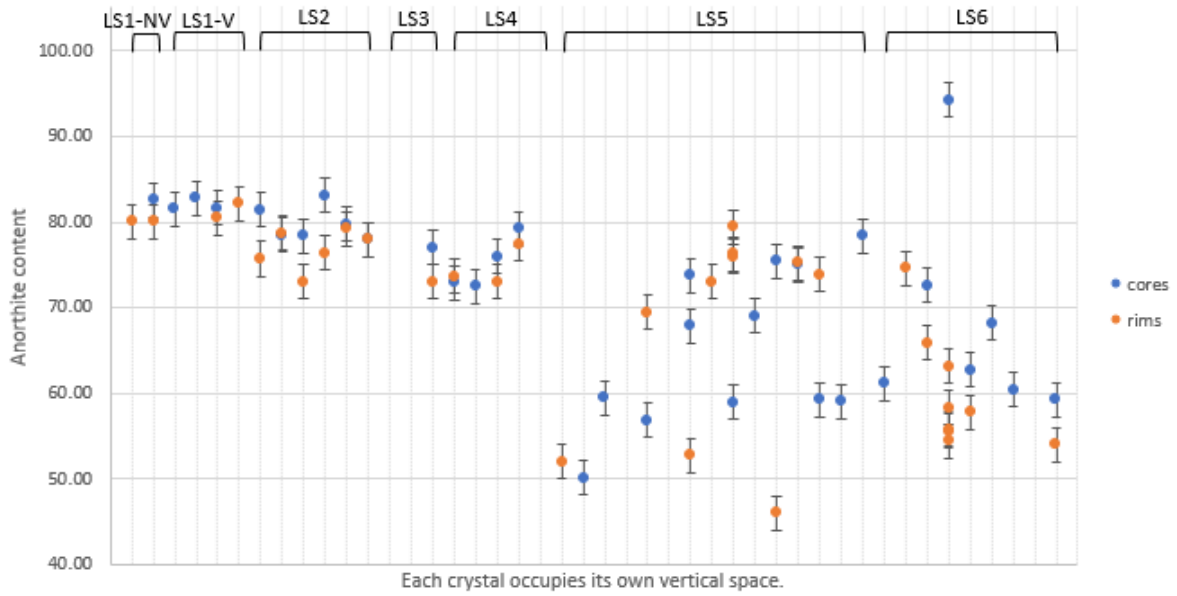

Figure 38. Lake Shannon plagioclase core and rim data. Each crystal occupies its own vertical space. Extent of each rock sample is indicated in brackets in the upper area of the plot.

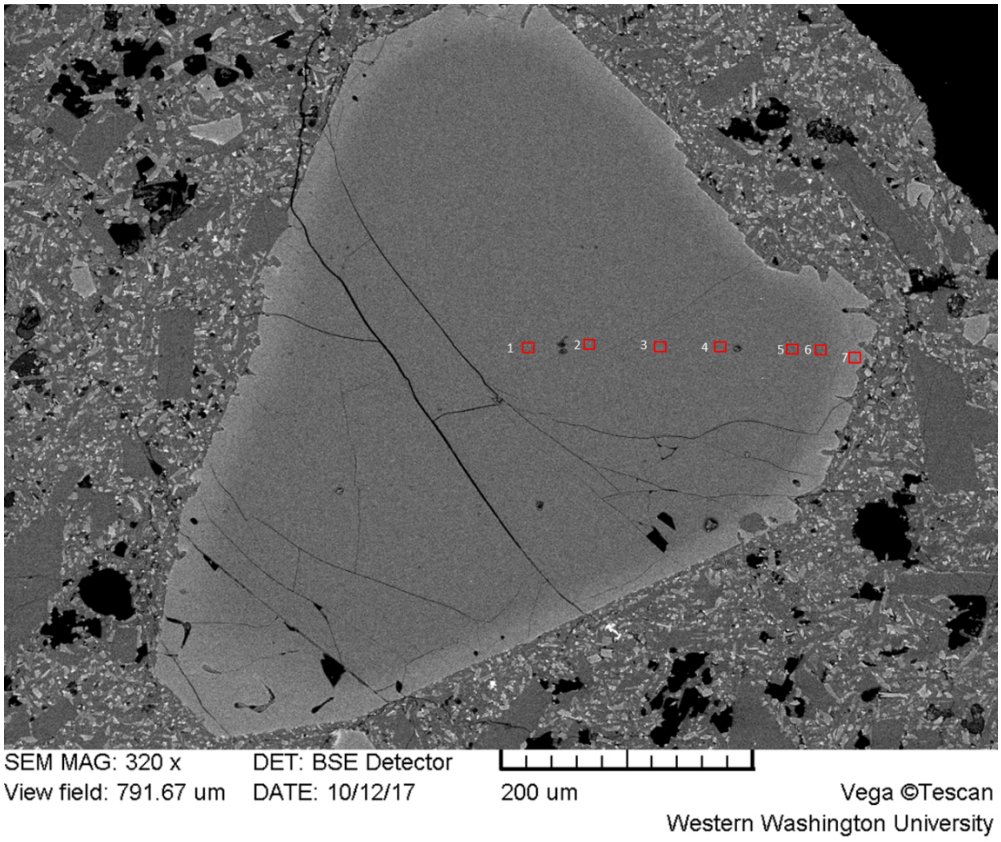

Figure 39. SEM image of LS4_ol1, an example of a normally zoned olivine crystal in the Lake Shannon flow. Note the sudden decrease in forsterite content very proximal to the rim, indicated by a lightening in color.

Figure 40. Schematic illustration of Lake Shannon population 1 olivine crystals.

Figure 41. Schematic illustration of Lake Shannon population 2 olivine crystals. Darker red = more mafic.

Figure 42. Schematic illustration of Lake Shannon population 3 olivine crystals. Darker red = more mafic. Note the slightly less mafic core and rim compared to population 2 (Figure 39).

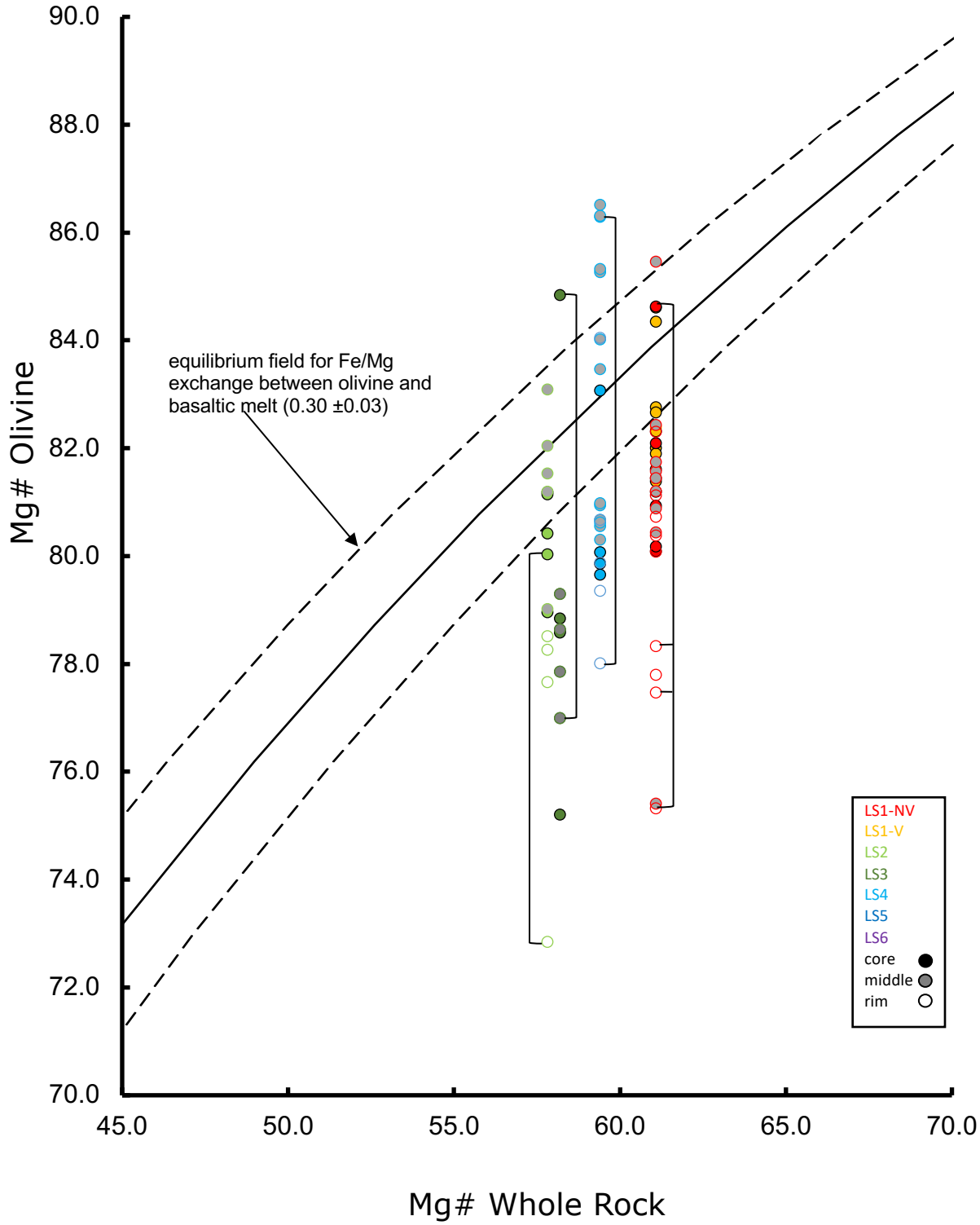

Figure 43. Olivine Rhodes plot showing equilibrium states of Lake Shannon olivine data. Brackets ([or]) connect cores and rims of zoned olivines.

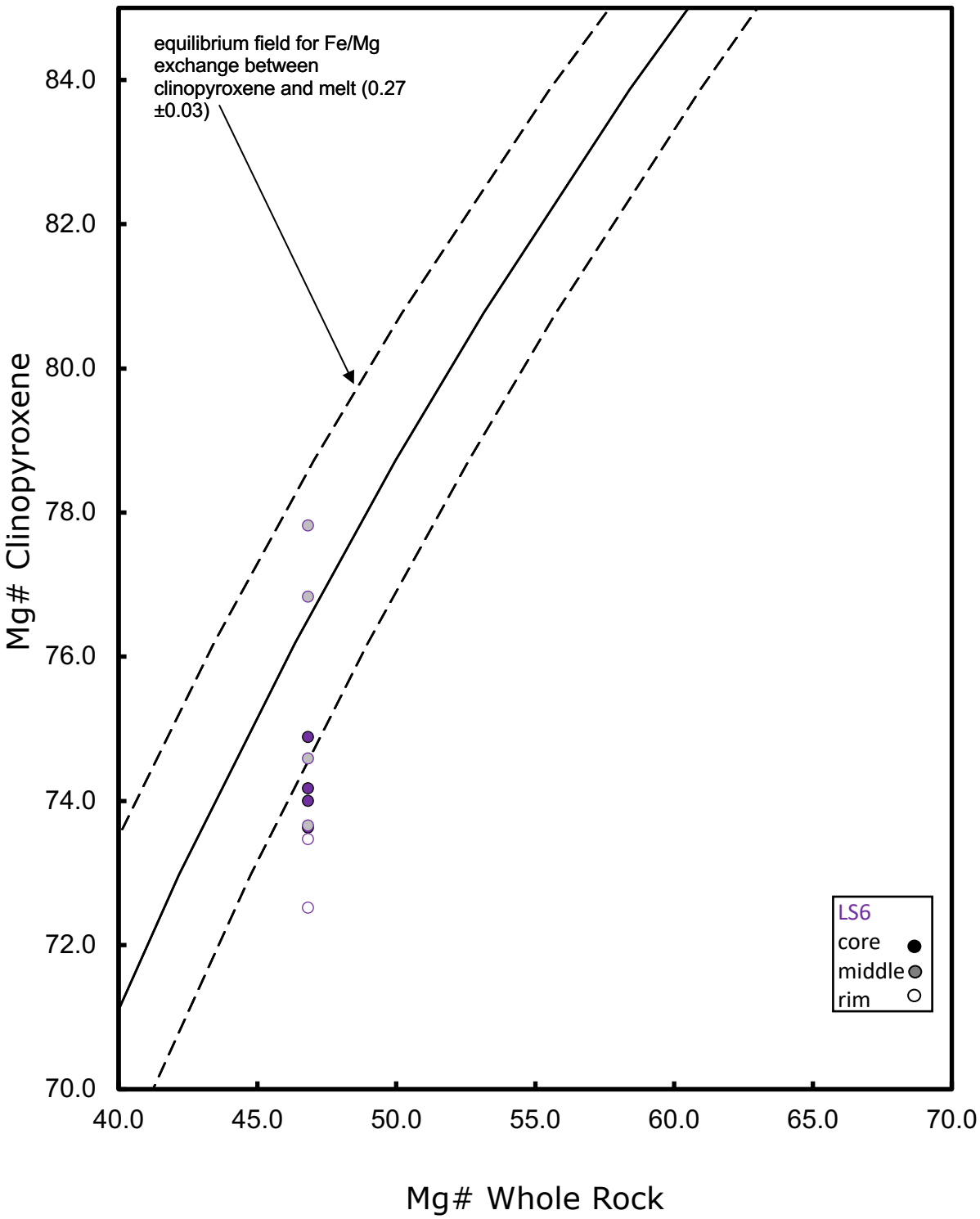

Figure 44. Clinopyroxene Rhodes plot showing equilibrium states of Lake Shannon clinopyroxene data. Note that although clinopyroxenes were also observed in LS5, no whole rock data was collected for the sample.

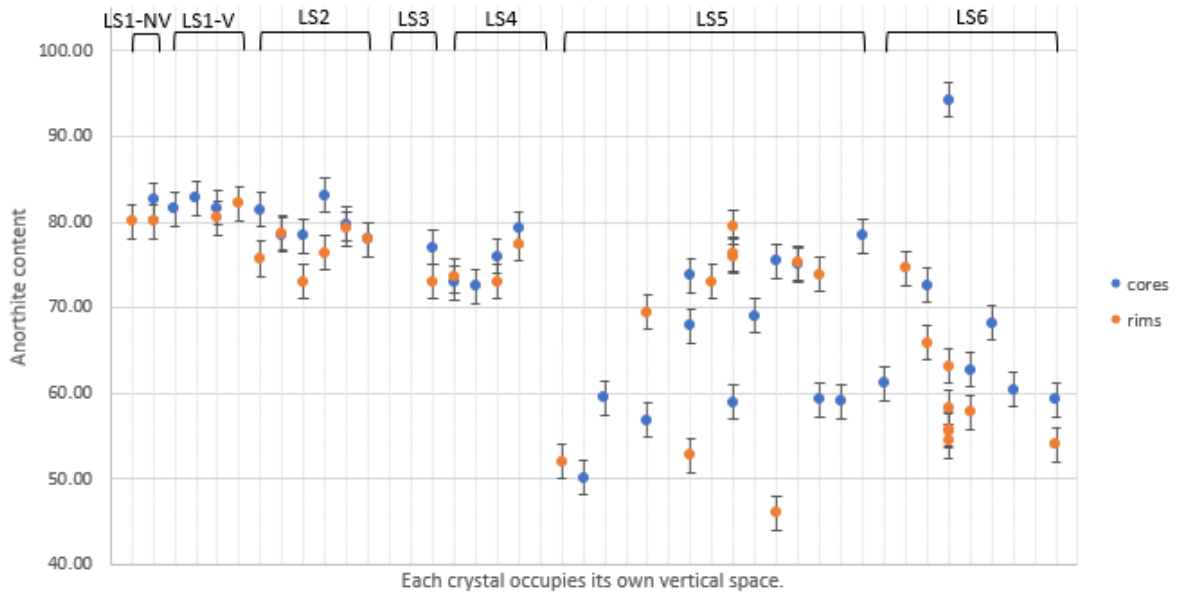

Figure 45. Lake Shannon plagioclase core and rim data. Each crystal occupies its own vertical space. Extent of each rock sample is indicated in brackets in the upper area of the plot.

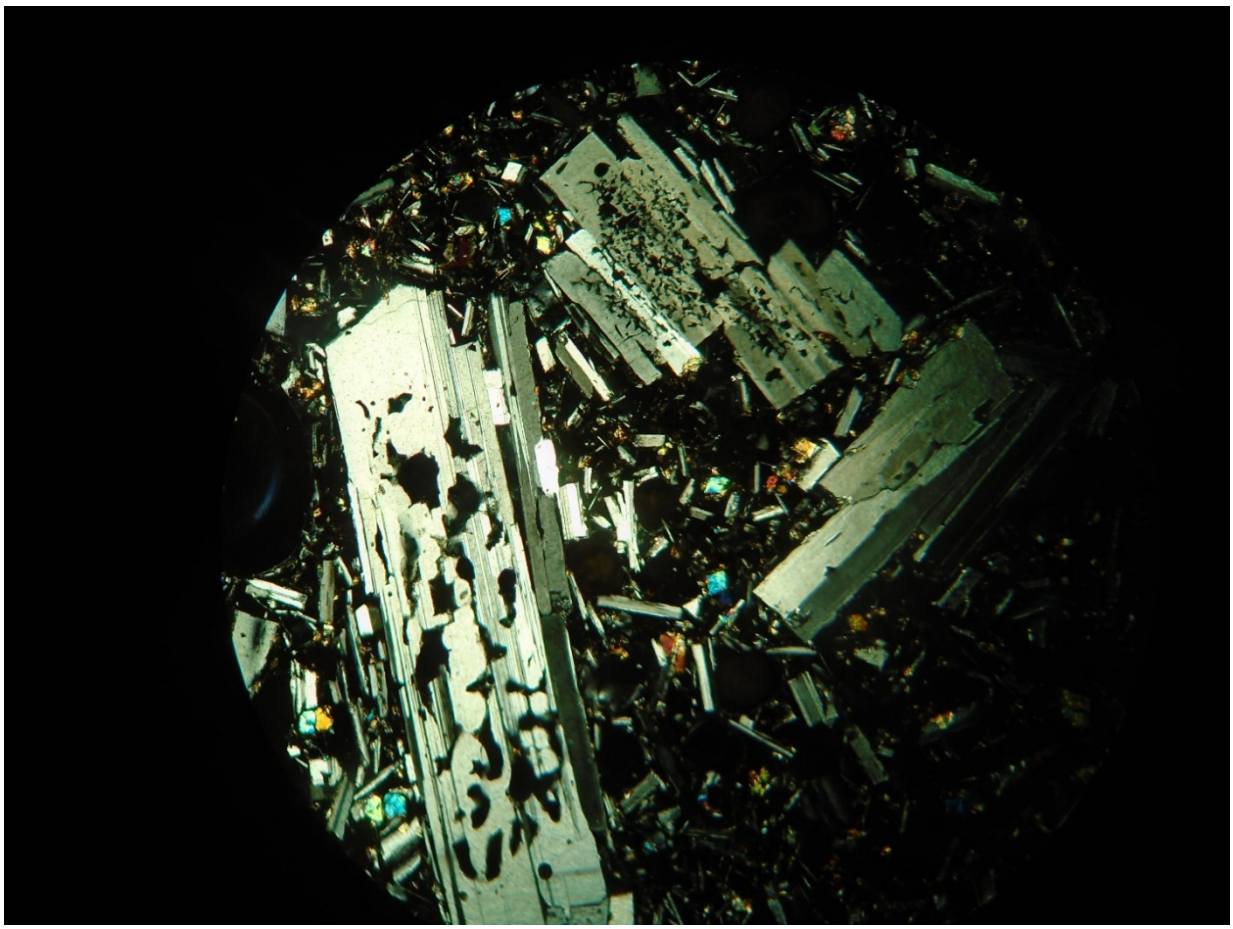

Figure 46. Cross-polarized light (XPL) view of sieved plagioclase crystals in LS1-V. Field of view diameter 2.5mm.

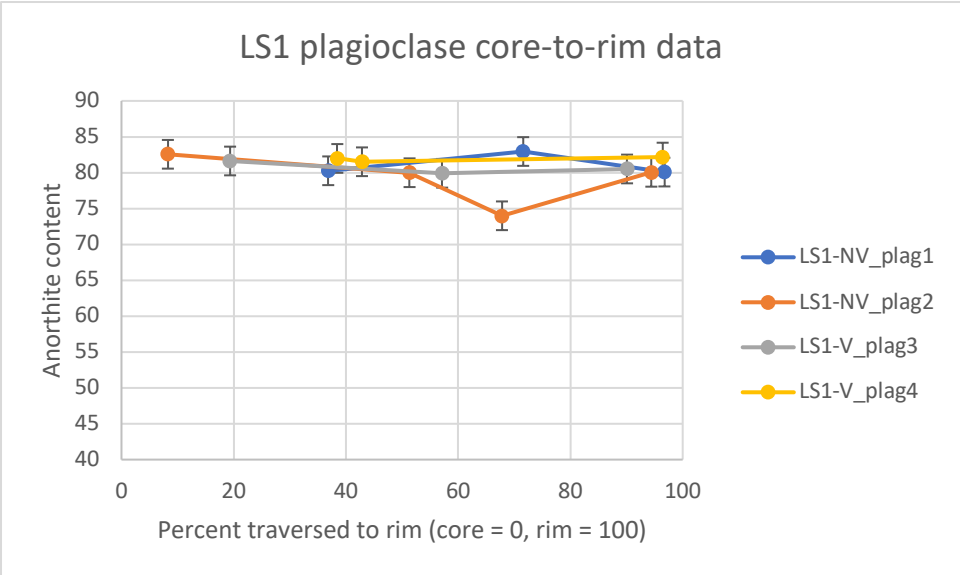

Figure 47. Core-to-rim traverses for LS1-NV and LS1-V plagioclase crystals.

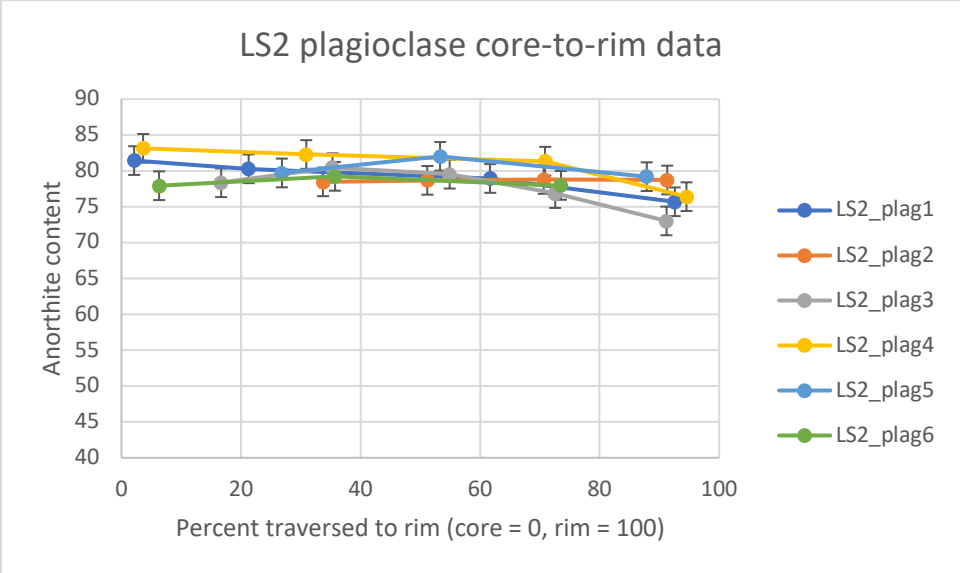

Figure 48. Core-to-rim traverses for LS2 plagioclase crystals. Note the more-or-less stable anorthite contents. Had enough time to diffuse with the “big magma body”

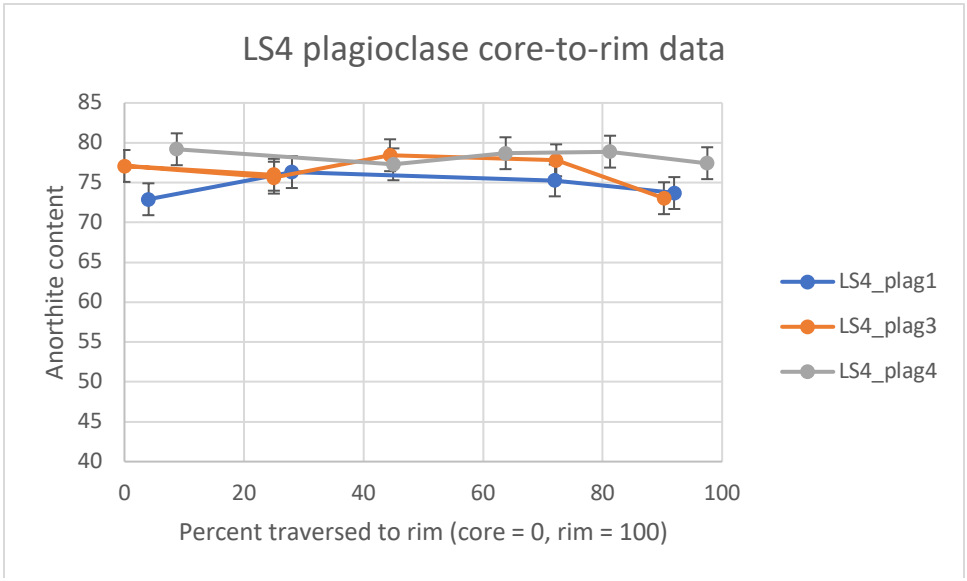

Figure 49. Core-to-rim traverses for LS4 plagioclase crystals.

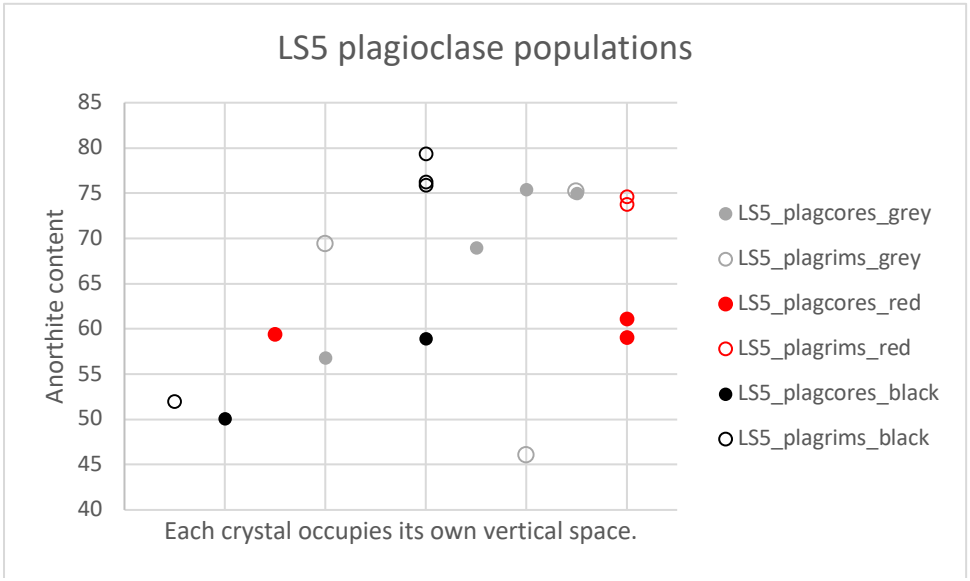

Figure 50. Color-coded diagram showing LS5 plagioclase data. Note the reversely zoned crystals found in all three magma components.

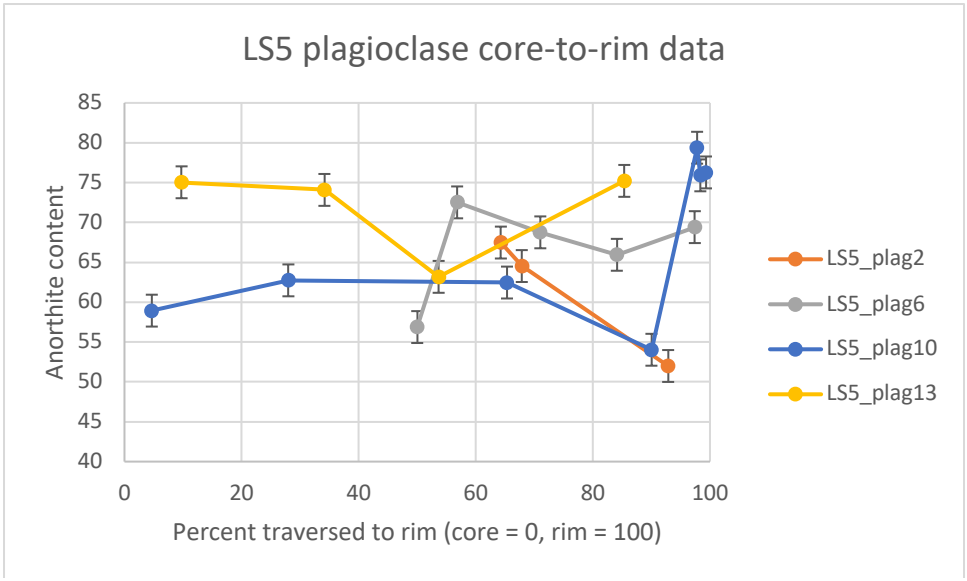

Figure 51. Core-to-rim traverses for LS4 plagioclase crystals.

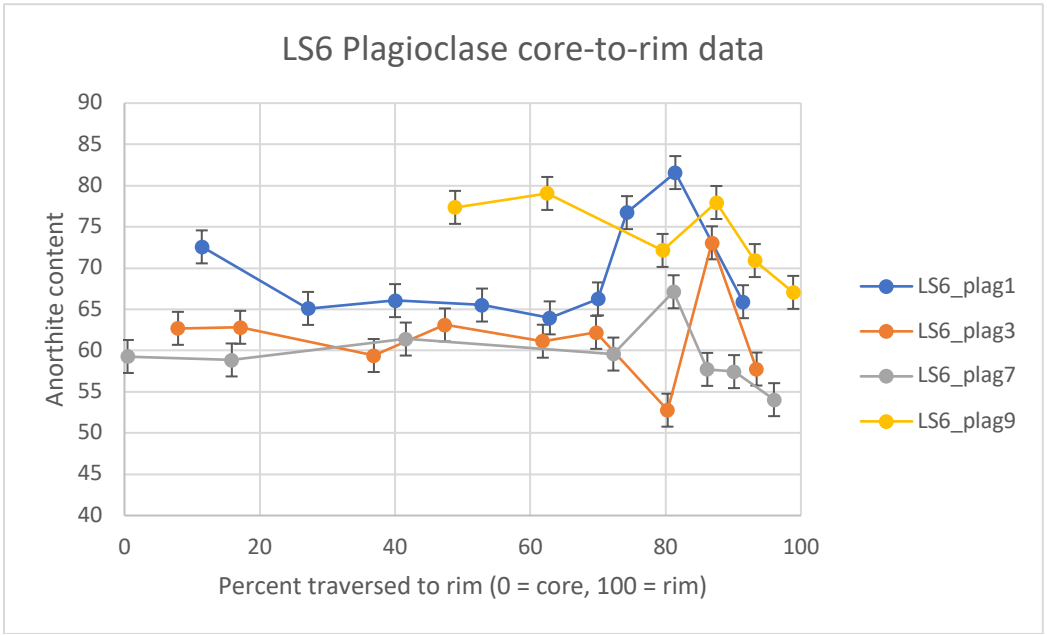

Figure 52. Core-to-rim traverses for LS6 plagioclase crystals. Note the jump upward in anorthite content at 80-90% traversed followed by a sharp decrease.

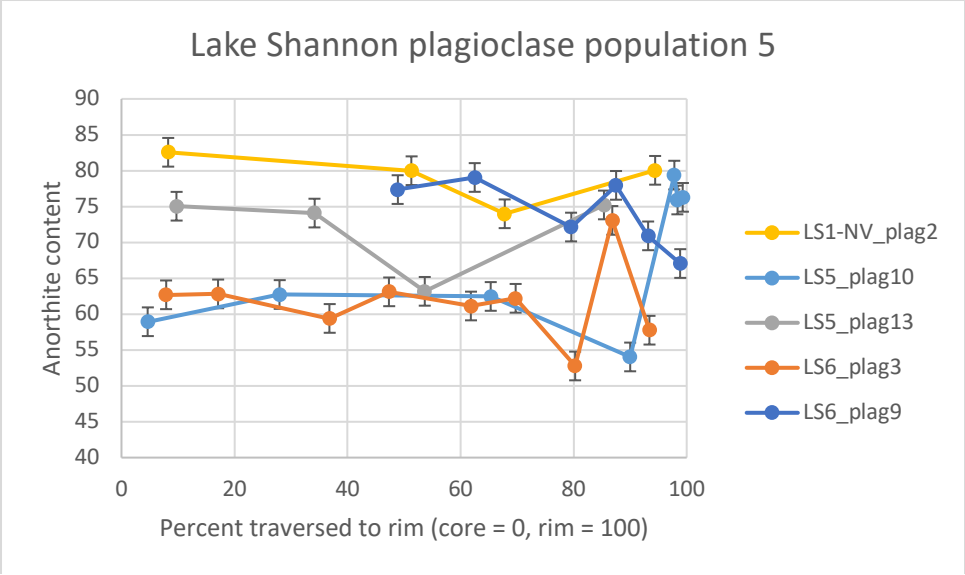

Figure 53. Lake Shannon plagioclase population 5 core-to-rim traverses. Note the decrease in anorthite content at 68-90% crystallization and subsequent increase.

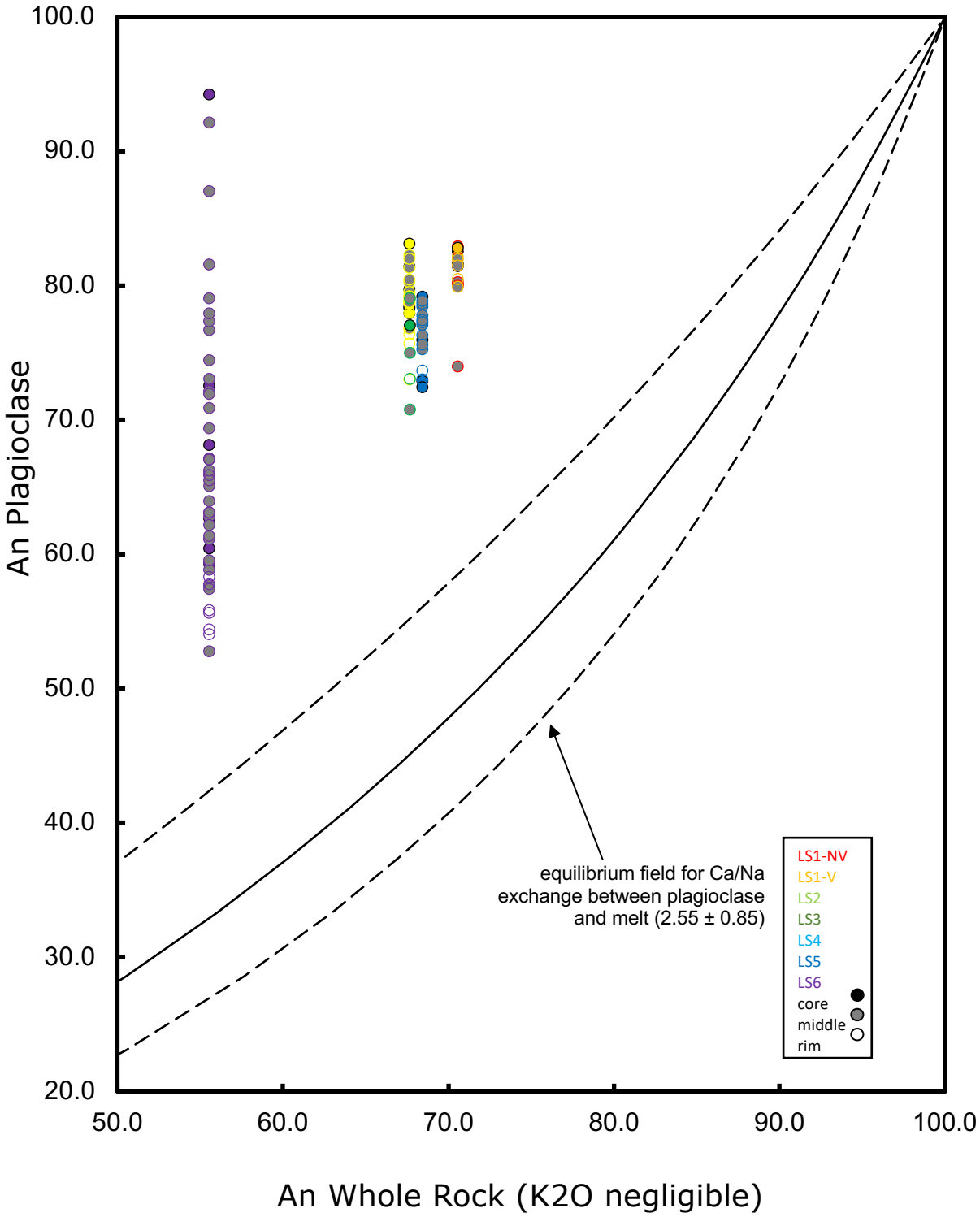

Figure 54. Plagioclase Rhodes plot showing equilibrium states of Lake Shannon plagioclase data. Note that with the Kd = 2.55 ± 0.85, all plagioclase data falls above the equilibrium field.

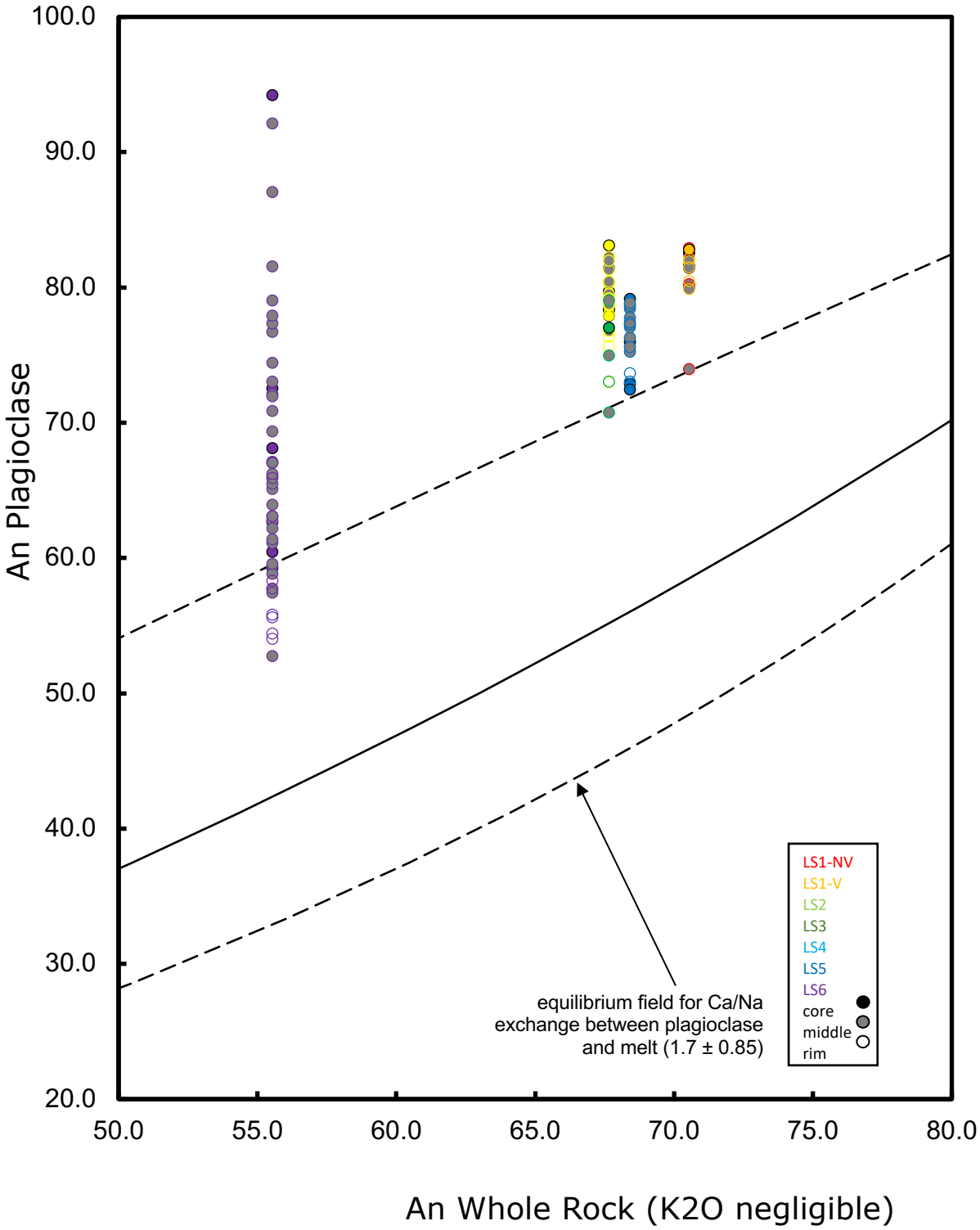

Figure 55. Plagioclase Rhodes plot showing equilibrium states of Lake Shannon plagioclase data. Note that with the Kd = 1.7 ± 0.85, all plagioclase data falls above the equilibrium field.

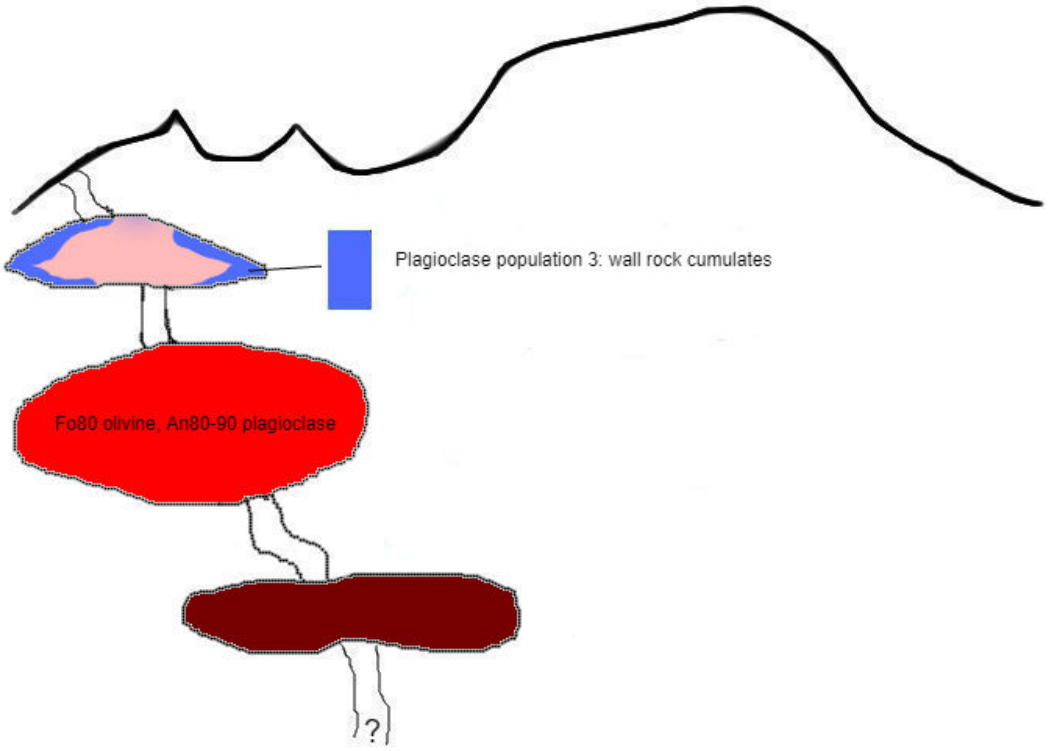

Figure 56. First possible scenario for Park Butte flow begins with olivine and plagioclase forming in equilibrium with their host magma: Fo80 olivine, An80-90 plagioclase.

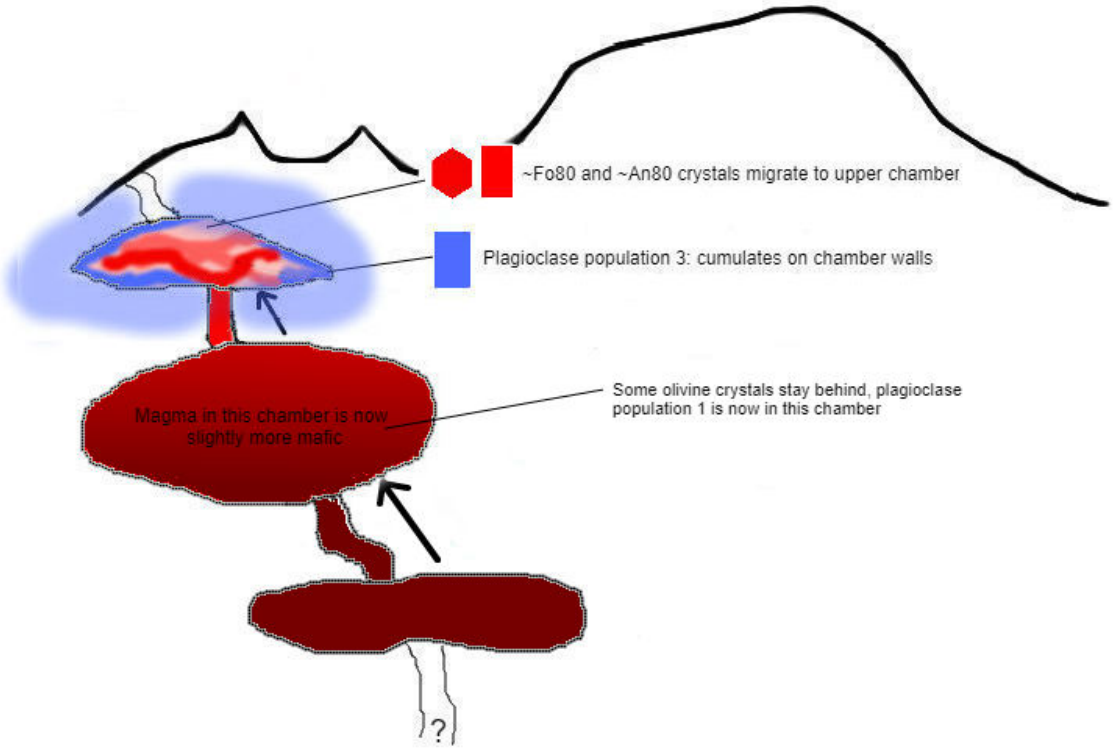

Figure 57. Injection of the middle chamber by a more mafic magma from below causes upward migration and displaces some of the olivine and plagioclase crystals into an upper, less mafic magma chamber. This injection causes the middle chamber to become slightly more mafic, and the olivine and plagioclase crystals which are left behind are in equilibrium with this new magma. The magma which migrates to the upper chamber mingles and partially mixes with the upper chamber magma, forming zoning patterns similar to those observed in the upper chamber in Figure 61,

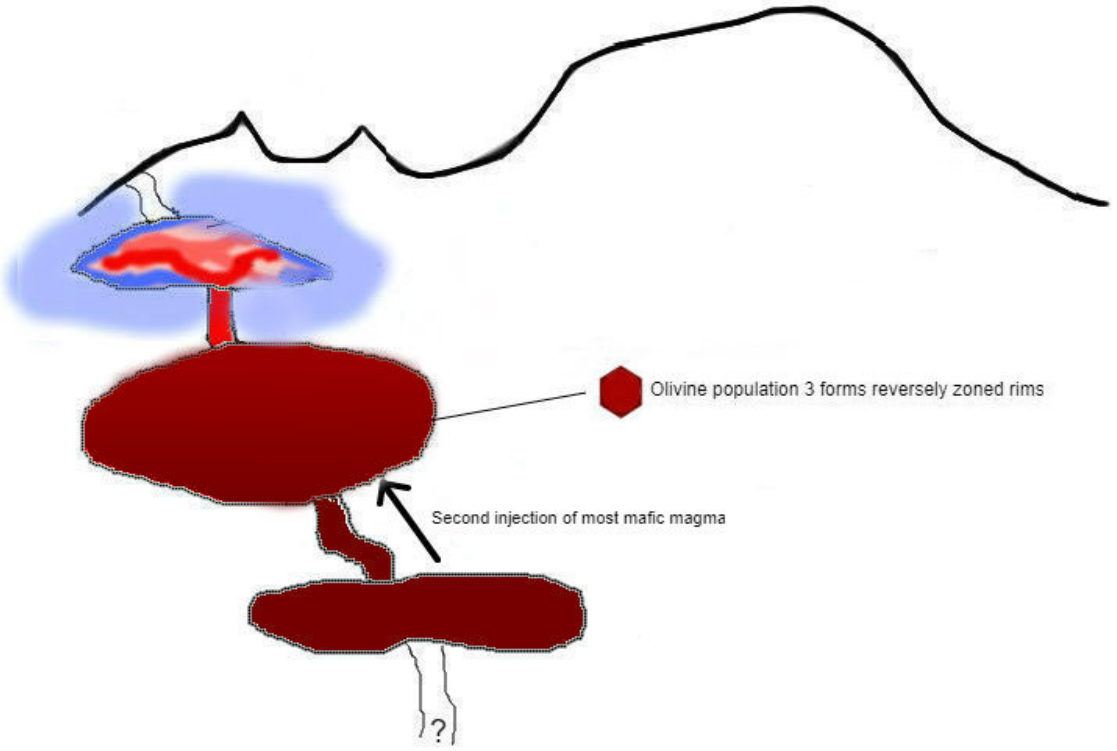

Figure 58. A second pulse of the most-mafic magma from below creates the reversely zoned rims of olivine population 3 and ultimately causes eruption (see Figure 62).

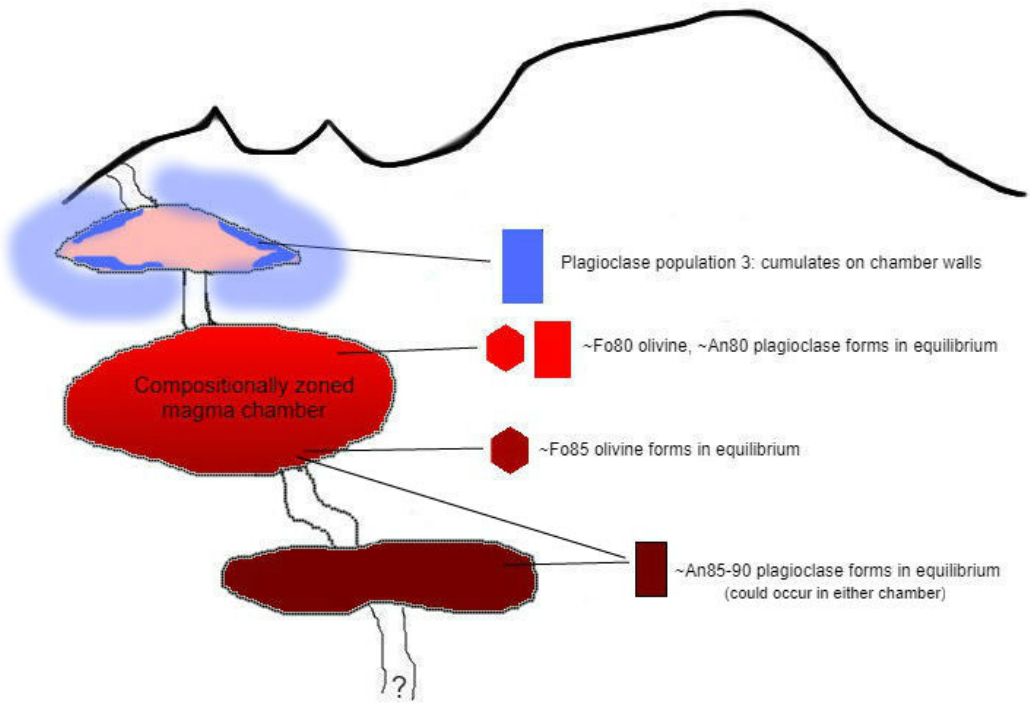

Figure 59. Second possible scenario for Park Butte flow begins with compositionally zoned magma chamber causing differential olivine (and possible plagioclase) core formation.

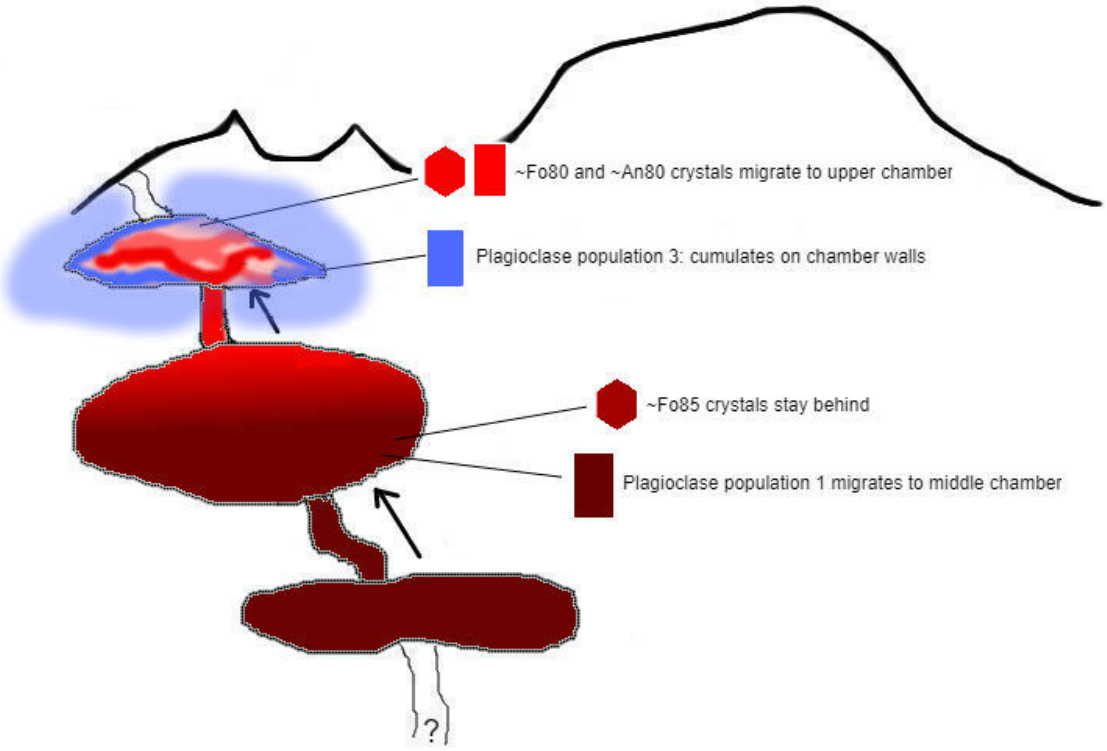

Figure 60. Injection of the middle chamber from below causes upward migration and displaces the upper portions of the central magma chamber into a less-mafic magma chamber. The higher-forsterite olivine crystals are left behind in the middle chamber.

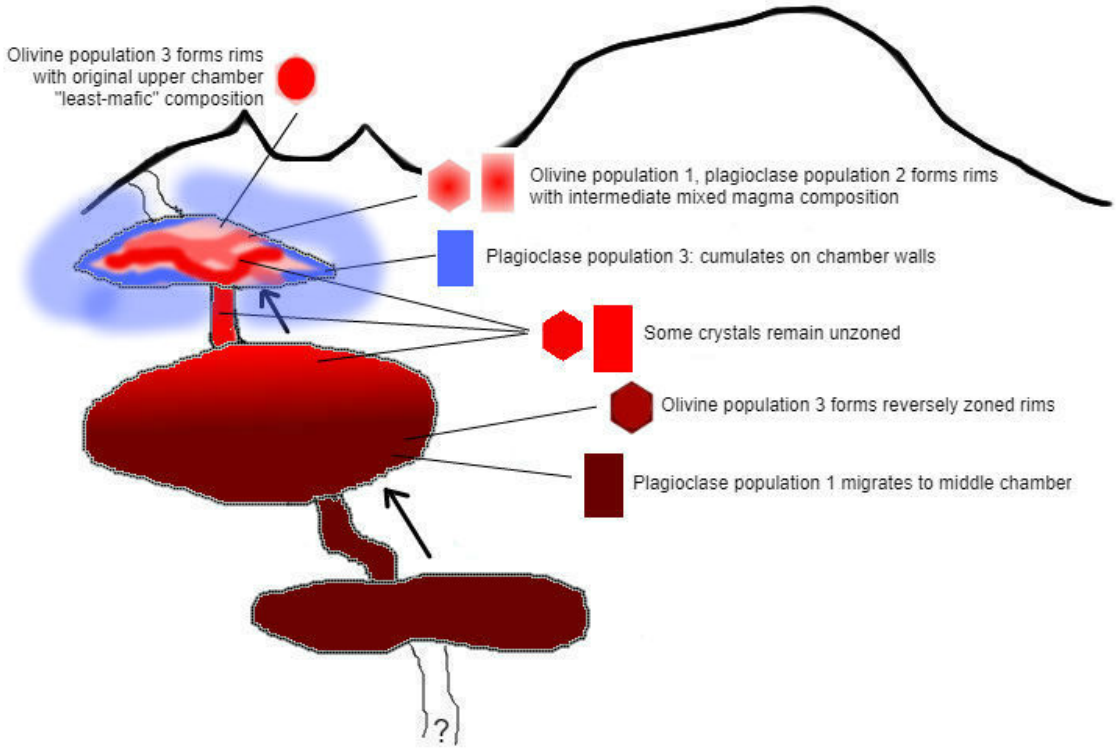

Figure 61. The migration described in Figure 60 creates the zoning patterns labelled in the figure: magma mingling and mixing creates differential rims on olivine populations 1 and 3, the mafic injection creates reversely zoned rims on olivine population 2.

Figure 62. Depressurization and increased temperature from this mafic injection cause exsolution of gasses and eruption. En route to the surface, some of the high-An plagioclase interacts with the low-An upper chamber magma and forms low-An rims.

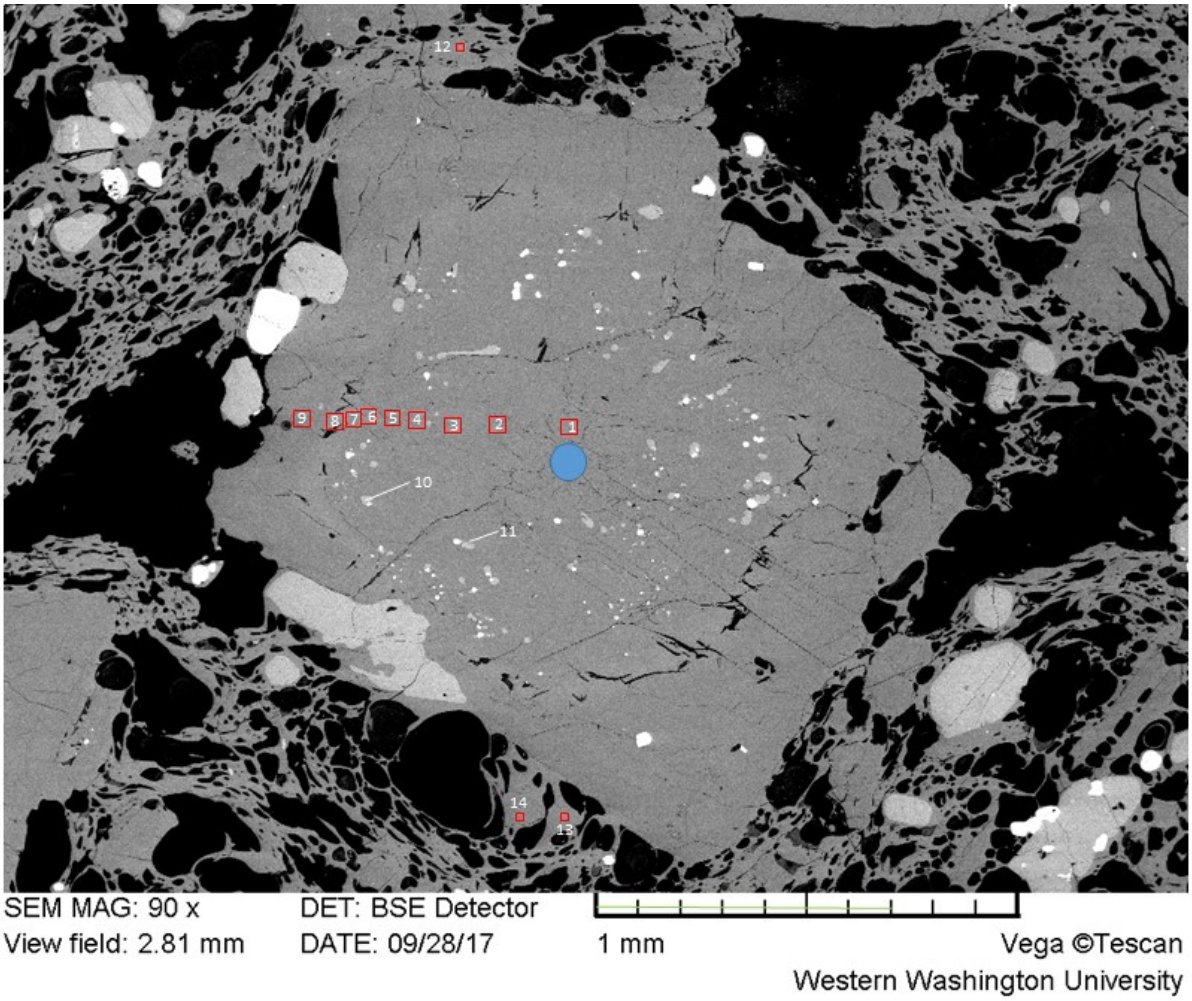

Figure 63. Scanning electron microscope (SEM) view of LS6_plag1. Points 7 and 8 represent the spike upward in anorthite content; note the reaction rim. Point 9 represents the decrease back to normal conditions.

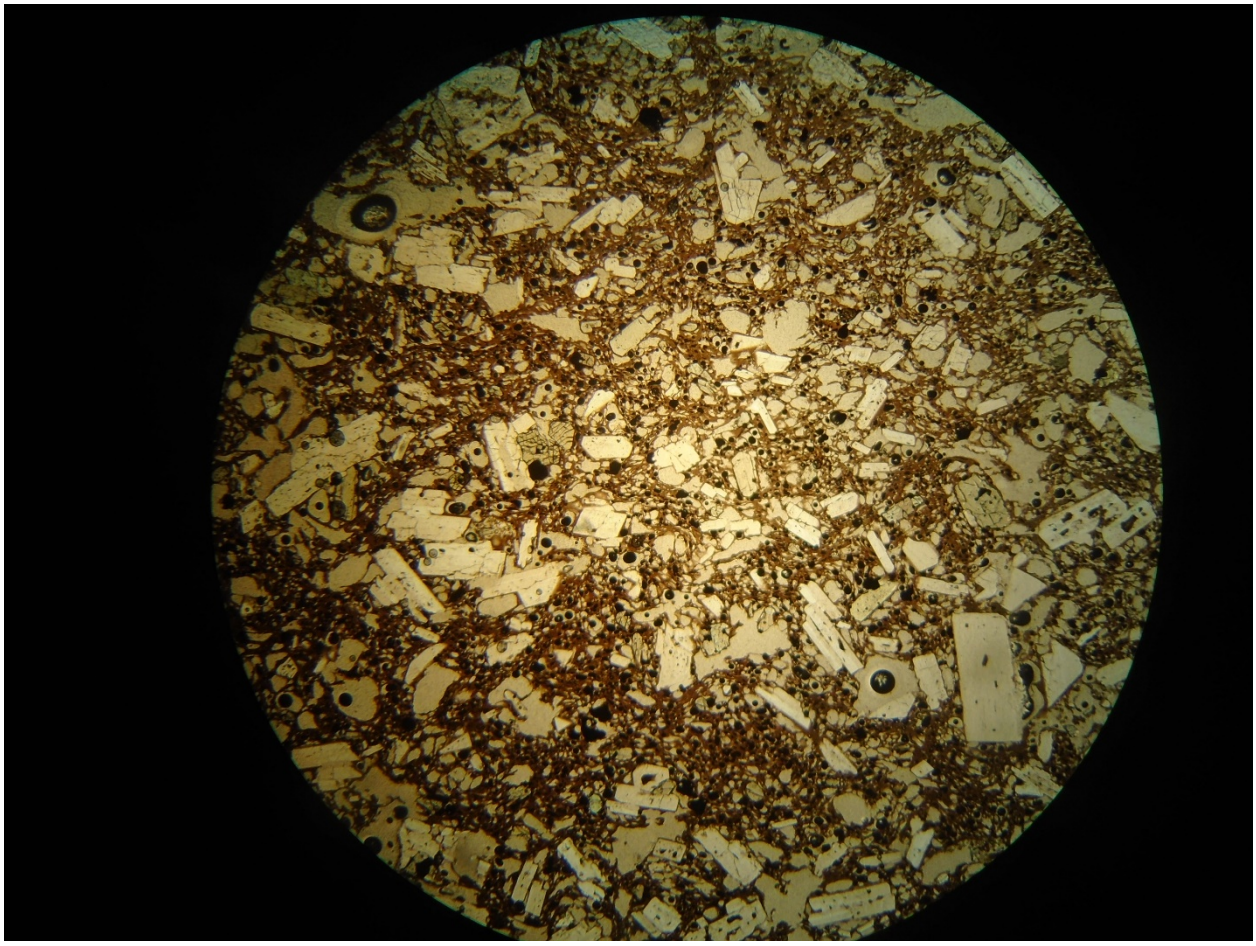

Figure 64. Plane-polarized light (PPL) image of Lake Shannon LS6 sample, showing brown glass (which appears basaltic in PPL) which is actually rhyolitic in composition (Figure 3).

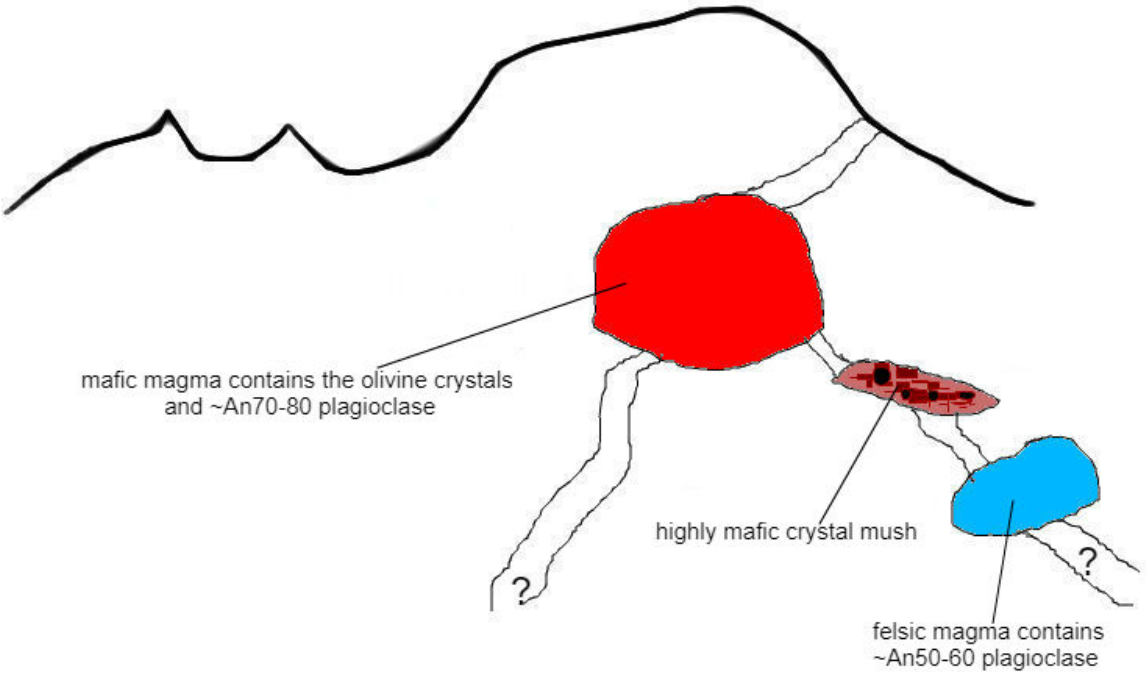

Figure 65. Schematic illustration of Lake Shannon flow relationships in the beginning stages.

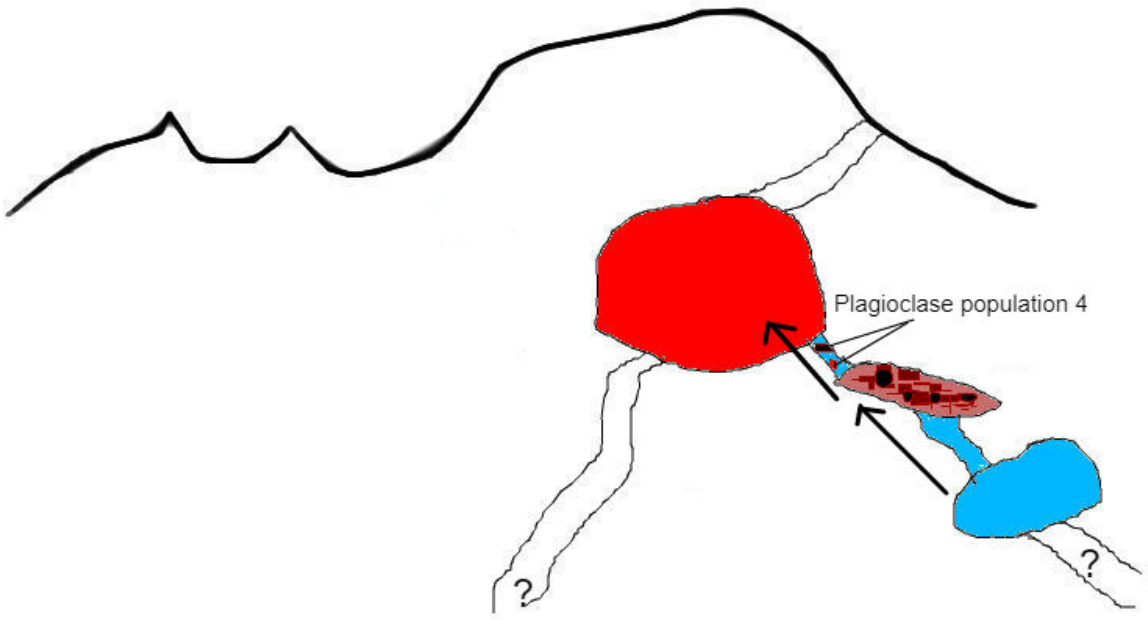

Figure 66. Schematic illustration of Lake Shannon flow relationships: felsic magma begins its travel and goes through a highly mafic crystal mush en route to the main mafic magma chamber.

Figure 67. Schematic illustration of Lake Shannon flow relationships: felsic magma continues into the mafic magma, mingles but does not mix for the most part.

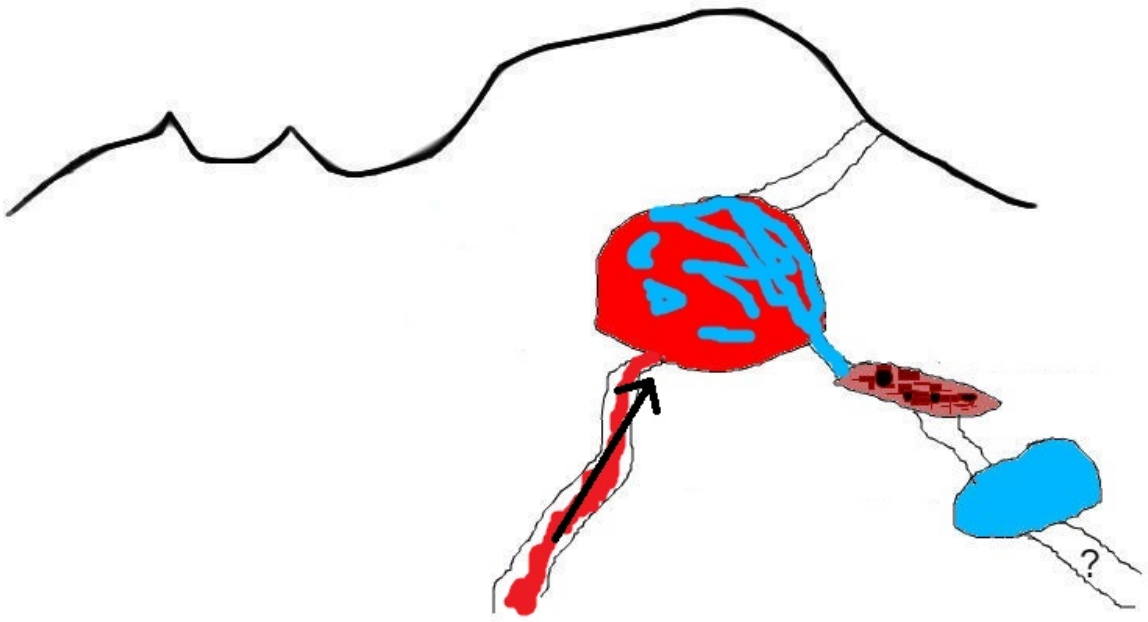

Figure 68. A pulse of mafic magma injects the main mafic magma chamber containing bits of all three main magma populations and causes eruption.